INTERNATIONAL JOURNAL FOR NUMERICAL METHODS IN ENGINEERING
Int. J. Numer. Meth. Engng 2002; **55**:191–231 (DOI: 10.1002/nme.492)

Classical and advanced multilayered plate elements based upon PVD and RMVT. Part 1: Derivation of finite element matrices

Erasmo Carrera*,† and Luciano Demasi

DIASP, Politecnico di Torino, Torino, Italy

SUMMARY

This paper deals with the formulation of finite plate elements for an accurate description of stress and strain fields in multilayered, thick plates subjected to static loadings in the linear, elastic cases. The so-called zig-zag form and interlaminar continuity are addressed in the considered formulations. Two variational statements, the *principle of virtual displacements* (*PVD*) and the *Reissner mixed variational theorem* (*RMVT*) are employed to derive finite element matrices. Transverse stress assumptions are made in the framework of RMVT and the resulting finite elements describe *a priori* interlaminar continuous transverse shear and normal stresses. Both modellings which preserve the number of variables independent of the number of layers (equivalent single-layer models, ESLM) and layer-wise models (LWM) in which the same variables are independent in each layer, have been treated. The order N of the expansions assumed for both displacement and transverse stress fields in the plate thickness direction z as well as the number of element nodes N_n have been taken as free parameters of the considered formulations. By varying N, N_n, variable treatment (LW or ESL) as well as variational statements (PVD and RMVT), a large number of newly finite elements have been presented. Finite elements that are based on PVD and RMVT have been called *classical* and *advanced*, respectively.

In order to write the matrices related to the considered plate elements in a concise form and to implement them in a computer code (see Part 2), extensive indicial notations have been set out. As a result, all the finite element matrices have been built from only five arrays that were called fundamental nuclei (four are related to RMVT applications and one to PVD cases). These arrays have 3×3 dimensions and are therefore constituted of only nine terms each. The different formulations are then obtained by expanding the indices that were introduced for the N-order expansion, for the number of nodes N_n and for the constitutive layers N_l. Compliances and/or stiffness are accumulated from layer to multilayered level according to the corresponding variable treatment (ESLM or LWM). The numerical evaluations and assessment for the presented plate elements have been provided in the companion paper (Part 2), where it has been concluded that it is convenient to refer to RMVT as a variational tool to formulate multilayered plate elements that are able to give a quasi-three-dimensional description of stress/strain fields in multilayered thick structures. Copyright © 2002 John Wiley & Sons, Ltd.

KEY WORDS: finite element; plates; multilayers; classical and mixed formulation; composite materials

*Correspondence to: Erasmo Carrera, Department of Aeronautics and Aerospace Engineering, Politecnico di Torino, Corso Duca degli Abruzzi, 24, 10129 Torino, Italy.
†E-mail: carrera@polito.it

Received 23 October 2000
Revised 4 April 2001

1. INTRODUCTION

Multilayered structures are increasingly used in aerospace, ships, automotive vehicles, advanced optical mirrors and semiconductor technologies. Examples of multilayered, anisotropic structures are sandwich constructions, composite structures made of orthotropic laminae, layered structures made of different isotropic layers (such as those employed for thermal protection) as well as intelligent structures embedding piezo-layers. In most of the applications, these structures mostly appear as flat (plates) or curved panels (shells). In this paper, attention has been restricted to flat geometries, although most of the presented derivations and techniques could be extended to shell cases. Examples of multilayered plates are given in Figure 1.

The analysis of multilayered, anisotropic structures is difficult when compared to one-layered ones made of traditional isotropic materials. A number of complicating effects arise when their mechanical behaviour as well as failure mechanisms have to be correctly understood. Interesting discussions on these effects have been reported by Pagano [1]. Some of these complicating effects have clearly been shown by early [2–4] and recent [5, 6] three-dimensional, elasticity solutions. Unfortunately, these elasticity solutions are only available in a very few cases, which are mainly restricted to sample geometries, loadings and boundary conditions as well as orthotropic behaviour of constitutive layers.

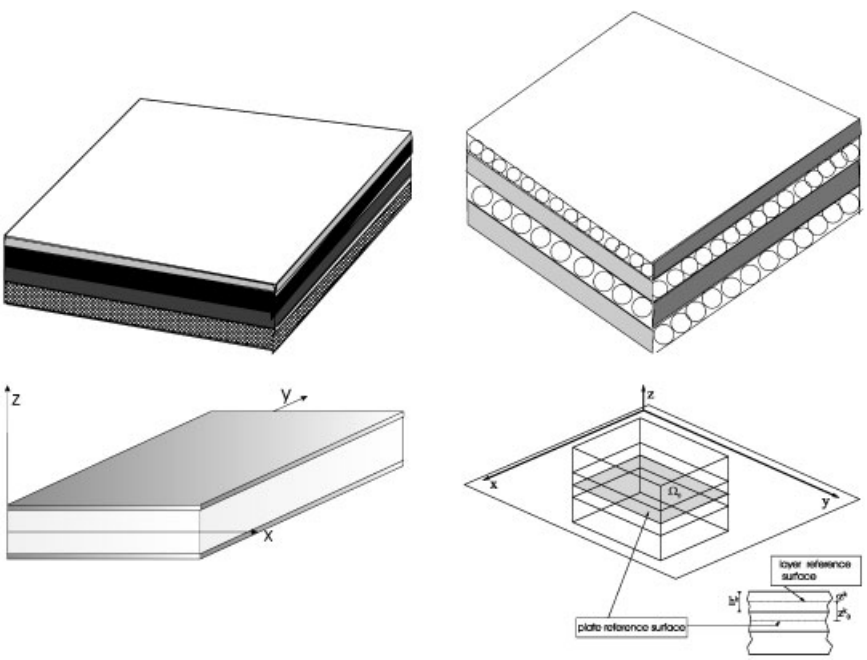

Figure 1. Examples of multilayered structures and plate geometries and notations. Plates (upper part) are made of layers of different materials (left) and by unidirectional fibres (right) and sandwich flat panel (lower, left part).

As far as two-dimensional modelling is concerned, the subject to which this paper is devoted, layered structures also require special attention. This is due to the intrinsic discontinuity of the thermomechanical properties at each layer-interface to which high shear and normal transverse deformability is associated. An accurate description of the stress and strain fields of these structures requires theories that are able to describe the so-called zig-zag (ZZ) form of displacement fields in the thickness z-direction as well as interlaminar continuous (IC) transverse shear and normal stresses (see [7, 2] as examples). Transverse and in-plane anisotropy of multilayered structures make it difficult to find closed-form solutions when these structures are subjected to the usual static and dynamical loadings of the environment to which these structures are exposed when in use. The use of approximated solutions is necessary in these cases. It can therefore be concluded that the use of both refined two-dimensional theories and computational methods become mandatory to solve practical problems related to multilayered structures.

A large number of refined theories and computational strategies have been proposed and implemented over the last four decades. Among the implemented computational strategies, the iterative techniques based on *a posteriori* evaluations developed by Noor and co-authors [8–10], the recent differential quadrature technique proposed by Malik [11], Malik and Bert [12] and recently applied by Teo and Liew [13], and the interesting boundary element formulation proposed by Davì [14] and recently applied by Davì [15], Davì and Milazzo [16] and Milazzo [17] are herein mentioned. Excellent overview papers are available on the topics of computational methods for multilayered structures analyses (see Section 2).

Among the several available computational methods, the finite element method (FEM) has played, and continues to play, a significant role. Most of the commercial codes that are used in small and large companies as well as in research centres are, in fact, finite element oriented. The subject of the present work consists of multilayered finite elements that are able to furnish an accurate description of strain/stress fields in multilayer flat structure analysis. Reissner's mixed variational theorem (RMVT) is used to derive what have been called *advanced*[‡] multilayered finite elements. As a main property, RMVT permits one to assume two independent fields for displacement and transverse stress variables. The resulting advanced finite elements therefore describe *a priori* interlaminar continuous transverse shear and normal stress fields. *Classical* finite elements with only displacement variables are formulated on the basis of the principle of virtual work (PVD) for comparison purposes. The number of both the order N of expansion in z and the number of nodes N_n of the elements are taken as free parameters of the considered RMVT and PVD formulations. As a result, apart from the new finite elements based on RMVT, a number of new classical FE based on PVD are proposed in this work.

In order to lower the number of equations related to the several presented finite elements as much as possible, the indicial notation already used in the first author's papers [18–21] has herein been extended to finite element applications. As a fundamental property, such an indicial notation has led to the writing of all the finite element matrices in terms of a few arrays, which are called *fundamental nuclei*, the dimension of which is 3×3. These fundamental nuclei are herein written at a layer level; such a choice has permitted the authors

[‡]The use of the word 'advanced' has been preferred by the authors, over a few others, such as 'refined', 'mixed' or 'higher order'.

to treat both modellings which preserve the number of variables independent of the number of layers (equivalent single-layer models, ESLM) and layer-wise models (LWM) in which the same variables are independent in each layer, at the same time. The variational statements and continuity requirements for stresses and displacements as well as non-homogeneous boundary conditions at each interface, for displacement and/or transverse stress variables, are used to derive matrices from layers to multilayers and from elements to structure levels.

This paper has been organized as follows. Section 2 outlines the necessary requirements (herein referred to as C_z^0-requirements) that should be taken into account for an accurate description of multilayered structures. Relevant contributions based on different approaches are briefly outlined. RMVT is introduced as a possible tool to completely meet the C_z^0-requirements. Available, relevant finite element implementations are also overviewed in this section. Section 3 quotes the preliminaries that are used in the subsequent sections. Geometries and Hooke's law in classical and mixed forms are given along with strain displacement relations and typical finite element descriptions. Section 4 briefly recalls the employed variational statements. RMVT and PVD are introduced along with their use in the framework of finite element applications. The used indicial notations are also explained in this section. Sections 5 and 6 describe the two-dimensional assumptions that one made on the displacements and transverse stresses. Section 7 derives the first 3×3 *fundamental nuclei* related to classical PVD applications. Section 8 derives the further four 3×3 *fundamental nuclei* related to RMVT applications. Section 9 discusses the possible treatment of stress variables for RMVT-based finite elements. Section 10 gives a summary of the derived multilayered finite elements along with concluding remarks.

Further derivations have been outlined in the form of appendices as follows. Appendix A reports an example that shows how the introduced indicial notations work. A well-known finite element based on PVD has been considered. Appendix B gives an example of loading vectors related to the finite element formulations that have been treated. Appendix C identifies the compliance/stiffness terms that require specific, numerical sub-integration schemes.

A companion paper (Part 2) has been written to provide numerical evaluations related to some of the herein proposed finite elements.

2. MODELLINGS AND FE IMPLEMENTATIONS

This section gives some insight into the peculiarities of two-dimensional modellings of multilayered plates (Section 2.1). Analytical developments are also considered in Section 2.1, while available, related finite element implementations are briefly discussed in Section 2.2.

The literature overview is not complete. A more exhaustive discussion on the several contributions that have been made in the recent past has been covered by recent state-of-the-art articles. Among these, one can mention the papers by Librescu and Reddy [22], Kapania and Raciti [23], Noor and Burton [9], Reddy and Robbins [24], Noor *et al.* [25], and the books by Librescu [26] and Reddy [27].

2.1. Two-dimensional modellings of multilayered structures

2.1.1. High transverse deformability. As far as two-dimensional modelling is concerned, the main task of multilayered constructions is related to the possibility of exhibiting

different mechanical–physical properties in the thickness plate direction. These are *transversely anisotropic* (TA) structures. In addition, anisotropic multilayered structures often show both higher transverse shear and normal flexibility, with respect to in-plane deformability, than traditional isotropic one-layered ones. These are *transversely high deformable* (THD) structures. For instance, laminated structures made of advanced composite materials presently used in aerospace structures could exhibit high values of Young's moduli orthotropic ratio ($E_L/E_T = E_L/E_z = 5$–40, where L denotes the fibre directions while T and z are two-directions orthogonal to L) and low transverse shear moduli ratio ($G_{LT}/E_T \approx G_{TT}/E_T = 1/10$–$1/200$), leading to higher transverse shear and normal stress deformability than in isotropic cases.

As a direct consequence of both TA and THD, well-known thin-plate theories [28–30] that were originally developed for traditional isotropic one-layer structures could be inadequate to predict the response of multilayered structures. Extension of thin-plate theories to multilayered structures are often denoted as *classical lamination theories* (CLT); see Jones [31] as an example. Transverse shear as well as normal strains are, in fact, postulated to be negligible with respect to the other strains in CLT plate analyses.

Improvements of thin-plate theories should be made according to the well-known *Koiter's recommendation* (KR) [32]: a refinement of Kirchhoff thin-plate theory is indeed meaningless, in general, unless the effects of transverse shear and normal stresses are taken into account at the same time. A great deal of contributions have been presented in the literature in which thin-plate and improved theories, already known for isotropic one-layered structures, have been extended to multilayered structures. Extensions of Reissner [33] and/or Mindlin [34] refined-type models, which violate KR and include only transverse shear strains, to layered structures are known as the *shear deformation theory* (SDT) (*or first-order SDT*, $FSDT$); see Yang *et al.* [35], Whitney [7] and the recent book by Reddy [27]. KR can be retained by including both transverse shear and normal strains, as done by Hildebrand *et al.* [36]. Examples of applications of these types of models to laminated structures can be found in the works by Sun and Whitney [37] and Lo *et al.* [38]. These are all known as *higher-order theories* (HOT).

2.1.2. Zig-zag effects and interlaminar continuity: C_z^0-requirements. In addition to the discussed refinements known for one-layer plates made of isotropic materials, the layered construction introduces further complicating effects. Transverse discontinuous mechanical properties cause, in fact, displacement fields $\mathbf{u} = (u_1, u_2, u_3)$ (bold letters denote arrays, while subscripts 1, 2, 3, denote the components in the x, y, z, directions, respectively) in the thickness direction which can exhibit rapid changes and different slopes in correspondence to each layer interface (see Figures 1 and 2). This is known as the *zig-zag* (ZZ) form of displacement field in the thickness shell direction. Although in-plane stresses $\boldsymbol{\sigma}_p = (\sigma_{11}, \sigma_{22}, \sigma_{12})$ can in general be discontinuous, equilibrium reasons, i.e. the Cauchy theorem, demand continuous transverse stresses $\boldsymbol{\sigma}_n = (\sigma_{13}, \sigma_{23}, \sigma_{33})$ at each layer interface (see Figure 3). This is often referred to in the literature as *interlaminar continuity* (IC) of transverse shear and normal stresses. Figure 2 shows, from a qualitative point of view, what could be the scenario of displacement $\mathbf{u}$ and transverse stress $\boldsymbol{\sigma}_n$ distributions in a multilayered structure in exact solutions and/or experiments. Stresses at the interfaces are displayed in Figure 3. In-plane components, which can be discontinuous, are also depicted for comparison. Figures 2 and 3 show that both displacement and transverse stresses, due to compatibility and equilibrium reasons, respectively, are C^0-continuous functions in the thickness z direction. $\mathbf{u}$ and $\boldsymbol{\sigma}_n$ have, in the most general case,

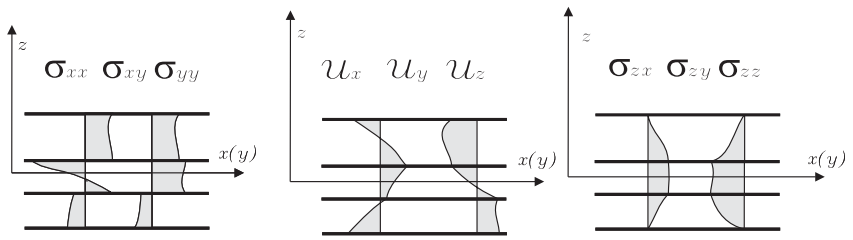

Figure 2. C_z^0-requirements. Displacement and stress (in-plane and transverse) fields in the thickness plate direction. Three-layered plate.

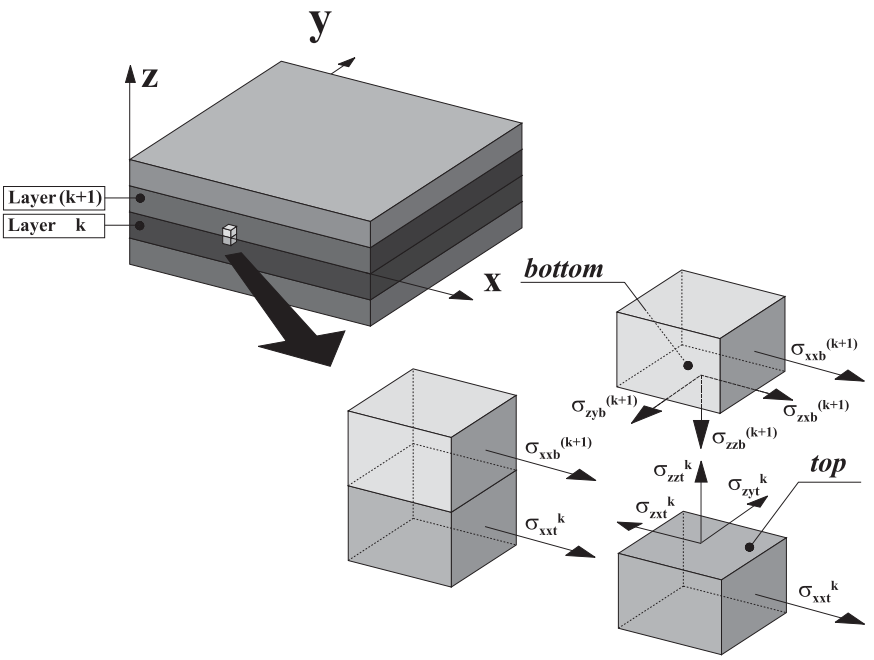

Figure 3. Details of the stress states at the interface between two consecutive layers.

discontinuous first derivatives with correspondence to each interface where the mechanical properties change. In References [18, 39], ZZ and IC were referred to as C_z^0-requirements. The fulfilment of C_z^0-requirements is a crucial point of two-dimensional modelling of multilayered structures.

The extension *sic et simpliciter* of CLT, FSDT and HOT to multilayered plates does not permit the fulfilment of the C_z^0-requirements, that is, ZZ and IC are not addressed by the mentioned CLT, SDT and HOT. An exception is given by Vlasov's [40] SDT-type theory which permits fulfilment of the homogeneous conditions for the transverse shear stresses in correspondence to the top and bottom shell/plate surfaces. Reddy [41, 42] and Reddy and

Phan [43] have shown that such simple inclusion could lead to significant improvement, with respect to SDT, in tracing the static and dynamic response of thick laminated structures.

The theories mentioned above all have the number of unknown variables that are independent of the number of constitutive layers N_l. Following Reddy [27], these types of theories are here grouped as *equivalent single-layer models* (*ESLM*). A possible, natural manner of including the ZZ effect could be implemented by applying CLT, FSDT or HOT at a layer level, that is, each layer is seen as an independent plate and compatibility of displacement is then imposed as a constraint. In these cases, *layer-wise models* (*LWM*) are obtained. Relevant examples of these types of theories are those found in the articles by Srinivas [44], who applied CLT in each layer, and Cho *et al.* [45], who implemented the HOT by Lo *et al.* [38] in each layer. Generalizations on these types of theories were given by Nosier *et al.* [46] and Reddy [27], who expressed the displacement variables in the thickness direction in terms of Lagrange polynomials (interface values were used as unknown variables), therefore permitting an easy linkage of compatibility conditions at each interface.

Literature has shown that LWM provides much better results than those related to ESLM-type analyses. The overviewed ESL or LW models, being formulated with only displacement unknowns, cannot describe *a priori* IC for the transverse shear and normal stresses, i.e. C_z^0-requirements are not completely fulfilled. Apart from the previously discussed contributions, special mention should be made of those works in which the description of both IC and ZZ effects is addressed. Among these, one should mention the pioneering paper by Lekhnitskii [47, 48] that was originally developed for beams, and which describes interlaminar continuous transverse shear stress as well as ZZ effects, and the plate/shell theories by Ambartsumian [49]. Lekhnitskii's theory was extended to plates by Ren [50] and Ren and Owen [51], while Ambartsumian's theory was first extended to unsymmetric plate cases by Whitney [7] and then to shell geometries by Rath and Das [52]. Hundreds of papers have been published that are based on the Ambartsumian–Whitney–Rath–Das theory (see the overview papers already mentioned at the beginning of this section). Most of the works based on these types of theories do not account for the interlaminar continuous transverse normal stress σ_{33} description, i.e. KR is discarded.

2.1.3. Use of RMVT. All the previously discussed theories are formulated on the basis of displacement variables. These types of theories are not designed to *a priori* describe interlaminar continuous transverse stresses. A post-processing procedure is required to recover $\boldsymbol{\sigma}_n$ stresses. Post-processing can be avoided if and only if stress assumptions are made. In-plane and transverse stresses can be assumed in the framework of mixed variational principles (see [41, 53]). *Reissner's mixed variational theorem consists of a mixed principle designed for multilayered structures*. RMVT, in fact, restricts the stress assumptions to transverse components. Murakami [54–56] was the first to apply RMVT to multilayered structures by assuming two independent fields for displacement and transverse stress variables. Toledano and Murakami [57, 58] showed that RMVT does not experience any particular difficulty when including transverse normal stresses in a plate theory.

A more comprehensive evaluation of LW and ESL theories was considered by Carrera [19, 20] where applications to the static analysis of plates were presented. Subsequent works extended the analysis to the dynamics case [21]. In References [19–21, 59–64], Carrera showed that RMVT leads to a quasi-three-dimensional description of the in-plane and out-of plane response. In particular, transverse stresses were determined *a priori* with excellent accuracy.

One should conclude that RMVT appears to be a natural tool to completely and *a priori* fulfil the C_z^0-requirements in both LW and ESL cases. An exhaustive review in RMVT has been recently proposed by Carrera in Reference [65].

2.2. Finite element implementations

Many finite elements have been proposed which were based on the approaches mentioned in the last section. Others based on some special finite element techniques (such as hybrid) have also been proposed. Some of these are briefly discussed in the next two subsections. A third subsection overviews available finite element implementation based on RMVT.

2.2.1. Implementation of refined two-dimensional theories. Early papers concerning laminated plate elements including transverse shear effects SDT have been developed by Pryor and Barker [66], Noor [67], Noor and Mathers [68], Panda and Natarayan [69], Reddy [70] and Kant and Kommineni [71]. Reduced, selective integration [72] and the assumed shear strain concept [73, 74] are known techniques to contrast shear locking and spurious modes associated to these implementations. Many refinements of SDT-type elements have been proposed (see the overview papers by Pandya and Kant [75], Reddy [76] and Barboni and Gaudenzi [77]).

Dozens of finite elements have been proposed that are based on the Ambartsumian–Whitney–Rath–Das-type theory. Among these, the recent works by Cho and Parmeter [78], Aitharaju and Averill [79], Idlbi *et al*. [80], Cho and Averill [81] and Polit and Touratier [82] can be mentioned.

Layer-wise finite elements have been discussed by Pinsky and Kim [83], Reddy [84], Robbin's and Reddy [85], Gaudenzi *et al.* [86], and more recently by Botello *et al.* [87].

The finite element models based on ESL or LW approaches have their own advantages/disadvantages in terms of solution accuracy and/or solution economy. However, these approaches can be combined to lead to the so-called 'multiple-method' or 'global/local technique': an LW description is used in those zones of the structures in which an accurate description is required while ESL is left for the remaining parts. Examples of these approaches can be found in Reddy [27]. Similar techniques, denoted as 'sub-laminate approaches', have recently been developed in the already mentioned Cho and Averill article [81], in the framework of zig-zag-type theories. The so-called 'hierarchy' finite elements for laminated plates were discussed by Babuska *et al.* [88] for similar reasons. The analytical derivations and numerical evaluations were restricted to laminated strips. Similar approaches, named 's-version', were used by Fish and Markolefas [89]. Finite elements based on asymptotic expansion of three-dimensional elasticity equations have been discussed by Turn *et al.* [90].

2.2.2. Mixed and hybrid FE. Discussions on mixed finite elements can be read in the interesting articles reported in the book by Atluri *et al.* [53]. Hybrid stress finite elements are based on a modified complementary energy statement in which equilibrating intra-element stresses and, independently, intra-element or element boundary displacements are interpolated in terms of stress parameter and nodal displacement, respectively. The stress parameters are then eliminated on an element level and a stiffness matrix is obtained. Four-node hybrid stress laminated plate elements, including transverse shear effects, have been developed by Mau and Pian [91] and Spilker *et al.* [92, 93]. Stress fields were defined for each layer (in the ESLM) or for the laminate (for the ESLM case) with interlayer traction continuity and upper/lower

laminate traction-free conditions enforced exactly. More recently, three-dimensional hybrid stress elements have been proposed by Moriya [94] and Liou and Sun [95] and a partial hybrid stress element was developed by Jing and Liao [96]. Partial mixed finite elements have been proposed by Auricchio and Sacco [97] which were based on a re-elaboration of the classical Hellingher–Reissner mixed functional. These were directed to the building of improved FSDT-type finite elements.

2.2.3. Available plate elements based on RMVT. The first FE approach to multilayered structures by means of RMVT is due to Jing and Liao [96]. A partial hybrid formulation was presented; a self-equilibrated stress field was restricted to the three in-plane stresses. As usual in hybrid formulation, stress unknowns were eliminated at an element level in the implemented finite hexahedron element for each layer. The results were restricted to cross-ply plates and showed good accuracy with respect to the exact solution and improvements with respect to other refined analyses.

Application of RMVT to develop standard finite elements was proposed by Rao and Meyer-Piening [98]. The Toledano and Murakami [57, 58] theory was used. Stress unknowns were eliminated before introducing FE approximations by employing a technique that is equivalent to the so-called weak form of Hooke's law (WFHL), which was introduced in Reference [18], that is, only displacements were taken as nodal variables in the ESLM framework. Applications were quoted for laminate and sandwich plates and were related to eight-noded plate isoparametric elements.

The extension of the standard Reissner–Mindlin model to multilayered structures was discussed by Carrera [99]. The obtained finite plate elements (four, eight and nine nodes) were denoted with the acronym RMZC (Reissner–Mindlin zig-zag interlaminar continuity). The weak form of Hooke's law proposed in Reference [18] was used to eliminate transverse shear stress variables. The numerical efficiency of the RMZC FE model was tested for non-linear problems in subsequent works. Large deflection of post-buckling was analysed by Carrera and Kröplin [100]. Non-linear dynamics problems were solved by Carrera and Krause [101]. Applications to linear and non-linear multilayered plates embedding piezo-layers were given by Carrera [102]. Extensive application to sandwich plates was quoted by Carrera [59] while extension to shells has recently been provided by Brank and Carrera [74].

It can be concluded that no study is available in which a systematic application of RMVT to develop ESLM as well as LW advanced multilayered plate elements is made. This is the subject of the present paper, in which PVD applications are mainly developed for comparison purposes.

3. PRELIMINARY ASSUMPTIONS

3.1. Geometry and notations for multilayered plates

The geometry and co-ordinate system of the laminated plates of N_l layers have been shown in Figure 1. The integer k, which is extensively used as both subscripts or superscripts, denotes the layer number that starts from the plate bottom. x and y are the plate middle surface Ω^k co-ordinates. Ω_0 and Ω will be also used to denote the reference surface. Γ^k is the layer boundary on Ω^k. z and z_k are the plate and layer thickness co-ordinates; h and h_k denote plate and layer thickness, respectively. $\zeta_k = 2z_k/h_k$ is the non-dimensional local plate co-ordinate;

A_k will denote the k-layer thickness domain. Symbols not affected by k subscripts/superscripts refer to the whole plate.

3.2. Hooke's law for orthotropic lamina in the material reference system

The laminae are considered to be homogeneous and to operate in the linear elastic range. By employing stiffness coefficients, Hooke's law for the anisotropic k-lamina is written in the form $\sigma_i = C_{ij}\varepsilon_j$, where the sub-indices i and j, ranging from 1 to 6, stand for the index couples $11, 22, 33, 13, 23$ and 12, respectively. The material is assumed to be orthotropic, as specified, by $C_{14} = C_{24} = C_{34} = C_{64} = C_{15} = C_{25} = C_{35} = C_{65} = 0$. This implies that σ_{13}^k and σ_{23}^k only depend on ε_{13}^k and ε_{23}^k. In matrix form,

$$\begin{bmatrix} \sigma_{11} \\ \sigma_{22} \\ \sigma_{12} \\ \sigma_{13} \\ \sigma_{23} \\ \sigma_{33} \end{bmatrix} = \begin{bmatrix} C_{11} & C_{12} & 0 & 0 & 0 & C_{13} \\ C_{12} & C_{22} & 0 & 0 & 0 & C_{23} \\ 0 & 0 & C_{66} & 0 & 0 & 0 \\ 0 & 0 & 0 & C_{55} & 0 & 0 \\ 0 & 0 & 0 & 0 & C_{44} & 0 \\ C_{13} & C_{23} & 0 & 0 & 0 & C_{33} \end{bmatrix} \begin{bmatrix} \varepsilon_{11} \\ \varepsilon_{22} \\ \varepsilon_{12} \\ \varepsilon_{13} \\ \varepsilon_{23} \\ \varepsilon_{33} \end{bmatrix} \tag{1}$$

3.2.1. Hooke' law for orthotropic lamina in the plate reference system. Multilayered plates are often composed of layers made up with different orientation. It is therefore of interest to write the previous Hooke's law from the material axis 1, 2, 3 into the reference (or problem) Cartesian system x, y, z.

$$\boldsymbol{\sigma}_m = [\sigma_{11} \;\; \sigma_{22} \;\; \sigma_{12} \;\; \sigma_{13} \;\; \sigma_{23} \;\; \sigma_{33}]^{\mathrm{T}} \tag{2}$$

$$\boldsymbol{\varepsilon}_m = [\varepsilon_{11} \;\; \varepsilon_{22} \;\; \varepsilon_{12} \;\; \varepsilon_{13} \;\; \varepsilon_{23} \;\; \varepsilon_{33}]^{\mathrm{T}} \tag{3}$$

$$\boldsymbol{\sigma} = [\sigma_{xx} \;\; \sigma_{yy} \;\; \sigma_{xy} \;\; \sigma_{xz} \;\; \sigma_{yz} \;\; \sigma_{zz}]^{\mathrm{T}} \tag{4}$$

$$\boldsymbol{\varepsilon} = [\varepsilon_{xx} \;\; \varepsilon_{yy} \;\; \varepsilon_{xy} \;\; \varepsilon_{xz} \;\; \varepsilon_{yz} \;\; \varepsilon_{zz}]^{\mathrm{T}} \tag{5}$$

The relations between the coefficient in the two reference system are:

$$\boldsymbol{\sigma} = \mathbf{T}\boldsymbol{\sigma}_m \tag{6}$$

$$\boldsymbol{\varepsilon}_m = \mathbf{T}^{\mathrm{T}}\boldsymbol{\varepsilon} \tag{7}$$

$$\boldsymbol{\sigma}_m = \mathbf{C}\boldsymbol{\varepsilon}_m \tag{8}$$

Upon substitution of Equation (7) into Equation (8) and by using Equation (6), one has

$$\boldsymbol{\sigma} = \mathbf{T}\mathbf{C}\mathbf{T}^{\mathrm{T}}\boldsymbol{\varepsilon} = \tilde{\mathbf{C}}\boldsymbol{\varepsilon} \tag{9}$$

3.2.2. Mixed form of Hooke's law. For our convenience, stresses and strains are grouped into two sets, in-plane and out-of-plane (transverse) components:

$$\boldsymbol{\sigma}_p = [\sigma_{xx} \;\; \sigma_{yy} \;\; \sigma_{xy}]^{\mathrm{T}}, \;\; \boldsymbol{\sigma}_n = [\sigma_{xz} \;\; \sigma_{yz} \;\; \sigma_{zz}]^{\mathrm{T}} \tag{10}$$

$$\boldsymbol{\varepsilon}_p = [\varepsilon_{xx} \;\; \varepsilon_{yy} \;\; \varepsilon_{xy}]^{\mathrm{T}}, \;\; \boldsymbol{\varepsilon}_n = [\varepsilon_{xz} \;\; \varepsilon_{yz} \;\; \varepsilon_{zz}]^{\mathrm{T}} \tag{11}$$

The same is done for the matrices:

$$\tilde{\mathbf{C}}_{pp} = \begin{bmatrix} \tilde{C}_{11} & \tilde{C}_{12} & \tilde{C}_{16} \\ \tilde{C}_{12} & \tilde{C}_{22} & \tilde{C}_{26} \\ \tilde{C}_{16} & \tilde{C}_{26} & \tilde{C}_{66} \end{bmatrix}, \quad \tilde{\mathbf{C}}_{pn} = \begin{bmatrix} 0 & 0 & \tilde{C}_{13} \\ 0 & 0 & \tilde{C}_{23} \\ 0 & 0 & \tilde{C}_{36} \end{bmatrix} \tag{12}$$

$$\tilde{\mathbf{C}}_{np} = \begin{bmatrix} 0 & 0 & 0 \\ 0 & 0 & 0 \\ \tilde{C}_{13} & \tilde{C}_{23} & \tilde{C}_{36} \end{bmatrix}, \quad \tilde{\mathbf{C}}_{nn} = \begin{bmatrix} \tilde{C}_{55} & \tilde{C}_{45} & 0 \\ \tilde{C}_{45} & \tilde{C}_{44} & 0 \\ 0 & 0 & \tilde{C}_{33} \end{bmatrix} \tag{13}$$

Hooke's law is therefore rewritten as

$$\begin{bmatrix} \boldsymbol{\sigma}_p \\ \boldsymbol{\sigma}_n \end{bmatrix} = \begin{bmatrix} \tilde{\mathbf{C}}_{pp} & \tilde{\mathbf{C}}_{pn} \\ \tilde{\mathbf{C}}_{np} & \tilde{\mathbf{C}}_{nn} \end{bmatrix} \begin{bmatrix} \boldsymbol{\varepsilon}_p \\ \boldsymbol{\varepsilon}_n \end{bmatrix} \tag{14}$$

That is,

$$\boldsymbol{\sigma}_p = \tilde{\mathbf{C}}_{pp}\boldsymbol{\varepsilon}_p + \tilde{\mathbf{C}}_{pn}\boldsymbol{\varepsilon}_n \tag{15}$$

$$\boldsymbol{\sigma}_n = \tilde{\mathbf{C}}_{np}\boldsymbol{\varepsilon}_p + \tilde{\mathbf{C}}_{nn}\boldsymbol{\varepsilon}_n \tag{16}$$

$$\boldsymbol{\sigma}_p = \mathbf{C}_{pp}\boldsymbol{\varepsilon}_p + \mathbf{C}_{pn}\boldsymbol{\sigma}_n \tag{17}$$

$$\boldsymbol{\varepsilon}_n = \mathbf{C}_{np}\boldsymbol{\varepsilon}_p + \mathbf{C}_{nn}\boldsymbol{\sigma}_n \tag{18}$$

Equations (17) and (18) represent the mixed form of Hooke's law. Such a form plays a fundamental role in the use of RMVT. The relations between the two forms of Hooke's law are

$$\begin{aligned} \mathbf{C}_{pp} &= \tilde{\mathbf{C}}_{pp} - \tilde{\mathbf{C}}_{pn}(\tilde{\mathbf{C}}_{nn})^{-1}\tilde{\mathbf{C}}_{np} \\ \mathbf{C}_{pn} &= \tilde{\mathbf{C}}_{pn}(\tilde{\mathbf{C}}_{nn})^{-1} \\ \mathbf{C}_{np} &= -(\tilde{\mathbf{C}}_{nn})^{-1}\tilde{\mathbf{C}}_{np} \\ \mathbf{C}_{nn} &= (\tilde{\mathbf{C}}_{nn})^{-1} \end{aligned} \tag{19}$$

3.3. Strain–displacement relations

As one remains within the small deformation field, the strain components $\boldsymbol{\varepsilon}_p, \boldsymbol{\varepsilon}_n$ are linearly related to the displacements $\mathbf{u}$ according to the differential, geometrical relations,

$$\boldsymbol{\varepsilon}_p = \mathbf{D}_p \mathbf{u} \tag{20}$$

$$\boldsymbol{\varepsilon}_n = \mathbf{D}_n \mathbf{u} = (\mathbf{D}_{n\Omega} + \mathbf{D}_{nz})\mathbf{u} \tag{21}$$

where $\mathbf{u}$ denotes the array of the displacement components,

$$\mathbf{u} = [u_x \;\; u_y \;\; u_z]^{\mathrm{T}} \tag{22}$$

The differential matrices are

$$\mathbf{D}_p = \begin{bmatrix} \dfrac{\partial}{\partial x} & 0 & 0 \\ 0 & \dfrac{\partial}{\partial y} & 0 \\ \dfrac{\partial}{\partial y} & \dfrac{\partial}{\partial x} & 0 \end{bmatrix}, \quad \mathbf{D}_n = \begin{bmatrix} \dfrac{\partial}{\partial z} & 0 & \dfrac{\partial}{\partial x} \\ 0 & \dfrac{\partial}{\partial z} & \dfrac{\partial}{\partial y} \\ 0 & 0 & \dfrac{\partial}{\partial z} \end{bmatrix} \tag{23}$$

$$\mathbf{D}_{n\Omega} = \begin{bmatrix} 0 & 0 & \dfrac{\partial}{\partial x} \\ 0 & 0 & \dfrac{\partial}{\partial y} \\ 0 & 0 & 0 \end{bmatrix}, \quad \mathbf{D}_{nz} = \begin{bmatrix} \dfrac{\partial}{\partial z} & 0 & 0 \\ 0 & \dfrac{\partial}{\partial z} & 0 \\ 0 & 0 & \dfrac{\partial}{\partial z} \end{bmatrix} \tag{24}$$

3.4. Finite element description and shape functions

Following standard FEM, the unknown variables in the element domain are expressed in terms of their values with correspondence to the element nodes. According to the isoparametric description, displacements or stresses are expressed as follows:

$$\mathbf{u}_\tau^k = N_i \mathbf{q}_{\tau i}^k \quad (i = 1, 2, \ldots, N_n) \tag{25}$$

where

$$\mathbf{q}_{\tau i}^k = [q_{u_x \tau i}^k \;\; q_{u_y \tau i}^k \;\; q_{u_z \tau i}^k]^{\mathrm{T}} \tag{26}$$

and

$$\boldsymbol{\sigma}_{n\tau}^k = N_i \mathbf{g}_{\tau i}^k \quad (i = 1, 2, \ldots, N_n) \tag{27}$$

where

$$\mathbf{g}_{\tau i}^k = [g_{xz\tau i}^k \;\; g_{yz\tau i}^k \;\; g_{zz\tau i}^k]^{\mathrm{T}} \tag{28}$$

N_n is the number of the node of the element and it is taken as free parameter of the model. N_i are the shape functions and $\mathbf{q}_{\tau i}^k$, $\mathbf{g}_{\tau i}^k$ are nodal variables. ξ, η are the natural co-ordinates. Explicit forms can be found in one of the many books on FEM; a few cases are detailed in Part 2 [103].

4. RMVT AND PVD AND THEIR USE TO DEVELOP FINITE ELEMENTS

4.1. PVD and RMVT

For a complete and rigorous understanding of the foundations of RMVT, reference can be made to the articles by Professor Reissner [104, 105]. Readers can refer to these works for a systematic comprehension of the mathematical/variational background of Reissner's theorem. Here the author's aim is to try to give a simple interpretation of RMVT, starting from the basic concept of continuum mechanics and the well-known statements of calculus of variations (see [106, 41, 53]).

In solid mechanics, it is well-known that the principle of virtual displacement (PVD) involves only a compatible displacement field as a variable, and has as its Euler–Lagrange the conditions of balance of momenta and traction boundary conditions. Likewise, the dual form of PVD, i.e. the principle of virtual forces (PVF), involves a stress field that is equilibrated and satisfies the traction boundary conditions, alone as a variable and has as its Euler–Lagrange equations the kinematic compatibility conditions and displacement boundary conditions. If in PVD kinematic compatibility and displacement boundary conditions are introduced as conditions of constraint through Lagrange multipliers, which turn out to be stresses and surface traction, respectively, one then obtains the so-called Hu–Washizu variational principle. Likewise, if the condition of equilibrium of stresses is introduced as a constraint condition through a Lagrange multipliers field (which turns out to be displacement) into PVF, one is led to the so-called Hellingher–Reissner principles. Thus, the Hu–Washizu and Hellingher–Reissner principles, which involve that one field in the continuum as variables (some of which play the role of Lagrange multipliers to enforce certain constraint conditions), are often referred to as mixed variational principles.

This is the scenario in which RMVT can be simply interpreted as a particular case of the previously mentioned mixed principles in which *only* compatibility of transverse strain $\boldsymbol{\varepsilon}_n = (\varepsilon_{13}, \varepsilon_{23}, \varepsilon_{33})$ is enforced by means of Lagrange multipliers which, in this case, turns out to be transverse stresses $\delta\boldsymbol{\sigma}_n = (\delta\sigma_{13}, \delta\sigma_{23}, \delta\sigma_{33})$ (δ is the variational symbol). The word *only* signifies Reissner's intuition: for multilayered structure analyses, it is sufficient to restrict the mixed assumptions to transverse stresses. It is for such stresses that an independent field is, in fact, required to *a priori* and *completely* fulfil the C_z^0-require ments.

PVD assumes a displacement field $\mathbf{u}$ and puts three-dimensional indefinite equilibrium (and related equilibrium conditions at the boundary surfaces which are, for the sake of brevity, not written here) into a variational form. In the static case, these equations are

$$\sigma_{ij,i} = p_i, \quad i, j = 1, 2, 3 \tag{29}$$

$\mathbf{p} = (p_1, p_2, p_3)$ are volume loadings. The corresponding PVD integral, variational equation for a multilayered structure is written as

$$\int_V (\delta \boldsymbol{\varepsilon}_{p\mathrm{G}}^{\mathrm{T}} \boldsymbol{\sigma}_{p\mathrm{H}} + \delta \boldsymbol{\varepsilon}_{n\mathrm{G}}^{\mathrm{T}} \boldsymbol{\sigma}_{n\mathrm{H}}) \, \mathrm{d}V = \delta L_{\mathrm{e}} \tag{30}$$

V denotes the three-dimensional multilayered body volume while the subscript H underlines that stresses are computed via Hooke's law. The variation of the internal work has been split into in-plane and out-of-plane parts and involves stress from Hooke's law and strain from geometrical relations (subscript G). δL_{e} is the virtual variation of the work made by the external layer force $\mathbf{p}$.

RMVT can be simply constructed by adding the constraint equations for the transverse stresses to PVD. These equations can be built by evaluating transverse strains in two ways: by Hooke's law $\boldsymbol{\varepsilon}_{n\mathrm{H}}$ and by geometrical relations $\boldsymbol{\varepsilon}_{n\mathrm{G}}$. In formula

$$\boldsymbol{\varepsilon}_{n\mathrm{H}} - \boldsymbol{\varepsilon}_{n\mathrm{G}} = 0 \tag{31}$$

RMVT therefore states

$$\int_V (\delta \boldsymbol{\varepsilon}_{p\mathrm{G}}^{\mathrm{T}} \boldsymbol{\sigma}_{p\mathrm{H}} + \delta \boldsymbol{\varepsilon}_{n\mathrm{G}}^{\mathrm{T}} \boldsymbol{\sigma}_{n\mathrm{M}} + \delta \boldsymbol{\sigma}_{n\mathrm{M}}^{\mathrm{T}} (\boldsymbol{\varepsilon}_{n\mathrm{G}} - \boldsymbol{\varepsilon}_{n\mathrm{H}})) \, \mathrm{d}V = \delta L_{\mathrm{e}} \tag{32}$$

The third 'mixed' term variationally enforces the compatibility of the transverse strain components. Subscript M underlines that transverse stresses are those of the assumed model.

4.2. Use of RMVT and PVD to develop finite elements

RMVT and PVD can be used to derive governing equations of plate problems in a strong form. Examples of the use of RMVT to derive governing differential equations are given in the already mentioned papers, see Murakami [56] and Carrera [101] as examples. In the present work, these two variational tools are used to establish the weak form of equilibrium and compatibility according to finite element approximations.

In the so-called axiomatic approach, a certain displacement and/or stress fields are postulated in the plate z-direction. An interesting discussion on the implications of the axiomatic character of a given theory has been provided by Antona [107]. According to PVD and RMVT variational statements, multilayered plate elements could be formulated according to the following five steps.

1. Displacement and/or stress distributions in the thickness z plate direction are *postulated* by referring to a certain set of base functions (Sections 5 and 6).
2. Material behaviour is assigned, i.e. Hooke's law is given (Section 3.2).
3. A geometrical relation is given, i.e. a strain–displacement relation is assumed (Section 3.3).
4. A finite element description and shape functions are introduced (Section 3.4).
5. Variational statements are then used to establish in weak sense finite element matrices (Sections 7 and 8).

These developments are presented in the most general cases of N-order for the expansion of the unknown variable in the z-thickness co-ordinate. The number of the nodes N_n is also taken as a free parameter of the present work.

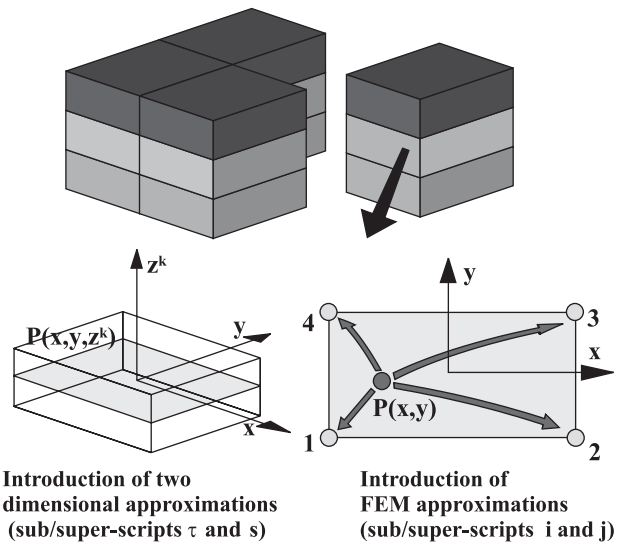

Figure 4. Summary of the introduced approximations and related indicial notations.

4.3. Summary of the introduced approximations, indicial notations and fundamental nuclei 3×3

In order to derive finite element matrices according to PVD or RMVT, the introduced approximations can be summarized in the following two points:

1. The three-dimensional problem is reduced to a two-dimensional one by postulating a certain behaviour in the plate thickness direction z. As a result, the unknown variables only depend on the x, y co-ordinates which are defined on Ω.
2. The unknowns on Ω are further expressed in terms of nodal variables via shape function assumptions.

Figure 4 shows a plate discretized in a certain number of finite elements. The dependence of the unknown variables on z is first eliminated via the introduction of two-dimensional approximations. The unknown variables are therefore only defined on a reference surface Ω. The dependence on x, y is further eliminated by introducing FE assumptions.

As far as indicial notations are concerned, one notices that the summands on the left-hand side of PVD and RMVT are products of stresses/strains times variations of stresses/strains and that each stress/strain array has three scalars. The two-dimensional and FE approximations (1) and (2) enumerated above are introduced in these stresses/strains as well as in their variations. In particular, in this paper the following sub/superscripts are used (Figure 4):

- τ, s sub–superscripts couple is used for the z-expansions for stresses/strains and their variation, respectively.
- i, j sub–superscripts couple is used for the number of nodes expansions for stresses/strains and their variations, respectively.

Hence PVD and RMVT statements lead to finite element matrices that could be written by means of simple arrays that have herein been called *fundamental nuclei*. These have 3×3 terms. By varying the introduced indexes, the generic term of the finite element matrices related to a given set of N and N_n values could be obtained. The used indicial notation has been designed for the computer implementations that are presented in the companion paper (Part 2) [103]. An example showing the way in which the indicial notation works is given in Appendix A.

5. DISPLACEMENT ASSUMPTIONS FOR PVD APPLICATIONS

In the framework of this paper, the behaviour of a displacement and/or transverse stress components f is postulated in the thickness plate z-directions according to a given expansion

$$f(x, y, z) = F_i(z)\ f_i(x, y), \quad i = 1, N^\star \tag{33}$$

It is intended that repeated indexes are summed over their ranges. The polynomials $F_i(z)$ constitute a set of independent functions. Such a base can be arbitrarily chosen: power of z, and combinations of Legendre polynomials will be considered in this paper. $N^\star$ denotes the number of the introduced terms.

In the case of classical models, formulated on the basis of PVD, the assumptions of Equation (33) are restricted to the displacement variables. Traditionally z power expansion is employed,

$$\mathbf{u} = \mathbf{u}_0 + z^r \mathbf{u}_r, \quad r = 1, 2, \ldots, N \tag{34}$$

The subscript 0 denotes displacement values with correspondence to the plate/shell reference surface Ω, not necessarily corresponding to the middle layer or multilayered surface. Linear and higher-order distributions in the z-direction are introduced by the r-polynomials. *N remains a free parameter of the model*. Different N values could be used for different variables.

In order to write the whole modellings in a unified notation, the above expansion is rewritten as

$$\mathbf{u} = F_t \mathbf{u}_t + F_b \mathbf{u}_b + F_r \mathbf{u}_r = F_\tau \mathbf{u}_\tau, \quad \tau = t, b, r, \quad r = 2, \ldots, N-1 \tag{35}$$

By comparing Equation (35) to Equation (34), one finds that subscript b denotes values corresponding to Ω ($\mathbf{u}_b = \mathbf{u}_0$) while subscript t refers to the highest-order term ($\mathbf{u}_t = \mathbf{u}_N$). The F_τ polynomials assume the following explicit form:

$$F_b = 1, \quad F_t = z^N, \quad F_r = z^r, \quad r = 2, \ldots, N-1 \tag{36}$$

where b and t subscripts will also signify, see below, values of the displacement and/or stress variables with correspondence to layer bottom and top surfaces, respectively.

The assumptions written at previous expansions can be made at layer or multilayered level. Layer-wise LW and equivalent single-layer (ESLM) descriptions correspond to the first and second cases, respectively. These are discussed separately in the following two subsections.

5.1. *Equivalent single-layer models (ESLM) with zig-zag function*

The displacement variables are the same in each of the N_l-layers. Resulting theories are well-known classical plate models.

It is possible to introduce zig-zag effects in the previous expansion and in the PVD framework by referring to Murakami's idea which was originally introduced in the framework of RMVT. Murakami [56] proposed to add a zig-zag function to Equation (33),

$$\mathbf{u} = \mathbf{u}_0 + (-1)^k \zeta_k \mathbf{u}_Z + z^{r-1}\mathbf{u}_r, \quad r = 2, \ldots, N \tag{37}$$

Subscript Z refers to the introduced zig-zag term. Note that the unknown variables $\mathbf{u}_0, \mathbf{u}_Z, \mathbf{u}_r$ are k-independent. The geometrical meaning of the zig-zag function is explained in Figure 3 of Part 2 of this paper. $\zeta_k = 2z_k/h_k$ is a non-dimensional layer co-ordinate (z_k is the physical co-ordinate of the k-layer whose thickness is h_k). The exponent k changes the sign of the zig-zag term in each layer. Such a trick permits one to reproduce the discontinuity of the first derivative of the displacement variables in the z-directions which physically comes from the intrinsic transverse anisotropy (TA) of multilayered structures (as depicted in Figure 2). By employing a unified notation, Equation (37) becomes

$$\mathbf{u} = F_t\mathbf{u}_t + F_b\mathbf{u}_b + F_r\mathbf{u}_r = F_\tau\mathbf{u}_\tau, \quad \tau = t, b, r, \quad r = 2, \ldots, N \tag{38}$$

Subscript t has been chosen to denote the zig-zag term ($\mathbf{u}_t = \mathbf{u}_Z$, $F_t = (-1)^k\zeta_k$).

5.2. *Layer-wise models (LWM)*

By assuming the expansion in Equation (34) in each layer, layer-wise description is obtained. Nevertheless, Taylor-type expansion of Equation (34) is not convenient for a layer-wise description. In fact, the fulfilment of continuity requirements for the displacement at interfaces, i.e. the C_z^0-requirements, could be easily introduced by using the interface variables as unknowns. A convenient combination of Legendre polynomials [56–58, 18] could be used as base functions:

$$\mathbf{u}^k = F_t\mathbf{u}_t^k + F_b\mathbf{u}_b^k + F_r\mathbf{u}_r^k = F_\tau\mathbf{u}_\tau^k \quad \tau = t, b, r, \quad r = 2, 3, \ldots, N, \quad k = 1, 2, \ldots, N_l \tag{39}$$

It is now intended that the subscripts t and b denote values related to the layer top and bottom surfaces, respectively. These two terms consist of the linear part of the expansion. The thickness functions $F_\tau(\zeta_k)$ have now been defined at the k-layer level,

$$F_t = \frac{P_0 + P_1}{2}, \quad F_b = \frac{P_0 - P_1}{2}, \quad F_r = P_r - P_{r-2}, \quad r = 2, 3, \ldots, N \tag{40}$$

in which $P_j = P_j(\zeta_k)$ is the Legendre polynomial of j-order defined in the ζ_k-domain: $-1 \leqslant \zeta_k \leqslant 1$. The chosen functions have the following properties:

$$\zeta_k = \begin{cases} 1, & F_t = 1,\ F_b = 0,\ F_r = 0 \\ -1, & F_t = 0,\ F_b = 1,\ F_r = 0 \end{cases} \tag{41}$$

The continuity of the displacement at each interface is easily linked,

$$\mathbf{u}_t^k = \mathbf{u}_b^{(k+1)}, \quad k = 1, N_l - 1 \tag{42}$$

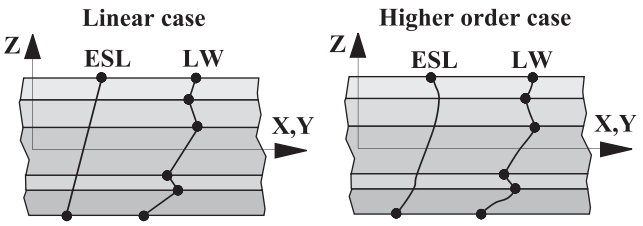

Figure 5. Examples of linear and higher-order field for both ESLM and LW variable description.

Examples of linear and higher-order fields in the multilayer for ESLM and LW description are shown in Figure 5.

6. DISPLACEMENT AND TRANSVERSE STRESS ASSUMPTIONS FOR RMVT APPLICATIONS

6.1. ESLM case

RMVT consists of a variational tool designed for multilayered structures. Appropriate applications of RMVT demand displacement fields which describe a zig-zag effect and transverse stresses which are continuous at the interfaces. The zig-zag effect can be included by referring to displacement fields quoted in Equations (37) and (39) for ESL and LW description, respectively. Equation (37) is not appropriate for ESL description of transverse stresses. Its extension to transverse shear and normal stress would violate Reissner's aims. In fact, the resulting stresses model does not fulfil homogeneous and non-homogeneous conditions at the plate top/bottom surface. The use of RMVT therefore demands layer-wise description of transverse stresses even though ESLM expansions are used for displacements. It is intended that in the presented derivations ESLM description is only related to displacement fields in RMVT applications.

Transverse stresses are assumed independent in each layer. The layer-wise description already used for displacements is extended to transverse stresses,

$$\boldsymbol{\sigma}_{n\mathrm{M}}^{k} = F_t \boldsymbol{\sigma}_{nt}^{k} + F_b \boldsymbol{\sigma}_{nb}^{k} + F_r \boldsymbol{\sigma}_{nr}^{k} = F_\tau \boldsymbol{\sigma}_{n\tau}^{k}, \quad \tau = t, b, r, \quad r = 2, 3, \ldots, N; \quad k = 1, 2, \ldots, N_l \tag{43}$$

The interlaminar transverse shear and normal stress continuity IC can therefore be linked by simply writing

$$\boldsymbol{\sigma}_{nt}^{k} = \boldsymbol{\sigma}_{nb}^{(k+1)}, \quad k = 1, N_l - 1 \tag{44}$$

In those cases in which the top/bottom plate/shell stress values are prescribed (zero or imposed values), the following additional equilibrium conditions must be accounted for:

$$\boldsymbol{\sigma}_{nb}^{1} = \bar{\boldsymbol{\sigma}}_{nb}, \quad \boldsymbol{\sigma}_{nt}^{N_l} = \bar{\boldsymbol{\sigma}}_{nt} \tag{45}$$

where the over-bar denotes the imposed values in correspondence to the plate boundary surfaces.

6.2. *Layer-wise models* (*LWM*)

Full layer-wise description can be introduced by simply extending the stress assumptions of the previous paragraph to displacement variables,

$$\begin{aligned} \mathbf{u}^k &= F_t\mathbf{u}_t^k + F_b\mathbf{u}_b^k + F_r\mathbf{u}_r^k = F_\tau\mathbf{u}_\tau^k, \qquad \tau = t,b,r, \quad r = 2,3,\ldots,N \\ \boldsymbol{\sigma}_{n\mathrm{M}}^k &= F_t\boldsymbol{\sigma}_{nt}^k + F_b\boldsymbol{\sigma}_{nb}^k + F_r\boldsymbol{\sigma}_{nr}^k = F_\tau\boldsymbol{\sigma}_{n\tau}^k, \quad k = 1,2,\ldots,N_l \end{aligned} \tag{46}$$

In addition to Equation (44) the compatibility of the displacement reads

$$\mathbf{u}_t^k = \mathbf{u}_b^{(k+1)}, \quad k = 1, N_l - 1 \tag{47}$$

Note that LW description does not require any zig-zag function for the simulation of zig-zag effects. C_z^0-requirements are completely and *a priori* fulfilled by Equations (44)–(47).

7. ESL AND LW FINITE ELEMENTS DEVELOPED ON THE BASIS OF PVD

7.1. *FEM matrices for the k-layer*

The assumed displacement field is first introduced in the expression for the strains, leading to

$$\boldsymbol{\varepsilon}_p^k = \mathbf{D}_p\mathbf{u}^k = \mathbf{D}_p(F_\tau\mathbf{u}_\tau^k) \tag{48}$$

$$\boldsymbol{\varepsilon}_n^k = \mathbf{D}_n\mathbf{u}^k = (\mathbf{D}_{n\Omega} + \mathbf{D}_{nz})(F_\tau\mathbf{u}_\tau^k) = \mathbf{D}_{n\Omega}(F_\tau\mathbf{u}_\tau^k) + F_{\tau,z}\mathbf{u}_\tau^k \tag{49}$$

in which the notation

$$F_{\tau,z} = \frac{\partial F_\tau}{\partial z} \tag{50}$$

has been introduced.

Secondly, finite element approximations are used to express the displacement in terms of their nodal values, via shape functions,

$$\mathbf{u}_\tau^k = N_i\mathbf{q}_{\tau i}^k \quad (i = 1,2,\ldots,N_n) \tag{51}$$

where N_n denotes the numbers of the nodes in the element while

$$\mathbf{q}_{\tau i}^k = [q_{u_x\tau i}^k \;\; q_{u_y\tau i}^k \;\; q_{u_z\tau i}^k]^{\mathrm{T}} \tag{52}$$

The base functions F_τ being independent of x and y, the strains can be written as

$$\boldsymbol{\varepsilon}_p^k = F_\tau\mathbf{D}_p(N_i\mathbf{I})\mathbf{q}_{\tau i}^k \tag{53}$$

$$\boldsymbol{\varepsilon}_n^k = F_\tau\mathbf{D}_{n\Omega}(N_i\mathbf{I})\mathbf{q}_{\tau i}^k + F_{\tau,z}N_i\mathbf{q}_{\tau i}^k \tag{54}$$

in which $\mathbf{I}$ is the identity matrix. By introducing the written strain–displacement relations (Equations (53) and (54)) along with Hooke's law (Equations (15) and (16)), the RHS of the PVD statement is

$$\begin{aligned}
\delta L^k_{\text{int}} = &\int_\Omega \delta\mathbf{q}^{k\mathrm{T}}_{\tau i}\mathbf{D}^{\mathrm{T}}_p(N_i\mathbf{I})\tilde{\mathbf{C}}^k_{pp}\left[\int_{A_k}(F_\tau F_s)\,\mathrm{d}z\right]\mathbf{D}_p(N_j\mathbf{I})\mathbf{q}^k_{sj}\,\mathrm{d}\Omega\\
&+\int_\Omega \delta\mathbf{q}^{k\mathrm{T}}_{\tau i}\mathbf{D}^{\mathrm{T}}_p(N_i\mathbf{I})\tilde{\mathbf{C}}^k_{pn}\left[\int_{A_k}(F_\tau F_s)\,\mathrm{d}z\right]\mathbf{D}_{n\Omega}(N_j\mathbf{I})\mathbf{q}^k_{sj}\,\mathrm{d}\Omega\\
&+\int_\Omega \delta\mathbf{q}^{k\mathrm{T}}_{\tau i}\mathbf{D}^{\mathrm{T}}_p(N_i\mathbf{I})\tilde{\mathbf{C}}^k_{pn}\left[\int_{A_k}(F_\tau F_{s_{,z}})\,\mathrm{d}z\right]N_j\mathbf{q}^k_{sj}\,\mathrm{d}\Omega\\
&+\int_\Omega \delta\mathbf{q}^{k\mathrm{T}}_{\tau i}\mathbf{D}^{\mathrm{T}}_{n\Omega}(N_i\mathbf{I})\tilde{\mathbf{C}}^k_{np}\left[\int_{A_k}(F_\tau F_s)\,\mathrm{d}z\right]\mathbf{D}_p(N_j\mathbf{I})\mathbf{q}^k_{sj}\,\mathrm{d}\Omega\\
&+\int_\Omega \delta\mathbf{q}^{k\mathrm{T}}_{\tau i}\mathbf{D}^{\mathrm{T}}_{n\Omega}(N_i\mathbf{I})\tilde{\mathbf{C}}^k_{nn}\left[\int_{A_k}(F_\tau F_s)\,\mathrm{d}z\right]\mathbf{D}_{n\Omega}(N_j\mathbf{I})\mathbf{q}^k_{sj}\,\mathrm{d}\Omega\\
&+\int_\Omega \delta\mathbf{q}^{k\mathrm{T}}_{\tau i}\mathbf{D}^{\mathrm{T}}_{n\Omega}(N_i\mathbf{I})\tilde{\mathbf{C}}^k_{nn}\left[\int_{A_k}(F_\tau F_{s_{,z}})\,\mathrm{d}z\right]N_j\mathbf{q}^k_{sj}\,\mathrm{d}\Omega\\
&+\int_\Omega \delta\mathbf{q}^{k\mathrm{T}}_{\tau i}N_i\tilde{\mathbf{C}}^k_{np}\left[\int_{A_k}(F_{\tau_{,z}} F_s)\,\mathrm{d}z\right]\mathbf{D}_p(N_j\mathbf{I})\mathbf{q}^k_{sj}\,\mathrm{d}\Omega\\
&+\int_\Omega \delta\mathbf{q}^{k\mathrm{T}}_{\tau i}N_i\tilde{\mathbf{C}}^k_{nn}\left[\int_{A_k}(F_{\tau_{,z}} F_s)\,\mathrm{d}z\right]\mathbf{D}_{n\Omega}(N_j\mathbf{I})\mathbf{q}^k_{sj}\,\mathrm{d}\Omega\\
&+\int_\Omega \delta\mathbf{q}^{k\mathrm{T}}_{\tau i}N_i\tilde{\mathbf{C}}^k_{nn}\left[\int_{A_k}(F_{\tau_{,z}} F_{s_{,z}})\,\mathrm{d}z\right]N_j\mathbf{q}^k_{sj}\,\mathrm{d}\Omega
\end{aligned}\tag{55}$$

Note again that subscripts τ and i have been used for the finite values of unknown variables while subscripts s and j have been introduced for their variations.

As usual in two-dimensional modellings the integration in the thickness direction can be made *a priori* by introducing the following layer integrals:

$$(\tilde{\mathbf{Z}}^{k\tau s}_{pp},\tilde{\mathbf{Z}}^{k\tau s}_{pn},\tilde{\mathbf{Z}}^{k\tau s}_{np},\tilde{\mathbf{Z}}^{k\tau s}_{nn}) = (\tilde{\mathbf{C}}^k_{pp},\tilde{\mathbf{C}}^k_{pn},\tilde{\mathbf{C}}^k_{np},\tilde{\mathbf{C}}^k_{nn})E_{\tau s}$$

$$(\tilde{\mathbf{Z}}^{k\tau s_{,z}}_{pn},\tilde{\mathbf{Z}}^{k\tau s_{,z}}_{nn},\tilde{\mathbf{Z}}^{k\tau_{,z} s}_{np},\tilde{\mathbf{Z}}^{k\tau_{,z} s}_{nn},\tilde{\mathbf{Z}}^{k\tau_{,z} s_{,z}}_{nn}) = (\tilde{\mathbf{C}}^k_{pn}E_{\tau s_{,z}},\tilde{\mathbf{C}}^k_{nn}E_{\tau s_{,z}},\tilde{\mathbf{C}}^k_{np}E_{\tau_{,z} s},\tilde{\mathbf{C}}^k_{nn}E^k_{\tau_{,z} s},\tilde{\mathbf{C}}^k_{nn}E_{\tau_{,z} s_{,z}})$$

$$(E_{\tau s},E_{\tau s_{,z}},E_{\tau_{,z} s},E_{\tau_{,z} s_{,z}}) = \int_{A_k}(F_\tau F_s,F_\tau F_{s_{,z}},F_{\tau_{,z}} F_s,F_{\tau_{,z}} F_{s_{,z}})\,\mathrm{d}z$$

Equation (55) is therefore written in the following form:

$$\delta L^k_{\text{int}} = \delta\mathbf{q}^{k\mathrm{T}}_{\tau i}\mathbf{K}^{k\tau s ij}\mathbf{q}^k_{sj}\tag{56}$$

where the following finite element matrix has been introduced:

$$\begin{aligned}\mathbf{K}^{k\tau sij} = {} & \lhd \mathbf{D}_p^{\mathrm{T}}(N_i\mathbf{I})[\tilde{\mathbf{Z}}_{pp}^{k\tau s}\mathbf{D}_p(N_j\mathbf{I}) + \tilde{\mathbf{Z}}_{pn}^{k\tau s}\mathbf{D}_{n\Omega}(N_j\mathbf{I}) + \tilde{\mathbf{Z}}_{pn}^{k\tau s,z}N_j] \\ & + \mathbf{D}_{n\Omega}^{\mathrm{T}}(N_i\mathbf{I})[\tilde{\mathbf{Z}}_{np}^{k\tau s}\mathbf{D}_p(N_j\mathbf{I}) + \tilde{\mathbf{Z}}_{nn}^{k\tau s}\mathbf{D}_{n\Omega}(N_j\mathbf{I}) + \tilde{\mathbf{Z}}_{nn}^{k\tau s,z}N_j] \\ & + N_i[\tilde{\mathbf{Z}}_{np}^{k\tau,zs}\mathbf{D}_p(N_j\mathbf{I}) + \tilde{\mathbf{Z}}_{nn}^{k\tau,zs}\mathbf{D}_{n\Omega}(N_j\mathbf{I}) + \tilde{\mathbf{Z}}_{nn}^{k\tau,zs,z}N_j]\rhd_\Omega \end{aligned} \tag{57}$$

The symbol $\lhd \ldots \rhd_\Omega$ has been introduced to denote integrals on Ω.

Note that the matrix $\mathbf{K}^{k\tau sij}$ is made by triplicate products of 3×3 arrays, so that $\mathbf{K}^{k\tau sij}$ is itself a 3×3 array. Such an array consists of the fundamental nucleus of finite element matrices related to PVD applications. The nine terms $\mathbf{K}^{k\tau sij}$ are:

$$\begin{aligned}
K_{xx}^{k\tau sij} = {} & \tilde{Z}_{pp11}^{k\tau s} \lhd N_{i,x}N_{j,x} \rhd_\Omega + \tilde{Z}_{pp16}^{k\tau s} \lhd N_{i,y}N_{j,x} \rhd_\Omega + \tilde{Z}_{pp16}^{k\tau s} \lhd N_{i,x}N_{j,y} \rhd_\Omega \\
& + \tilde{Z}_{pp66}^{k\tau s} \lhd N_{i,y}N_{j,y} \rhd_\Omega + \tilde{Z}_{nn55}^{k\tau,zs,z} \lhd N_iN_j \rhd_\Omega \\
K_{xy}^{k\tau sij} = {} & \tilde{Z}_{pp12}^{k\tau s} \lhd N_{i,x}N_{j,y} \rhd_\Omega + \tilde{Z}_{pp26}^{k\tau s} \lhd N_{i,y}N_{j,y} \rhd_\Omega + \tilde{Z}_{pp16}^{k\tau s} \lhd N_{i,x}N_{j,x} \rhd_\Omega \\
& + \tilde{Z}_{pp66}^{k\tau s} \lhd N_{i,y}N_{j,x} \rhd_\Omega + \tilde{Z}_{nn45}^{k\tau,zs,z} \lhd N_iN_j \rhd_\Omega \\
K_{xz}^{k\tau sij} = {} & \tilde{Z}_{pn13}^{k\tau s,z} \lhd N_{i,x}N_j \rhd_\Omega + \tilde{Z}_{pn36}^{k\tau s,z} \lhd N_{i,y}N_j \rhd_\Omega + \tilde{Z}_{nn55}^{k\tau,zs} \lhd N_iN_{j,x} \rhd_\Omega \\
& + \tilde{Z}_{nn45}^{k\tau,zs} \lhd N_iN_{j,y} \rhd_\Omega \\
K_{yx}^{k\tau sij} = {} & \tilde{Z}_{pp12}^{k\tau s} \lhd N_{i,y}N_{j,x} \rhd_\Omega + \tilde{Z}_{pp16}^{k\tau s} \lhd N_{i,x}N_{j,x} \rhd_\Omega + \tilde{Z}_{pp26}^{k\tau s} \lhd N_{i,y}N_{j,y} \rhd_\Omega \\
& + \tilde{Z}_{pp66}^{k\tau s} \lhd N_{i,x}N_{j,y} \rhd_\Omega + \tilde{Z}_{nn45}^{k\tau,zs,z} \lhd N_iN_j \rhd_\Omega \\
K_{yy}^{k\tau sij} = {} & \tilde{Z}_{pp22}^{k\tau s} \lhd N_{i,y}N_{j,y} \rhd_\Omega + \tilde{Z}_{pp26}^{k\tau s} \lhd N_{i,x}N_{j,y} \rhd_\Omega + \tilde{Z}_{pp26}^{k\tau s} \lhd N_{i,y}N_{j,x} \rhd_\Omega \\
& + \tilde{Z}_{pp66}^{k\tau s} \lhd N_{i,x}N_{j,x} \rhd_\Omega + \tilde{Z}_{nn44}^{k\tau,zs,z} \lhd N_iN_j \rhd_\Omega \\
K_{yz}^{k\tau sij} = {} & \tilde{Z}_{pn23}^{k\tau s,z} \lhd N_{i,y}N_j \rhd_\Omega + \tilde{Z}_{pn36}^{k\tau s,z} \lhd N_{i,x}N_j \rhd_\Omega + \tilde{Z}_{nn45}^{k\tau,zs} \lhd N_iN_{j,x} \rhd_\Omega \\
& + \tilde{Z}_{nn44}^{k\tau,zs} \lhd N_iN_{j,y} \rhd_\Omega \\
K_{zx}^{k\tau sij} = {} & \tilde{Z}_{nn55}^{k\tau s,zk} \lhd N_{i,x}N_j \rhd_\Omega + \tilde{Z}_{nn45}^{k\tau s,zk} \lhd N_{i,y}N_j \rhd_\Omega + \tilde{Z}_{np13}^{k\tau,zs} \lhd N_iN_{j,x} \rhd_\Omega \\
& + \tilde{Z}_{np36}^{k\tau,zs} \lhd N_iN_{j,y} \rhd_\Omega \\
K_{zy}^{k\tau sij} = {} & \tilde{Z}_{nn45}^{k\tau s,zk} \lhd N_{i,x}N_j \rhd_\Omega + \tilde{Z}_{nn44}^{k\tau s,zk} \lhd N_{i,y}N_j \rhd_\Omega + \tilde{Z}_{np23}^{k\tau,zs} \lhd N_iN_{j,y} \rhd_\Omega \\
& + \tilde{Z}_{np36}^{k\tau,zs} \lhd N_iN_{j,x} \rhd_\Omega \\
K_{zz}^{k\tau sij} = {} & \tilde{Z}_{nn55}^{k\tau sk} \lhd N_{i,x}N_{j,x} \rhd_\Omega + \tilde{Z}_{nn45}^{k\tau sk} \lhd N_{i,y}N_{j,x} \rhd_\Omega + \tilde{Z}_{nn45}^{k\tau sk} \lhd N_{i,x}N_{j,y} \rhd_\Omega \\
& + \tilde{Z}_{nn44}^{k\tau sk} \lhd N_{i,y}N_{j,y} \rhd_\Omega + \tilde{Z}_{nn33}^{k\tau,zs,z} \lhd N_iN_j \rhd_\Omega
\end{aligned} \tag{58}$$

By varying N and N_n, the finite element matrices of the k-layer corresponding to the implemented two-dimensional theories and number of nodes are obtained.

By introducing the external work of applied loadings, one has (see Appendix B for an example)

$$\delta \mathbf{q}_{\tau i}^{k\mathrm{T}} \mathbf{K}^{k\tau sij} \mathbf{q}_{sj}^{k} = \delta \mathbf{q}_{\tau i}^{k\mathrm{T}} \mathbf{P}_{\tau i}^{k}$$

By imposing the definition of virtual variations, PVD leads for each k-layer to the following equilibrium conditions:

$$\delta \mathbf{q}_{\tau i}^{k\mathrm{T}}: \quad \mathbf{K}^{k\tau sij} \mathbf{q}_{sj}^{k} = \mathbf{P}_{\tau i}^{k} \tag{59}$$

7.2. Assembly from layer to multilayer

In order to write the finite element matrix for the multilayered plate, for a given set of parameters N, N_n and N_l, the following steps must be implemented (global/local approaches mentioned in Section 2.2.1 should be taken into account at this stage):

1. The 3×3 fundamental nucleus of the matrix $\mathbf{K}^{k\tau sij}$ should be expanded according to the indexes τ, s and i, j. The expansion according to τ, s indexes is shown in Figure 6 (a four-noded element has been considered in this figure in conjunction to $N = 2$ expansions in z).
2. The obtained matrix must be written for each of the N_l-layers.
3. Resulting matrices are assembled from layer to multilayer level depending on the used variables descriptions.
   (a) In the case of ESLM, the variables and their variations being the same for each layer, these matrices are simply summed. That is, layer stiffness is accumulated layer by layer. Assemblage related to a three-layered plate is depicted in Figure 7.
   (b) Displacement variables are independent in each layer in the LW cases which require only continuity of displacement variables at the interface. This is formally shown in Figure 8.

8. ESL AND LW FINITE ELEMENTS DEVELOPED ON THE BASIS OF RMVT

The same steps made in the PVD case could be extended to RMVT formulated finite elements. Transverse normal stress variables along with displacement ones will now lead to four 3×3 fundamental nuclei. Three of them are related to equilibrium conditions; the other establishes compatibility conditions.

8.1. FEM matrices for the k-layer

The mixed form of Hooke's law for the k-layer is here rewritten as

$$\boldsymbol{\sigma}_{p\mathrm{H}}^{k} = \mathbf{C}_{pp}^{k} \boldsymbol{\varepsilon}_{p\mathrm{G}}^{k} + \mathbf{C}_{pn}^{k} \boldsymbol{\sigma}_{n\mathrm{M}}^{k} \tag{60}$$

$$\boldsymbol{\varepsilon}_{n\mathrm{H}}^{k} = \mathbf{C}_{np}^{k} \boldsymbol{\varepsilon}_{p\mathrm{G}}^{k} + \mathbf{C}_{nn}^{k} \boldsymbol{\sigma}_{n\mathrm{M}}^{k} \tag{61}$$

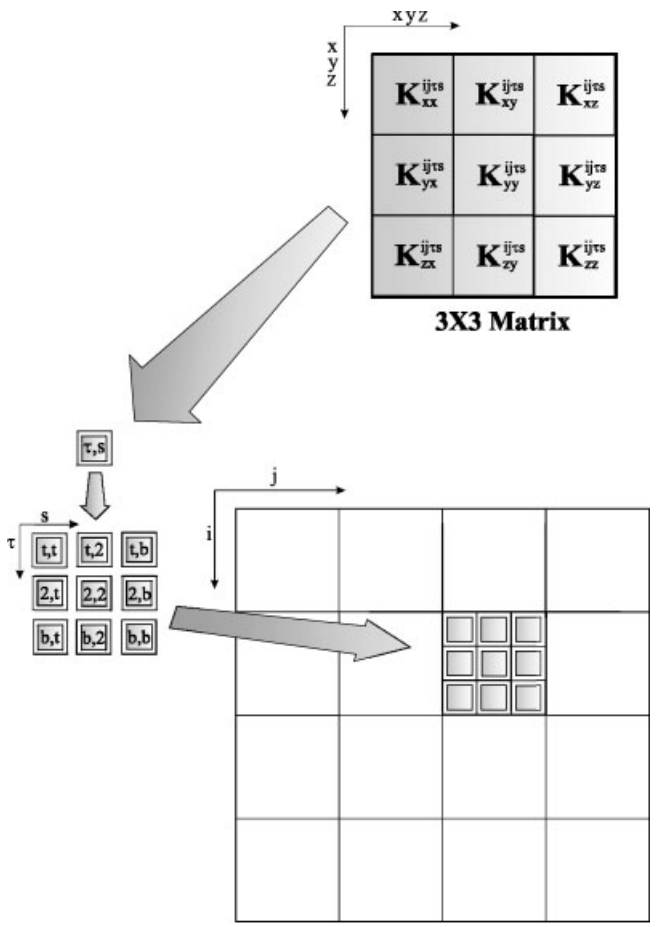

Figure 6. Expansion of the layer matrix from the correspondent 3×3 fundamental nuclei via τ and s indexes.

Transverse stress variables are expressed in terms of shape functions as done for the displacement ones,

$$\boldsymbol{\sigma}_{n\tau}^{k} = N_i \mathbf{g}_{\tau i}^{k} \quad (i = 1, 2, \ldots, N_n) \tag{62}$$

where

$$\mathbf{g}_{\tau i}^{k} = [g_{xz\tau i}^{k} \;\; g_{yz\tau i}^{k} \;\; g_{zz\tau i}^{k}]^{\mathrm{T}} \tag{63}$$

By introducing

$$\boldsymbol{\sigma}_{n\mathrm{M}}^{k} = F_\tau N_i \mathbf{g}_{\tau i}^{k} \tag{64}$$

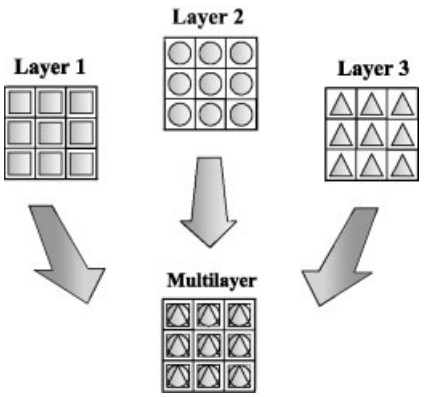

Figure 7. Assemblage from layer to multilayered level in ESLM description for a three-layered plate.

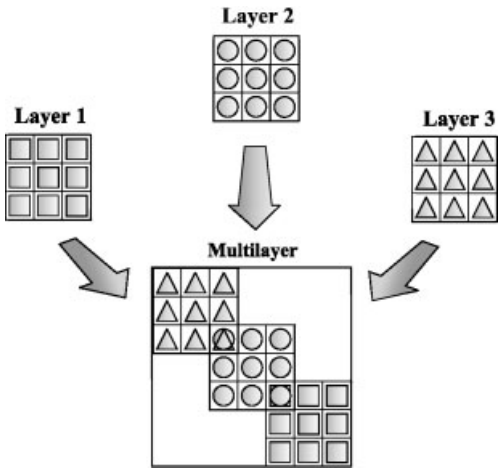

Figure 8. Assemblage from layer to multilayered level in LW description for a three-layered plate.

the left-hand side of RMVT becomes

$$\delta L_{\text{int}} = \int_v [\delta \boldsymbol{\varepsilon}_{pG}^{k\mathrm{T}} \mathbf{C}_{pp}^k \boldsymbol{\varepsilon}_{pG}^{k\mathrm{T}} + \delta \boldsymbol{\varepsilon}_{pG}^{k\mathrm{T}} \mathbf{C}_{pn}^k \boldsymbol{\sigma}_{nM}^k + \delta \boldsymbol{\varepsilon}_{nG}^{k\mathrm{T}} \boldsymbol{\sigma}_{nM}^k + \delta \boldsymbol{\sigma}_{nM}^{k\mathrm{T}} \boldsymbol{\varepsilon}_{nG}^k - \delta \boldsymbol{\sigma}_{nM}^{k\mathrm{T}} \mathbf{C}_{np}^k \boldsymbol{\varepsilon}_{pG}^{k\mathrm{T}} - \delta \boldsymbol{\sigma}_{nM}^k \mathbf{C}_{nn}^k \boldsymbol{\sigma}_{nM}^{k\mathrm{T}}] \, \mathrm{d}v \tag{65}$$

Upon substitution of (64), (53) and (54) one has

$$\begin{aligned}
\delta L_{\text{int}}^k = {} & \lhd \{\delta \mathbf{q}_{\tau i}^{k\mathrm{T}} [\mathbf{D}_p^{\mathrm{T}}(N_i \mathbf{I}) \mathbf{Z}_{pp}^{k\tau s} \mathbf{D}_p (N_j \mathbf{I})] \mathbf{q}_{sj}^k\} \rhd_\Omega + \lhd \{\delta \mathbf{q}_{\tau i}^{k\mathrm{T}} [\mathbf{D}_p^{\mathrm{T}}(N_i \mathbf{I}) \mathbf{Z}_{pn}^{k\tau s} N_j] \mathbf{g}_{sj}^k\} \rhd_\Omega \\
& + \lhd \{\delta \mathbf{q}_{\tau i}^{k\mathrm{T}} [\mathbf{D}_{n\Omega}^{\mathrm{T}}(N_i \mathbf{I}) E_{\tau s} N_j + E_{\tau_{,z} s} N_i N_j \mathbf{I}] g_{sj}^k\} \rhd_\Omega \\
& + \lhd \{\delta \mathbf{g}_{\tau i}^{k\mathrm{T}} [N_i E_{\tau s} \mathbf{D}_{n\Omega}(N_j \mathbf{I}) + E_{\tau s_{,z}} N_i N_j \mathbf{I}] q_{sj}^k\} \rhd_\Omega \\
& - \lhd \{\delta \mathbf{g}_{\tau i}^{k\mathrm{T}} [N_i \mathbf{Z}_{np}^{k\tau s} \mathbf{D}_p (N_j \mathbf{I})] \mathbf{q}_{sj}^k\} \rhd_\Omega - \lhd \{\delta \mathbf{g}_{\tau i}^{k\mathrm{T}} [N_i \mathbf{Z}_{nn}^{k\tau s} N_j] \mathbf{g}_{sj}^k\} \rhd_\Omega
\end{aligned}$$

where the following layer stiffness and compliance have been introduced:

$$(\mathbf{Z}_{pp}^{k\tau s}, \mathbf{Z}_{pn}^{k\tau s}, \mathbf{Z}_{np}^{k\tau s}, \mathbf{Z}_{nn}^{k\tau s}) = (\mathbf{C}_{pp}^{k}, \mathbf{C}_{pn}^{k}, \mathbf{C}_{np}^{k}, \mathbf{C}_{nn}^{k}) E_{\tau s}$$

so that

$$\delta L_{\text{int}}^{Rk} = \delta \mathbf{q}_{\tau i}^{k\mathrm{T}} [\mathbf{K}_{uu}^{k\tau sij} \mathbf{q}_{sj}^{k} + \mathbf{K}_{u\sigma}^{k\tau sij} \mathbf{g}_{sj}^{k}] + \delta \mathbf{g}_{\tau i}^{k\mathrm{T}} [\mathbf{K}_{\sigma u}^{k\tau sij} \mathbf{q}_{sj}^{k} + \mathbf{K}_{\sigma\sigma}^{k\tau sij} \mathbf{g}_{sj}^{k}] \tag{66}$$

where

$$\begin{aligned}
\mathbf{K}_{uu}^{k\tau sij} &= \triangleleft [\mathbf{D}_{p}^{\mathrm{T}}(N_i \mathbf{I}) \mathbf{Z}_{pp}^{k\tau s} \mathbf{D}_{p}(N_j \mathbf{I})] \triangleright_{\Omega} \\
\mathbf{K}_{u\sigma}^{k\tau sij} &= \triangleleft [\mathbf{D}_{p}^{\mathrm{T}}(N_i \mathbf{I}) \mathbf{Z}_{pn}^{k\tau s} N_j + \mathbf{D}_{n\Omega}^{\mathrm{T}}(N_i \mathbf{I}) E_{\tau s} N_j + E_{\tau_{,z} s} N_i N_j \mathbf{I}] \triangleright_{\Omega} \\
\mathbf{K}_{\sigma u}^{k\tau sij} &= \triangleleft [N_i E_{\tau s} \mathbf{D}_{n\Omega}(N_j \mathbf{I}) + E_{\tau s_{,z}} N_i N_j \mathbf{I} - N_i \mathbf{Z}_{np}^{k\tau s} \mathbf{D}_{p}(N_j \mathbf{I})] \triangleright_{\Omega} \\
\mathbf{K}_{\sigma\sigma}^{k\tau sij} &= \triangleleft [-N_i \mathbf{Z}_{nn}^{k\tau s} N_j] \triangleright_{\Omega}
\end{aligned} \tag{67}$$

By imposing the definition of virtual variations, the RMVT leads to the following equilibrium and compatibility equations:

$$\begin{aligned}
\delta \mathbf{q}_{\tau i}^{k\mathrm{T}}: &\quad \mathbf{K}_{uu}^{k\tau sij} \mathbf{q}_{sj}^{k} + \mathbf{K}_{u\sigma}^{k\tau sij} \mathbf{g}_{sj}^{k} = \mathbf{P}_{\tau i}^{k} \\
\delta \mathbf{g}_{\tau i}^{k\mathrm{T}}: &\quad \mathbf{K}_{\sigma u}^{k\tau sij} \mathbf{q}_{sj}^{k} + \mathbf{K}_{\sigma\sigma}^{k\tau sij} \mathbf{g}_{sj}^{k} = \mathbf{0}
\end{aligned} \tag{68}$$

As anticipated, four 3×3 fundamental nuclei have been obtained. In explicit form these hold:

$$\begin{aligned}
K_{uuxx}^{k\tau sij} &= Z_{pp11}^{k\tau s} \triangleleft N_{i,x} N_{j,x} \triangleright_{\Omega} + Z_{pp16}^{k\tau s} \triangleleft N_{i,y} N_{j,x} \triangleright_{\Omega} + Z_{pp16}^{k\tau s} \triangleleft N_{i,x} N_{j,y} \triangleright_{\Omega} + Z_{pp66}^{k\tau s} \triangleleft N_{i,y} N_{j,y} \triangleright_{\Omega} \\
K_{uuxy}^{k\tau sij} &= Z_{pp12}^{k\tau s} \triangleleft N_{i,x} N_{j,y} \triangleright_{\Omega} + Z_{pp26}^{k\tau s} \triangleleft N_{i,y} N_{j,y} \triangleright_{\Omega} + Z_{pp16}^{k\tau s} \triangleleft N_{i,x} N_{j,x} \triangleright_{\Omega} + Z_{pp66}^{k\tau s} \triangleleft N_{i,y} N_{j,x} \triangleright_{\Omega} \\
K_{uuxz}^{k\tau sij} &= 0 \\
K_{uuyx}^{k\tau sij} &= Z_{pp12}^{k\tau s} \triangleleft N_{i,y} N_{j,x} \triangleright_{\Omega} + Z_{pp16}^{k\tau s} \triangleleft N_{i,x} N_{j,x} \triangleright_{\Omega} + Z_{pp26}^{k\tau s} \triangleleft N_{i,y} N_{j,y} \triangleright_{\Omega} + Z_{pp66}^{k\tau s} \triangleleft N_{i,x} N_{j,y} \triangleright_{\Omega} \\
K_{uuyy}^{k\tau sij} &= Z_{pp22}^{k\tau s} \triangleleft N_{i,y} N_{j,y} \triangleright_{\Omega} + Z_{pp26}^{k\tau s} \triangleleft N_{i,x} N_{j,y} \triangleright_{\Omega} + Z_{pp26}^{k\tau s} \triangleleft N_{i,y} N_{j,x} \triangleright_{\Omega} + Z_{pp66}^{k\tau s} \triangleleft N_{i,x} N_{j,x} \triangleright_{\Omega} \\
K_{uuyz}^{k\tau sij} &= 0 \\
K_{uuzx}^{k\tau sij} &= 0 \\
K_{uuzy}^{k\tau sij} &= 0 \\
K_{uuzz}^{k\tau sij} &= 0
\end{aligned} \tag{69}$$

$$
\begin{aligned}
K^{k\tau sij}_{u\sigma xx} &= E_{\tau,zs} \lhd N_i N_j \rhd_\Omega \\
K^{k\tau sij}_{u\sigma xy} &= 0 \\
K^{k\tau sij}_{u\sigma xz} &= Z^{k\tau s}_{pn13} \lhd N_{i,x} N_j \rhd_\Omega + Z^{k\tau s}_{pn36} \lhd N_{i,y} N_j \rhd_\Omega \\
K^{k\tau sij}_{u\sigma yx} &= 0 \\
K^{k\tau sij}_{u\sigma yy} &= E_{\tau,zs} \lhd N_i N_j \rhd_\Omega \\
K^{k\tau sij}_{u\sigma yz} &= Z^{k\tau s}_{pn23} \lhd N_{i,y} N_j \rhd_\Omega + Z^{k\tau s}_{pn36} \lhd N_{i,x} N_j \rhd_\Omega \\
K^{k\tau sij}_{u\sigma zx} &= E_{\tau s} \lhd N_{i,x} N_j \rhd_\Omega \\
K^{k\tau sij}_{u\sigma zy} &= E_{\tau s} \lhd N_{i,y} N_j \rhd_\Omega \\
K^{k\tau sij}_{u\sigma zz} &= E_{\tau,zs} \lhd N_i N_j \rhd_\Omega
\end{aligned}
\tag{70}
$$

$$
\begin{aligned}
K^{k\tau sij}_{\sigma uxx} &= E_{\tau s,z} \lhd N_i N_j \rhd_\Omega \\
K^{k\tau sij}_{\sigma uxy} &= 0 \\
K^{k\tau sij}_{\sigma uxz} &= E_{\tau s} \lhd N_i N_{j,x} \rhd_\Omega \\
K^{k\tau sij}_{\sigma uyx} &= 0 \\
K^{k\tau sij}_{\sigma uyy} &= E_{\tau s,z} \lhd N_i N_j \rhd_\Omega \\
K^{k\tau sij}_{\sigma uyz} &= E_{\tau s} \lhd N_i N_{j,y} \rhd_\Omega \\
K^{k\tau sij}_{\sigma uzx} &= -Z^{k\tau s}_{np13} \lhd N_i N_{j,x} \rhd_\Omega - Z^{k\tau s}_{np36} \lhd N_i N_{j,y} \rhd_\Omega \\
K^{k\tau sij}_{\sigma uzy} &= -Z^{k\tau s}_{np23} \lhd N_i N_{j,y} \rhd_\Omega - Z^{k\tau s}_{np36} \lhd N_i N_{j,x} \rhd_\Omega \\
K^{k\tau sij}_{\sigma uzz} &= E_{\tau s,z} \lhd N_i N_j \rhd_\Omega
\end{aligned}
\tag{71}
$$

$$
\mathbf{K}^{k\tau sij}_{\sigma\sigma} = \begin{bmatrix}
-Z^{k\tau s}_{nn55} \lhd N_i N_j \rhd_\Omega & -Z^{k\tau s}_{nn45} \lhd N_i N_j \rhd_\Omega & 0 \\
-Z^{k\tau s}_{nn45} \lhd N_i N_j \rhd_\Omega & -Z^{k\tau s}_{nn44} \lhd N_i N_j \rhd_\Omega & 0 \\
0 & 0 & -Z^{k\tau s}_{nn33} \lhd N_i N_j \rhd_\Omega
\end{bmatrix}
\tag{72}
$$

As done for the PVD case, by expanding the (τ, s) as well as (i, j) couples of indices, the finite element matrix for the given k-layer is obtained.

8.2. *Assembly of matrices from layer to multilayer level*

In order to obtain multilayer matrices, the procedure already described for the PVD case must be applied. The LW case perfectly follows what is written for the PVD case.

Some difference arises because the ESL–RMVT formulation demands LW description for the stresses. In these cases, $\mathbf{K}^{k\tau sij}_{\sigma\sigma}$ follows the LW PVD case while $\mathbf{K}^{k\tau sij}_{uu}$ follows the ESL PVD case. A mixed LW and ESL assembly procedure has to be implemented for the other two matrices $\mathbf{K}^{k\tau sij}_{u\sigma}$ and $\mathbf{K}^{k\tau sij}_{\sigma u}$ This is described in Figure 9 for a three-layer case and the $\mathbf{K}^{k\tau sij}_{\sigma u}$ case (N and N_l are fixed to the values 2 and 3, respectively).

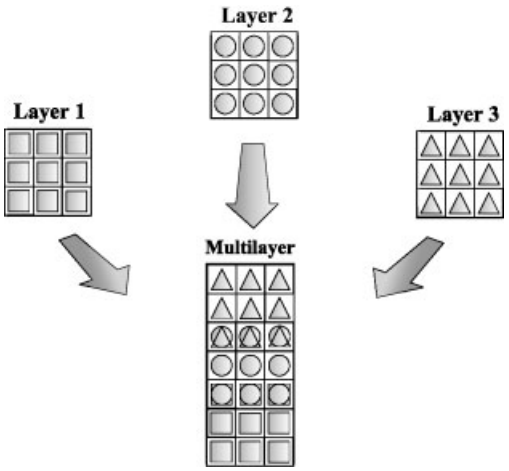

Figure 9. Assemblage from layer to multilayered level related to $K_{\sigma u}$-type matrix in the mixed case and ESLM description, for a three-layered plate.

9. TREATMENT OF STRESS VARIABLES

Mixed formulation offers several possibilities as far as the treatment of stress variables is concerned. Stress variables can be expressed in terms of the displacement ones. This can be done at layer level, multilayer level or structure level. As an alternative, stress variables can be retained and full mixed implementation is then obtained.

These methods are discussed in the following sections. For the sake of simplicity, attention has been restricted to the particular case of homogeneous boundary conditions, that is no transverse stresses are applied at any interface.

9.1. Elimination of stress variables at layer level

Let us consider a plate loaded by concentrated loadings. After expansion of (τ, s) and (i, j) indexes, the four mixed matrices

$$\mathbf{K}_{uu}^{k\tau sij}, \mathbf{K}_{u\sigma}^{k\tau sij}, \mathbf{K}_{\sigma u}^{k\tau sij}, \mathbf{K}_{\sigma\sigma}^{k\tau sij}$$

lead to corresponding layer matrices that are denoted by

$$\mathbf{K}_{uu}^{k}, \mathbf{K}_{u\sigma}^{k}, \mathbf{K}_{\sigma u}^{k}, \mathbf{K}_{\sigma\sigma}^{k}$$

RMVT can therefore be written as

$$\delta\mathbf{q}^{k\mathrm{T}}[\mathbf{K}_{uu}^{k}\mathbf{q}^{k} + \mathbf{K}_{u\sigma}^{k}\mathbf{g}^{k}] + \delta\mathbf{g}^{k\mathrm{T}}[\mathbf{K}_{\sigma u}^{k}\mathbf{q}^{k} + \mathbf{K}_{\sigma\sigma}^{k}\mathbf{g}^{k}] = \delta L_{\mathrm{est}}^{k} \tag{73}$$

This leads to, for each layer, the following set of governing equations:

$$\begin{aligned} \mathbf{K}_{uu}^{k}\mathbf{q}^{k} + \mathbf{K}_{u\sigma}^{k}\mathbf{g}^{k} &= \mathbf{P}^{k} \\ \mathbf{K}_{\sigma u}^{k}\mathbf{q}^{k} + \mathbf{K}_{\sigma\sigma}^{k}\mathbf{g}^{k} &= \mathbf{0} \end{aligned} \tag{74}$$

The second equation is then solved in terms of displacements by means of the so-called static-condensation technique. The first equation becomes

$$[\mathbf{K}_{uu}^{k} - \mathbf{K}_{u\sigma}^{k}(\mathbf{K}_{\sigma\sigma}^{k})^{-1}\mathbf{K}_{\sigma u}^{k}]\mathbf{q}^{k} = \mathbf{P}^{k} \tag{75}$$

By introducing

$$\mathbf{K}_{\text{mixed}}^{k} = [\mathbf{K}_{uu}^{k} - \mathbf{K}_{u\sigma}^{k}(\mathbf{K}_{\sigma\sigma}^{k})^{-1}\mathbf{K}_{\sigma u}^{k}] \tag{76}$$

one has

$$\mathbf{K}_{\text{mixed}}^{k}\mathbf{q}^{k} = \mathbf{P}^{k} \tag{77}$$

Such a matrix assumes the role that stiffness matrix $\mathbf{K}$ plays in PVD applications. It is to be pointed out that $\mathbf{K}^{k}$ and $\mathbf{K}_{\text{mixed}}^{k}$ consist of two completely different matrices; the differential operator in them as well as stiffness/compliances are completely different. Nevertheless, as will be demonstrated in Part 2 of this work, PVD and RMVT will lead to the same results if applied to one-layered structures (see Table IV of Part 2 [103]).

The matrix $\mathbf{K}_{\text{mixed}}^{k}$ must be assembled in a similar manner as those used for the PVD case. Loadings require to be assembled too. At the very end, for the whole multilayer one has

$$\mathbf{K}_{\text{mixed}}\mathbf{q} = \mathbf{P} \tag{78}$$

Assembly from element to structure level is made as usual in the finite element technique. At the structure level, the governing finite element system is

$$\mathbf{K}_{\text{mixed}}^{\text{S}}\mathbf{q}^{\text{S}} = \mathbf{P}^{\text{S}} \tag{79}$$

where superscript S denotes that arrays are those at the structure level.

9.2. Elimination of stress variables at element level

Let us expand the layer matrices

$$\mathbf{K}_{uu}^{k}, \mathbf{K}_{u\sigma}^{k}, \mathbf{K}_{\sigma u}^{k}, \mathbf{K}_{\sigma\sigma}^{k}$$

to multilayered element level, according to the procedure described in Section 8.2,

$$\mathbf{K}_{uu}, \mathbf{K}_{u\sigma}, \mathbf{K}_{\sigma u}, \mathbf{K}_{\sigma\sigma}$$

RMVT is then written as

$$\delta\mathbf{q}^{\text{T}}[\mathbf{K}_{uu}\mathbf{q} + \mathbf{K}_{u\sigma}\mathbf{g}] + \delta\mathbf{g}^{\text{T}}[\mathbf{K}_{\sigma u}\mathbf{q} + \mathbf{K}_{\sigma\sigma}\mathbf{g}] = \delta L_{\text{est}} \tag{80}$$

This leads to the following governing equations at element level:

$$\begin{aligned} \mathbf{K}_{uu}\mathbf{q} + \mathbf{K}_{u\sigma}\mathbf{g} &= \mathbf{P} \\ \mathbf{K}_{\sigma u}\mathbf{q} + \mathbf{K}_{\sigma\sigma}\mathbf{g} &= \mathbf{0} \end{aligned} \tag{81}$$

Static condensation is then applied at this stage,

$$[\mathbf{K}_{uu} - \mathbf{K}_{u\sigma}(\mathbf{K}_{\sigma\sigma})^{-1}\mathbf{K}_{\sigma u}]\mathbf{q} = \mathbf{P} \tag{82}$$

By introducing

$$\mathbf{K}^{\star}_{\text{mixed}} = [\mathbf{K}_{uu} - \mathbf{K}_{u\sigma}(\mathbf{K}_{\sigma\sigma})^{-1}\mathbf{K}_{\sigma u}] \tag{83}$$

one has the governing equations written in terms of only displacement variables,

$$\mathbf{K}^{\star}_{\text{mixed}}\mathbf{q} = \mathbf{P} \tag{84}$$

At structure level, one has

$$\mathbf{K}^{\star\,\text{S}}_{\text{mixed}}\mathbf{q}^{\text{S}} = \mathbf{P}^{\text{S}} \tag{85}$$

Transverse stresses are then calculated *a posteriori.*

9.3. Elimination of stress variables at structure level

Following similar steps that have been discussed above, the layer matrix is assembled at multilayered level and then at structure level,

$$\mathbf{K}^{\text{S}}_{uu}, \mathbf{K}^{\text{S}}_{u\sigma}, \mathbf{K}^{\text{S}}_{\sigma u}, \mathbf{K}^{\text{S}}_{\sigma\sigma}$$

RMVT is then written as

$$\delta\mathbf{q}^{\text{ST}}[\mathbf{K}^{\text{S}}_{uu}\mathbf{q}^{\text{S}} + \mathbf{K}^{\text{S}}_{u\sigma}\mathbf{g}^{\text{S}}] + \delta\mathbf{g}^{\text{ST}}[\mathbf{K}^{\text{S}}_{\sigma u}\mathbf{q}^{\text{S}} + \mathbf{K}^{\text{S}}_{\sigma\sigma}\mathbf{g}^{\text{S}}] = \delta L^{\text{S}}_{\text{est}} \tag{86}$$

which leads to the following governing equations:

$$\begin{aligned} \mathbf{K}^{\text{S}}_{uu}\mathbf{q}^{\text{S}} + \mathbf{K}^{\text{S}}_{u\sigma}\mathbf{g}^{\text{S}} &= \mathbf{P}^{\text{S}} \\ \mathbf{K}^{\text{S}}_{\sigma u}\mathbf{q}^{\text{S}} + \mathbf{K}^{\text{S}}_{\sigma\sigma}\mathbf{g}^{\text{S}} &= \mathbf{0} \end{aligned} \tag{87}$$

Static condensation can be applied at this stage,

$$[\mathbf{K}^{\text{S}}_{uu} - \mathbf{K}^{\text{S}}_{u\sigma}(\mathbf{K}^{\text{S}}_{\sigma\sigma})^{-1}\mathbf{K}^{\text{S}}_{\sigma u}]\mathbf{q}^{\text{S}} = \mathbf{P}^{\text{S}} \tag{88}$$

By introducing

$$\mathbf{K}^{\star\star\,\text{S}}_{\text{mixed}} = [\mathbf{K}^{\text{S}}_{uu} - \mathbf{K}^{\text{S}}_{u\sigma}(\mathbf{K}^{\text{S}}_{\sigma\sigma})^{-1}\mathbf{K}^{\text{S}}_{\sigma u}] \tag{89}$$

One has

$$\mathbf{K}^{\star\star\,\text{S}}_{\text{mixed}}\mathbf{q}^{\text{S}} = \mathbf{P}^{\text{S}} \tag{90}$$

which has only displacement variables as nodal unknowns.

9.4. Full mixed case

For the full mixed case, the governing equations with stress variables are obtained. This leads to the following system of governing equations:

$$\begin{aligned} \mathbf{K}^{\mathrm{S}}_{uu}\mathbf{q}^{\mathrm{S}} + \mathbf{K}^{\mathrm{S}}_{u\sigma}\mathbf{g}^{\mathrm{S}} &= \mathbf{P}^{\mathrm{S}} \\ \mathbf{K}^{\mathrm{S}}_{\sigma u}\mathbf{q}^{\mathrm{S}} + \mathbf{K}^{\mathrm{S}}_{\sigma\sigma}\mathbf{g}^{\mathrm{S}} &= \mathbf{0} \end{aligned} \tag{91}$$

For convenience, the following arrays are introduced:

$$\mathbf{h} = \begin{bmatrix} \mathbf{q} \\ \mathbf{g} \end{bmatrix} \tag{92}$$

$$\mathbf{P}^{f} = \begin{bmatrix} \mathbf{P} \\ \mathbf{0} \end{bmatrix} \tag{93}$$

$$\mathbf{K}_{f} = \begin{bmatrix} \mathbf{K}_{uu} & \mathbf{K}_{u\sigma} \\ \mathbf{K}_{\sigma u} & \mathbf{K}_{\sigma\sigma} \end{bmatrix} \tag{94}$$

The resulting global system of linear algebraic equations is

$$\mathbf{K}_{f}\mathbf{h} = \mathbf{P}^{f} \tag{95}$$

in which both displacement and stress variables appear as problem unknowns.

Different stress treatments would lead to different governing FE matrices and to different results. For the sake of completeness the so-called weak form of Hooke's law, established by Carrera [18], should be mentioned as a further possibility for the treatment of stress variables.

10. SUMMARY OF THE PRESENTED FINITE ELEMENTS AND CONCLUDING REMARKS

This paper has formulated multilayer finite plate elements according to the following statements:

- Two-dimensional theories that consider each layer as an independent plate (layerwise) as well as plate theories that consider all the layers as a single plate (equivalent single layer) have been considered.
- Linear and higher-order fields are considered for the two-dimensional expansion in the thickness direction. The order N of such an expansion has been taken as a free parameter of the derived formulations.
- The number of element nodes N_n has also been taken as a free parameter of the considered plate finite elements.
- Classical formulations with only displacement variables have been addressed in the framework of the principle of virtual displacements.

- Advanced formulations have been developed in the framework of Reissner's mixed variational theorem which consists of a variational tool designed for multilayered structure applications. Displacements and interlaminar continuous transverse stresses (shear and normal components) are assumed in the RMVT case.

Depending on the used variational statement (PVD or RMVT), variable descriptions (LWM or ESLM), order of the used expansion N, number of nodes N_n, a large number of multilayered plate elements have been derived. In order to lower the number of the formulas related to the different finite element matrices as much as possible, extensive use of indicial notations has been proposed in this work. Such an indicial notation, which was mainly invented for computer implementation, has permitted the authors to write all the considered FE matrices in terms of only five arrays (one for PVD and four for RMVT applications). These arrays have been called fundamental nuclei and were derived at a layer level. Each of them is of dimension 3×3. Multilayer arrays are constructed by imposing the continuity requirements for stresses and/or displacements, according to the variational statements that have been used.

Implementation of some of the derived finite elements is given in Part 2 of this work [103], where it is mainly concluded that RMVT can be considered a natural tool to analyse multilayered structures. RMVT, in fact, leads to a quasi-three-dimensional description of the stress fields of layered plates.

APPENDIX A: AN EXAMPLE SHOWING HOW THE INDICIAL NOTATION WORKS

This appendix shows how indicial notation works for a simple case. A particular plate element related to PVD applications has been chosen. These elements will be denoted by the acronym ED1 in Part 2 of this work: E for equivalent single layer, D for displacement approaches based upon PVD and 1 to signify that it consists of first-order linear expansion in z. ED1 finite element consists of one of the most popular plate elements. It is in fact the closest to the Reissner–Mindlin plate theories (ED1 cases include transverse normal strain/stress effects).

The functions used in the z-expansions are Equation (43),

$$F_b = 1, \quad F_t = z$$

The corresponding layer integrals are in this case

$$\begin{aligned}
E_{bb} &= \int_{A_k} F_t F_t \, \mathrm{d}z = \int_{A_k} \mathrm{d}z = z_{k-1} - z_k = h_k \\
E_{bt} &= \int_{A_k} F_t F_b \, \mathrm{d}z = \int_{A_k} z \, \mathrm{d}z = \frac{1}{2}(z_{k-1}^2 - z_k^2) \\
E_{tb} &= \int_{A_k} F_b F_t \, \mathrm{d}z = \int_{A_k} z \, \mathrm{d}z = \frac{1}{2}(z_{k-1}^2 - z_k^2) \\
E_{tt} &= \int_{A_k} F_b F_b \, \mathrm{d}z = \int_{A_k} z^2 \, \mathrm{d}z = \frac{1}{3}(z_{k-1}^3 - z_k^3)
\end{aligned} \tag{A1}$$

ED1 corresponds to the ESLM case of Figure 5 (left), that is stiffness terms in the correspondent fundamental nuclei are summed over k-range. In other words, layer stiffness is

accumulated from layer to multilayered level. At this stage, we can denote the accumulated multilayer stiffness by referring to notations usually used for laminate analysis [27, 31]:

$$\begin{aligned} A_{IJ} &= \sum_{k=1}^{N_l} C_{ij}^k \int_{A_k} F_b F_b \,\mathrm{d}z \;= \sum_{k=1}^{N_l} C_{ij}^k h_k \\ B_{IJ} &= \sum_{k=1}^{N_l} C_{ij}^k \int_{A_k} F_b F_t \,\mathrm{d}z \;= \sum_{k=1}^{N_l} C_{ij}^k \tfrac{1}{2}(z_{k-1}^2 - z_k^2), \quad I,J = 1,6 \\ D_{IJ} &= \sum_{k=1}^{N_l} C_{ij}^k \int_{A_k} F_t F_t \,\mathrm{d}z \;= \sum_{k=1}^{N_l} C_{ij}^k \tfrac{1}{3}(z_{k-1}^3 - z_k^3) \end{aligned} \tag{A2}$$

which correspond to well-known in-plane, coupling and bending plate stiffness.

By using these stiffnesses, the fundamental nuclei related to ED1 finite element can be expanded as far as τ and s superscripts are concerned. As a result, the finite element stiffness matrix related to i,j node is obtained. It takes the form of $(2\times 3)\times(3\times 2)$ arrays in which the terms

$$Z_{pp}^{k\tau s}, Z_{pn}^{k\tau s}, Z_{np}^{k\tau s}, Z_{nn}^{k\tau s}$$

are opportunely replaced by the plate stiffnesses

$$A_{IJ}, B_{IJ}, D_{IJ}$$

according to the following substitution:

$$\begin{aligned} Z_{pp}^{kbb}, Z_{pn}^{kbb}, Z_{np}^{kbb}, Z_{nn}^{kbb} &\rightsquigarrow A_{IJ} \\ Z_{pp}^{kbt}, Z_{pn}^{kbt}, Z_{np}^{kbt}, Z_{nn}^{kbt} &\rightsquigarrow B_{IJ} \\ Z_{pp}^{ktb}, Z_{pn}^{ktb}, Z_{np}^{ktb}, Z_{nn}^{ktb} &\rightsquigarrow B_{IJ}, \\ Z_{pp}^{ktt}, Z_{pn}^{ktt}, Z_{np}^{ktt}, Z_{nn}^{ktt} &\rightsquigarrow D_{IJ} \end{aligned} \qquad I,J = 1,6 \tag{A3}$$

The resulting 36 terms of this matrix are:

$$K_{xx}^{ttij} = \int_\Omega (D_{11}N_{i,x}N_{j,x} + D_{16}N_{i,y}N_{j,x} + D_{16}N_{i,x}N_{j,y} +; + D_{66}N_{i,y}N_{j,y} + A_{55}N_iN_j)\,\mathrm{d}\Omega$$

$$K_{xx}^{tbij} = \int_\Omega (B_{11}N_{i,x}N_{j,x} + B_{16}N_{i,y}N_{j,x} + B_{16}N_{i,x}N_{j,y} +; + B_{66}N_{i,y}N_{j,y})\,\mathrm{d}\Omega$$

$$K_{xx}^{btij} = \int_\Omega (B_{11}N_{i,x}N_{j,x} + B_{16}N_{i,y}N_{j,x} + B_{16}N_{i,x}N_{j,y} +; + B_{66}N_{i,y}N_{j,y})\,\mathrm{d}\Omega$$

$$K_{xx}^{bbij} = \int_\Omega (A_{11}N_{i,x}N_{j,x} + A_{16}N_{i,y}N_{j,x} + A_{16}N_{i,x}N_{j,y} +; + A_{66}N_{i,y}N_{j,y})\,\mathrm{d}\Omega$$

$$
\begin{aligned}
K_{xy}^{ttij} &= \int_{\Omega} (D_{12}N_{i,x}N_{j,y} + D_{26}N_{i,y}N_{j,y} + D_{16}N_{i,x}N_{j,x} + D_{66}N_{i,y}N_{j,x} + A_{45}N_iN_j)\,\mathrm{d}\Omega \\
K_{xy}^{tbij} &= \int_{\Omega} (B_{12}N_{i,x}N_{j,y} + B_{26}N_{i,y}N_{j,y} + B_{16}N_{i,x}N_{j,x} + B_{66}N_{i,y}N_{j,x})\,\mathrm{d}\Omega \\
K_{xy}^{btij} &= \int_{\Omega} (B_{12}N_{i,x}N_{j,y} + B_{26}N_{i,y}N_{j,y} + B_{16}N_{i,x}N_{j,x} + B_{66}N_{i,y}N_{j,x})\,\mathrm{d}\Omega \\
K_{xy}^{bbij} &= \int_{\Omega} (A_{12}N_{i,x}N_{j,y} + A_{26}N_{i,y}N_{j,y} + A_{16}N_{i,x}N_{j,x} + A_{66}N_{i,y}N_{j,x})\,\mathrm{d}\Omega \\
K_{xz}^{ttij} &= \int_{\Omega} (B_{13}N_{i,x}N_j + B_{36}N_{i,y}N_j + B_{55}N_iN_{j,x} + B_{45}N_iN_{j,y})\,\mathrm{d}\Omega \\
K_{xz}^{tbij} &= \int_{\Omega} (A_{55}N_iN_{j,x} + A_{45}N_iN_{j,y})\,\mathrm{d}\Omega \\
K_{xz}^{btij} &= \int_{\Omega} (B_{13}N_{i,x}N_j + B_{36}N_{i,y}N_j)\,\mathrm{d}\Omega \\
K_{xz}^{bbij} &= 0 \\
K_{yx}^{ttij} &= \int_{\Omega} (D_{12}N_{i,y}N_{j,x} + D_{16}N_{i,x}N_{j,x} + D_{26}N_{i,y}N_{j,y} + D_{66}N_{i,x}N_{j,y} + A_{45}N_iN_j)\,\mathrm{d}\Omega \\
K_{yx}^{tbij} &= \int_{\Omega} (B_{12}N_{i,y}N_{j,x} + B_{16}N_{i,x}N_{j,x} + B_{26}N_{i,y}N_{j,y} + B_{66}N_{i,x}N_{j,y})\,\mathrm{d}\Omega \\
K_{yx}^{btij} &= \int_{\Omega} (B_{12}N_{i,y}N_{j,x} + B_{16}N_{i,x}N_{j,x} + B_{26}N_{i,y}N_{j,y} + B_{66}N_{i,x}N_{j,y})\,\mathrm{d}\Omega \\
K_{yx}^{bbij} &= \int_{\Omega} (A_{12}N_{i,y}N_{j,x} + A_{16}N_{i,x}N_{j,x} + A_{26}N_{i,y}N_{j,y} + A_{66}N_{i,x}N_{j,y})\,\mathrm{d}\Omega \\
K_{yy}^{ttij} &= \int_{\Omega} (D_{22}N_{i,y}N_{j,y} + D_{26}N_{i,x}N_{j,y}D_{26}N_{i,y}N_{j,x} + D_{66}N_{i,x}N_{j,x} + A_{44}N_iN_j)\,\mathrm{d}\Omega \\
K_{yy}^{ttij} &= \int_{\Omega} (B_{22}N_{i,y}N_{j,y} + B_{26}N_{i,x}N_{j,y}B_{26}N_{i,y}N_{j,x} + B_{66}N_{i,x}N_{j,x})\,\mathrm{d}\Omega \\
K_{yy}^{ttij} &= \int_{\Omega} (B_{22}N_{i,y}N_{j,y} + B_{26}N_{i,x}N_{j,y}B_{26}N_{i,y}N_{j,x} + B_{66}N_{i,x}N_{j,x})\,\mathrm{d}\Omega \\
K_{yy}^{ttij} &= \int_{\Omega} (A_{22}N_{i,y}N_{j,y} + A_{26}N_{i,x}N_{j,y}A_{26}N_{i,y}N_{j,x} + A_{66}N_{i,x}N_{j,x})\,\mathrm{d}\Omega \\
K_{yz}^{ttij} &= \int_{\Omega} (B_{23}N_{i,y}N_j + B_{36}N_{i,x}N_j + B_{45}N_iN_{j,x} + B_{44}N_iN_{j,y})\,\mathrm{d}\Omega \\
K_{yz}^{tbij} &= \int_{\Omega} (B_{23}N_{i,y}N_j + B_{36}N_{i,x}N_j)\,\mathrm{d}\Omega \\
K_{yz}^{btij} &= \int_{\Omega} (B_{45}N_iN_{j,x} + B_{44}N_iN_{j,y})\,\mathrm{d}\Omega \\
K_{yz}^{bbij} &= 0
\end{aligned}
\tag{A4}
\tag{A5}
$$

$$
\begin{aligned}
K_{zx}^{ttij} &= \int_{\Omega} (B_{55}N_{i,x}N_j + B_{45}N_{i,y}N_j + B_{13}N_iN_{j,x} + B_{36}N_iN_{j,y})\,\mathrm{d}\Omega \\
K_{zx}^{ttij} &= \int_{\Omega} (B_{55}N_{i,x}N_j + B_{45}N_{i,y}N_j)\,\mathrm{d}\Omega \\
K_{zx}^{ttij} &= \int_{\Omega} (B_{13}N_iN_{j,x} + B_{36}N_iN_{j,y})\,\mathrm{d}\Omega \\
K_{zx}^{ttij} &= 0 \\
K_{zy}^{ttij} &= \int_{\Omega} (B_{45}N_{i,x}N_j + B_{44}N_{i,y}N_j + B_{23}N_iN_{j,y} + Z_{36}N_iN_{j,x})\,\mathrm{d}\Omega \\
K_{zy}^{ttij} &= \int_{\Omega} (B_{45}N_{i,x}N_j + B_{44}N_{i,y}N_j)\,\mathrm{d}\Omega \\
K_{zy}^{ttij} &= \int_{\Omega} (+B_{23}N_iN_{j,y} + Z_{36}N_iN_{j,x})\,\mathrm{d}\Omega \\
K_{zy}^{ttij} &= 0 \\
K_{zz}^{\tau sij} &= \int_{\Omega} (D_{55}N_{i,x}N_{j,x} + D_{45}N_{i,y}N_{j,x} + D_{45}N_{i,x}N_{j,y} + D_{44}N_{i,y}N_{j,y} + A_{33}N_iN_j)\,\mathrm{d}\Omega \\
K_{zz}^{\tau sij} &= \int_{\Omega} (B_{55}N_{i,x}N_{j,x} + B_{45}N_{i,y}N_{j,x} + B_{45}N_{i,x}N_{j,y} + B_{44}N_{i,y}N_{j,y})\,\mathrm{d}\Omega \\
K_{zz}^{\tau sij} &= \int_{\Omega} (B_{55}N_{i,x}N_{j,x} + B_{45}N_{i,y}N_{j,x} + B_{45}N_{i,x}N_{j,y} + B_{44}N_{i,y}N_{j,y})\,\mathrm{d}\Omega \\
K_{zz}^{\tau sij} &= \int_{\Omega} (A_{55}N_{i,x}N_{j,x} + A_{45}N_{i,y}N_{j,x}A_{45}N_{i,x}N_{j,y} + A_{44}N_{i,y}N_{j,y})\,\mathrm{d}\Omega
\end{aligned}
\tag{A6}
$$

The integral on Ω has been explicitly written. Note that it is a multilayered level matrix. By varying the superscripts i, j over the element node N_n the full $6N_n \times 6N_n$ matrix is obtained.

The written explicit expression of stiffness matrix will never be used in computer implementations. In fact, these implementations will build stiffness matrices by making appropriate loops around the five derived fundamental nuclei (see Part 2).

APPENDIX B: APPLIED LOADING VECTORS

The technique employed to derive finite element stiffness/compliance matrices can be applied to derive consistent loading arrays. An example is given in this appendix, which deals with a distribution of pressure acting on the k-layer and applied on a plane parallel to the reference surface Ω which is distant $\zeta^k = \zeta_1^k$. The external work made by these pressure distributions is

$$
\delta L_P^k = \int_{\Omega_1} \delta \mathbf{u}^{k\mathrm{T}}(x, y, \zeta_1^k)\mathbf{P}^k(x, y, \zeta_1^k)\,\mathrm{d}\Omega_1 \tag{B1}
$$

where Ω_1 is the domain on which the pressure acts and $\mathbf{P}^k(x, y, \zeta_1^k)$ is the array which denotes the pressure.

Since $\Omega_1 = \Omega$ for plates, Equation (B1) becomes

$$\delta L_P^k = \delta \mathbf{q}_{\tau i}^{k\mathrm{T}} \; F_\tau^1 \; F_s^1 \; {}_i N_j \mathbf{p}_s^k \triangleright_\Omega \mathbf{a}_{sj}^k \tag{B2}$$

In case more pressure loadings are applied corresponding to more than one plane, the related terms must be summed. In formula

$$\delta L_P^k = \delta \mathbf{q}_{\tau i}^{k\mathrm{T}} \; F_\tau^m \; F_s^m \triangleleft N_i N_j \mathbf{p}_s^k \triangleright_\Omega \mathbf{a}_{sj}^k, \quad m = t, r, b, \quad r = 2, 3, \ldots, N \tag{B3}$$

At least top and bottom layer surface pressure are included in the previous equation. By introducing

$$\mathbf{D}^{k\tau sij} = F_\tau^m \; F_s^m \triangleleft N_i N_j \mathbf{p}_s^k \triangleright_\Omega \tag{B4}$$

one has

$$\delta L_P^k = \delta \mathbf{q}_{\tau i}^{k\mathrm{T}} \; \mathbf{D}^{k\tau sij} \mathbf{a}_{sj}^k \tag{B5}$$

$\mathbf{D}^{k\tau sij}$ plays the role of fundamental nucleus. In explicit form, it holds that

$$\mathbf{D}^{k\tau sij} = F_\tau^m \; F_s^m \begin{bmatrix} \triangleleft N_i N_j \, p_{xs}^k \triangleright_\Omega & 0 & 0 \\ 0 & \triangleleft N_i N_j \, p_{ys}^k \triangleright_\Omega & 0 \\ 0 & 0 & \triangleleft N_i N_j \, p_{zs}^k \triangleright_\Omega \end{bmatrix} \tag{B6}$$

At the very end, one notices that by introducing

$$\mathbf{P}_{\tau i}^{k\mathrm{eq}} = \mathbf{D}^{k\tau sij} \mathbf{a}_{sj}^k \tag{B7}$$

Equation (B5) becomes

$$\delta L_P^k = \delta \mathbf{q}_{\tau i}^{k\mathrm{T}} \mathbf{P}_{\tau i}^{k\mathrm{eq}} \tag{B8}$$

The array $\mathbf{P}_{\tau i}^{k\mathrm{eq}}$ therefore assumes the meaning of the loading array variationally equivalent to the applied pressure.

APPENDIX C: IDENTIFICATION OF TERMS RELATED TO TRANSVERSE STRESSES AND STRAINS

Owing to numerical reasons, such as shear locking mechanisms [108], it is essential to distinguish stiffness/compliance terms related to different transverse stress components. These terms are, in fact, treated with different numerical integration schemes in the companion paper (Part 2), where numerical evaluations are given.

C.1. PVD cases

The Hooke's law matrix can be conveniently arranged in the following form:

$$\boldsymbol{\sigma}^k = (\tilde{\mathbf{C}}^{kp} + \tilde{\mathbf{C}}^{k\ddagger} + \tilde{\mathbf{C}}^{k\dagger}) \boldsymbol{\varepsilon}^k \tag{C1}$$

By splitting in-plane and out-of-plane contribution, one has

$$\boldsymbol{\sigma}_p^k = \tilde{\mathbf{C}}_{pp}^k \boldsymbol{\varepsilon}_p^k + \tilde{\mathbf{C}}_{pn}^k \boldsymbol{\varepsilon}_n^k \tag{C2}$$

$$\boldsymbol{\sigma}_n^k = \delta_\dagger \tilde{\mathbf{C}}_{np}^k \boldsymbol{\varepsilon}_p^k + (\delta_\ddagger \tilde{\mathbf{C}}_{nn}^{k\ddagger} + \delta_\dagger \tilde{\mathbf{C}}_{nn}^{k\dagger}) \boldsymbol{\varepsilon}_n^k \tag{C3}$$

where

$$\tilde{\mathbf{C}}_{nn}^{k\ddagger} = \begin{bmatrix} \tilde{C}_{55}^k & \tilde{C}_{45}^k & 0 \\ \tilde{C}_{45}^k & \tilde{C}_{44}^k & 0 \\ 0 & 0 & 0 \end{bmatrix}, \quad \tilde{\mathbf{C}}_{nn}^{k\dagger} = \begin{bmatrix} 0 & 0 & 0 \\ 0 & 0 & 0 \\ 0 & 0 & \tilde{C}_{33}^k \end{bmatrix}$$

For our convenience, the symbols $\delta_\dagger$ $\delta_\ddagger$ have been introduced. Such symbols permit one to evaluate in a different manner shear and normal components.

In order to outline transverse strain contribution ε_{zz}^k, geometrical relations are then written in the following form:

$$\boldsymbol{\varepsilon}_p^k = F_\tau \mathbf{D}_p (N_i \mathbf{I}) \mathbf{q}_{\tau i}^k \tag{C4}$$

$$\boldsymbol{\varepsilon}_n^k = F_\tau \mathbf{D}_{n\Omega} (N_i \mathbf{I}) \mathbf{q}_{\tau i}^k + F_{\tau_{,z}} (N_i \mathbf{I}_\delta) \mathbf{q}_{\tau i}^k \tag{C5}$$

where

$$\mathbf{I}_\delta = \begin{bmatrix} 1 & 0 & 0 \\ 0 & 1 & 0 \\ 0 & 0 & \delta \end{bmatrix} \tag{C6}$$

ε_{zz}^k is therefore written as

$$\varepsilon_{zz}^k = F_{\tau_{,z}} \delta (N_i q_{u_z \tau i}^k) \tag{C7}$$

$\varepsilon_{zz}^k = 0$ is simply obtained by forcing $\delta = 0$.

The stiffness matrix can be written as

$$\begin{aligned} \mathbf{K}^{k\tau sij} = {} & \lhd \mathbf{D}_p^{\mathrm{T}} (N_i \mathbf{I}) [\tilde{\mathbf{Z}}_{pp}^{k\tau s} \mathbf{D}_p (N_j \mathbf{I}) + \tilde{\mathbf{Z}}_{pn}^{k\tau s} \mathbf{D}_{n\Omega} (N_j \mathbf{I}) + \tilde{\mathbf{Z}}_{pn}^{k\tau s_{,z}} (N_j \mathbf{I}_\delta)] \\ & + \mathbf{D}_{n\Omega}^{\mathrm{T}} (N_i \mathbf{I}) [\delta_\dagger \tilde{\mathbf{Z}}_{np}^{k\tau s} \mathbf{D}_p (N_j \mathbf{I}) + (\delta_\ddagger \tilde{\mathbf{Z}}_{nn}^{k\ddagger\tau s} + \delta_\dagger \tilde{\mathbf{Z}}_{nn}^{k\dagger\tau s}) \mathbf{D}_{n\Omega} (N_j \mathbf{I}) \\ & + (\delta_\ddagger \tilde{\mathbf{Z}}_{nn}^{k\ddagger\tau s_{,z}} + \delta_\dagger \tilde{\mathbf{Z}}_{nn}^{k\dagger\tau s_{,z}}) (N_j \mathbf{I}_\delta)] + (N_i \mathbf{I}_\delta) [\delta_\dagger \tilde{\mathbf{Z}}_{np}^{k\tau_{,z} s} \mathbf{D}_p (N_j \mathbf{I}) \\ & + (\delta_\ddagger \tilde{\mathbf{Z}}_{nn}^{k\ddagger\tau_{,z} s} + \delta_\dagger \tilde{\mathbf{Z}}_{nn}^{k\dagger\tau_{,z} s}) \mathbf{D}_{n\Omega} (N_j \mathbf{I}) + (\delta_\ddagger \tilde{\mathbf{Z}}_{nn}^{k\ddagger\tau_{,z} s_{,z}} + \delta_\dagger \tilde{\mathbf{Z}}_{nn}^{k\dagger\tau_{,z} s_{,z}}) (N_j \mathbf{I}_\delta)] \rhd_\Omega \end{aligned} \tag{C8}$$

where

$$(\tilde{\mathbf{Z}}_{nn}^{k\ddagger\tau s}, \tilde{\mathbf{Z}}_{nn}^{k\dagger\tau s}) = (\tilde{\mathbf{C}}_{nn}^{k\ddagger} E_{\tau s}, \tilde{\mathbf{C}}_{nn}^{k\dagger} E_{\tau s})$$

$$(\tilde{\mathbf{Z}}_{nn}^{k\ddagger\tau s_{,z}}, \tilde{\mathbf{Z}}_{nn}^{k\ddagger\tau_{,z}s}, \tilde{\mathbf{Z}}_{nn}^{k\ddagger\tau_{,z}s_{,z}}) = (\tilde{\mathbf{C}}_{nn}^{k\ddagger}E_{\tau s_{,z}}, \tilde{\mathbf{C}}_{nn}^{k\ddagger}E_{\tau_{,z}s}^{k}, \tilde{\mathbf{C}}_{nn}^{k\ddagger}E_{\tau_{,z}s_{,z}})$$

$$(\tilde{\mathbf{Z}}_{nn}^{k\dagger\tau s_{,z}}, \tilde{\mathbf{Z}}_{nn}^{k\dagger\tau_{,z}s}, \tilde{\mathbf{Z}}_{nn}^{k\dagger\tau_{,z}s_{,z}}) = (\tilde{\mathbf{C}}_{nn}^{k\dagger}E_{\tau s_{,z}}, \tilde{\mathbf{C}}_{nn}^{k\dagger}E_{\tau_{,z}s}^{k}, \tilde{\mathbf{C}}_{nn}^{k\dagger}E_{\tau_{,z}s_{,z}})$$

As far as the reduced/selective integration technique is concerned, it is intended that:

- Normal integration denoted by the IN scheme (see Part 2) signifies that all the terms are fully integrative (full integration by using 3×3 and 2×2 Gaussian points for eight- or nine- and four-noded plates, respectively).
- Selective integration denoted by the IS scheme signifies that terms that have been put in a single rectangle must be calculated by reduced integration (it is intended that the reduced integration scheme is obtained by the full one by reducing the grid of one unity).
- Selective integration denoted by the IS2 scheme signifies that both terms that have been put in single and double rectangles must be calculated according to reduced integration.

C.2. RMVT cases

Following what was done above, $\sigma_{xz}^{k}, \sigma_{yz}^{k}; \sigma_{zz}^{k}$ (the fundamental array related to RMVT applications) are obtained in the following forms:

$$\begin{aligned}
\mathbf{K}_{uu}^{k\tau sij} &= \lhd [\mathbf{D}_{p}^{\mathrm{T}}(N_i\mathbf{I})\mathbf{Z}_{pp}^{k\tau s}\mathbf{D}_{p}(N_j\mathbf{I})]\rhd_{\Omega} \\
\mathbf{K}_{u\sigma}^{k\tau sij} &= \lhd [\mathbf{D}_{p}^{\mathrm{T}}(N_i\mathbf{I}_z)\mathbf{Z}_{pn}^{k\tau s}N_j + \mathbf{D}_{n\Omega}^{\mathrm{T}}(N_i\mathbf{I}_z)E_{\tau s}N_j + E_{\tau_{,z}s}N_iN_j\mathbf{I}_z\mathbf{I}_{\delta}]\rhd_{\Omega} \\
\mathbf{K}_{\sigma u}^{k\tau sij} &= \lhd [N_iE_{\tau s}\mathbf{D}_{n\Omega}(N_j\mathbf{I}_z) + E_{\tau s_{,z}}N_iN_j\mathbf{I}_z\mathbf{I}_{\delta} - N_i\mathbf{Z}_{np}^{k\tau s}\mathbf{D}_{p}(N_j\mathbf{I}_z)]\rhd_{\Omega} \\
\mathbf{K}_{\sigma\sigma}^{k\tau sij} &= \lhd [-(N_i\mathbf{I}_z)\mathbf{Z}_{nn}^{k\tau s}(N_j\mathbf{I}_z)]\rhd_{\Omega}
\end{aligned} \tag{C9}$$

where

$$\mathbf{I}_z = \begin{bmatrix} \delta_T & 0 & 0 \\ 0 & \delta_T & 0 \\ 0 & 0 & \delta_z \end{bmatrix}, \quad \mathbf{I}_{\delta} = \begin{bmatrix} 1 & 0 & 0 \\ 0 & 1 & 0 \\ 0 & 0 & \delta \end{bmatrix} \tag{C10}$$

Note that $\mathbf{K}_{uu}^{k\tau sij}$ is not influenced by $\sigma_{xz}^{k}, \sigma_{yz}^{k}; \sigma_{zz}^{k}$.

REFERENCES

1. Pagano NJ. Stress fields in composite laminates. *International Journal of Solids and Structures* 1978; **14**: 385–400.
2. Pagano NJ. Exact solutions for composite laminates in cylindrical bending. *Journal of Composite Materials* 1969; **3**:398–411.
3. Pagano NJ. Exact solutions for rectangular bi-direction composites and sandwich plates. *Journal of Composite Materials* 1970; **4**:20–34.
4. Pagano NJ, Hatfield SJ. Elastic behavior of multilayered bidirectional composites. *American Institute of Aeronautics and Astronautics Journal* 1972; **10**:931–933.
5. Vel SS, Batra RC. Analytical solution for rectangular thick plates subjected to arbitrary boundary conditions. *American Institute of Aeronautics and Astronautics Journal* 1999; **37**:1464–1473.
6. Vel SS, Batra RC. A generalized plane strain deformation of thick anisotropic composite laminates plates. *International Journal of Solids and Structures* 2000; **37**:715–733.

7. Whitney JM. The effects of transverse shear deformation on the bending of laminated plates. *Journal of Composite Materials* 1969; **3**:534–547.
8. Noor AK, Burton WS. Stress and free vibration analyses of multilayered composite plates. *Composite Structures* 1989; **11**:183–204.
9. Noor AK, Burton WS. Assessment of shear deformation theories for multilayered composite plates. *Applied Mechanics Review* 1989; **41**:1–18.
10. Noor AK, Burton WS, Peters JM. Predictor corrector procedures for stress and free vibration analysis of multilayered composite plates and shells. *Computer Methods in Applied Mechanics and Engineering* 1990; **82**:341–363.
11. Malik M. Differential quadrature method in computational mechanics: new development and applications. *Ph.D. Dissertation*, University of Oklahoma, Oklahoma, 1994.
12. Malik M, Bert CW. Differential quadrature analysis of free vibration of symmetric cross-ply laminates with shear deformation and rotatory inertia. *Shock and Vibration* 1995; **2**:321–338.
13. Teo TM, Liew KM. Three-dimensional elasticity solutions to some orthotropic plate problems. *International Journal of Solids and Structures* 1999; **36**:5301–5326.
14. Davì G. A general boundary integral formulation for numerical solutions of bended multilayer sandwich plates. *Proceedings of the 11th International Conference on Boundary Element Method* 1989; **1**:23–35.
15. Davì G. Stress field in general composite laminates. *American Institute of Aeronautics and Astronautics Journal* 1996; **34**:2604–2608.
16. Davì G, Milazzo A. Bending stress fields in composite laminate beams by a boundary integral formulation. *Composite Structures* 1999; **71**:267–276.
17. Milazzo A. Interlaminar stress in laminated composite beam-type structures under shear/bending. *American Institute of Aeronautics and Astronautics Journal* 2000; **38**:687–694.
18. Carrera E. A class of two-dimensional theories for anisotropic multilayered plates analysis. *Accademia delle Scienze di Torino*, Memorie Scienze Fisiche, 19–20 (1995–1996); 1–39.
19. Carrera E. Mixed layer-wise models for multilayered plates analysis. *Composite Structures* 1998; **43**:57–70.
20. Carrera E. Evaluation of layer-wise mixed theories for laminated plates analysis. *American Institute of Aeronautics and Astronautics Journal* 1998; **26**:830–839.
21. Carrera E. Layer-wise mixed models for accurate vibration analysis of multilayered plates. *Journal of Applied Mechanics* 1998; **65**:820–828.
22. Librescu L, Reddy JN. A critical review and generalization of transverse shear deformable anisotropic plates. *Euromech Colloquium 219*, Kassel, September 1986; *Refined Dynamical Theories of Beams, Plates and Shells and their Applications*. Elishakoff, Irretier (eds). Springer: Berlin, 1987; 32–43.
23. Kapania RK, Raciti S. Recent advances in analysis of laminated beams and plates. *American Institute of Aeronautics and Astronautics Journal* 1989; **27**:923–946.
24. Reddy JN, Robbins DH. Theories and computational models for composite laminates. *Applied Mechanics Review* 1994; **47**:147–165.
25. Noor AK, Burton S, Bert CW. Computational model for sandwich panels and shells. *Applied Mechanics Review* 1996; **49**:155–199.
26. Librescu L. *Elasto-statics and Kinetics of Anisotropic and Heterogeneous Shell-Type Structures*. Noordhoff Int.: Leyden, Netherlands, 1975.
27. Reddy JN. *Mechanics of Laminated Composite Plates. Theory and Analysis.* CRC Press: Boca Raton FL, 1997.
28. Cauchy AL. Sur l'equilibre et le mouvement d'une plaque solide. *Exercises de Matematique* 1828; **3**:328–355.
29. Poisson SD. Memoire sur l'equilibre et le mouvement des corps elastique. *Memoires de l'Academie des Sciences* 1829; **8**:357.
30. Kirchhoff G. Über das Gleichgewicht und die Bewegung einer elastishen Scheibe. *Zeitscheift fuer Angewandte Mathematik* 1850; **40**:51–88.
31. Jones RM. *Mechanics of Composite Materials*. McGraw-Hill: New York, 1975.
32. Koiter WT. A consistent first approximations in the general theory of thin elastic shells, *Proceedings of Symposium on the Theory of Thin Elastic Shells*, August 1959, North-Holland: Amsterdam, 1959; 12–23.
33. Reissner E. The effect of transverse shear deformation on the bending of elastic plates. *Journal of Applied Mechanics* 1945; **12**:69–76.
34. Mindlin. Influence of rotatory inertia and shear in flexural motions of isotropic elastic plates. *Journal of Applied Mechanics* 1951; **18**:1031–1036.
35. Yang PC, Norris CH, Stavsky Y. Elastic Wave propagation in heterogenous plates. *International Journal of Solids and Structures* 1966; **2**:665–684.
36. Hildebrand FB, Reissner E, Thomas GB. Notes on the foundations of the theory of small displacements of orthotropic shells. *NACA TN*-1833, Washington, DC, 1938.
37. Sun CT, Whitney JM. On the theories for the dynamic response of laminated plates. *American Institute of Aeronautics and Astronautics Journal* 1973; **11**:372–398.

38. Lo KH, Christensen RM, Wu EM. A higher-order theory of plate deformation, Part 2: laminated plates. *Journal of Applied Mechanics* 1977; **44**:669–676.
39. Carrera E. C_z^0 requirements—models for the two-dimensional analysis of multilayered structures. *Composite Structures* 1997; **37**:373–384.
40. Vlasov BF. On the equations of bending of plates. *Doklady Akademii Nauk Azerbeidzhanskoi SSR* 1957; **3**:955–979.
41. Reddy JN. *Energy and Variational Methods in Applied Mechanics.* Wiley: NY, 1984.
42. Reddy JN. A simple higher order theories for laminated composites plates. *Journal of Applied Mechanics* 1984; **52**:745–742.
43. Reddy JN, Phan ND. Stability and vibration of isotropic, orthotropic, and laminated plates according to a higher order shear deformation theory. *Journal of Sound and Vibration* 1985; **98**:157–170.
44. Srinivas S. A refined analysis of composite laminates. *Journal of Sound and Vibration* 1973; **30**:495–507.
45. Cho KN, Bert CW, Striz AG. Free vibrations of laminated rectangular plates analyzed by higher order individual-layer theory. *Journal of Sound and Vibration* 1991; **145**:429–442.
46. Nosier A, Kapania RK, Reddy JN. Free vibration analysis of laminated plates using a layer-wise theory. *American Institute of Aeronautics and Astronautics Journal* 1993; **31**:2335–2346.
47. Lekhnitskii SG. Strength calculation of composite beams. *Vestnik inzhen. i tekhnikov* 1935; (9).
48. Lekhnitskii SG. *Anisotropic Plates*. 2nd edn. Translated from the 2nd Russian edn, Tsai SW, Cheron (eds). Gordon and Breach: New York, 1968.
49. Ambartsumian SA. *Theory of Anisotropic Plates.* Translated from Russian by T. Cheron and Edited by J.E. Ashton Tech. Pub. Co., 1969.
50. Ren JG. A new theory for laminated plates. *Composite Science and Technology* 1986; **26**:225–239.
51. Ren JG, Owen DRJ. Vibration and buckling of laminated plates. *International Journal of Solids and Structures* 1989; **25**:95–106.
52. Rath BK, Das YC. Vibration of layered shells. *Journal of Sound and Vibration* 1973; **28**:737–757.
53. Atluri SN, Tong P, Murakawa H. Recent studies in hybrid and mixed finite element methods in mechanics. In *Hybrid and Mixed Finite Element Methods*. Atluri SN, Callagher RH, Zienkiewicz O (eds). Wiley: New York, 1983; 51–71.
54. Murakami H. A laminated beam theory with interlayer slip. *Journal of Applied Mechanics* 1984; **51**:551–559.
55. Murakami H. Laminated composite plate theory with improved in-plane responses. *ASME Proceedings of PVP Conference*, New Orleans, June 24–26, PVP-Vol. 98-2, 1985; 257–263.
56. Murakami H. Laminated composite plate theory with improved in-plane responses. *Journal of Applied Mechanics* 1986; **53**:661–666.
57. Toledano A, Murakami H. A high-order laminated plate theory with improved in-plane responses. *International Journal of Solids and Structures* 1987; **23**:111–131.
58. Toledano A, Murakami H. A composite plate theory for arbitrary laminate configurations. *Journal of Applied Mechanics* 1987; **54**:181–189.
59. Carrera E. A refined multilayered finite element model applied to linear and nonlinear analysis of sandwich structures. *Composite Science and Technology* 1998; **58**:1553–1569.
60. Carrera E. Transverse normal stress effects in multilayered plates. *Journal of Applied Mechanics* 1999; **66**: 1004–1012.
61. Carrera E. A study of transverse normal stress effects on vibration of multilayered plates and shells. *Journal of Sound and Vibration* 1999; **225**:803–829.
62. Carrera E. Single-layer vs. multi-layers plate modelings on the basis of Reissner's mixed theorem. *American Institute of Aeronautics and Astronautics Journal* 2000; **38**:342–343.
63. Carrera E. *A priori* vs *a posteriori* evaluation of transverse stresses in multilayered orthotropic plates. *Composite Structures* 2000; **48**:245–260.
64. Carrera E. An assessment of mixed and classical theories for thermal stress analysis of orthotropic plates. *Journal of Thermal Stress* 2000; **23**:797–831.
65. Carrera E. Developments, ideas and evaluations based upon the Reissner's mixed theorem in the modeling of multilayered plates and shells. *Applied Mechanics Review* 2001; **54**:301–329.
66. Pryor CW, Barker RM. A finite element analysis including transverse shear effect for applications to laminated plates. *American Institute of Aeronautics and Astronautics Journal* 1971; **9**:912–917.
67. Noor AK. Finite element analysis of anisotropic plates. *American Institute of Aeronautics and Astronautics Journal* 1972; **11**:289–307.
68. Noor AK, Mathers MD. Finite element analysis of anisotropic plates. *International Journal for Numerical Methods in Engineering* 1977; **11**:289–370.
69. Panda SC, Natarayan R. Finite element analysis of laminated composite plates. *International Journal for Numerical Methods in Engineering* 1979; **14**:69–79.
70. Reddy JN. A penalty plate-bending element for the analysis of laminated anisotropic composites plates. *International Journal for Numerical Methods in Engineering* 1980; **12**:1187–1206.

71. Kant T, Kommineni JR. Large amplitude free vibration analysis of cross-ply composite and sandwich laminates with a refined theory and C^0 finite elements. *Computers and Structures* 1989; **50**:123–134.
72. Kant T, Owen DRJ, Zienkiewicz OC. Refined higher order C^0 plate bending element. *Computers and Structures* 1982; **15**:177–183.
73. Bathe KJ, Dvorkin EN. A four node plate bending element based on Mindlin/Reissner plate theory and mixed interpolation. *International Journal for Numerical Methods in Engineering* 1985; **21**:367–383.
74. Brank B, Carrera E. Multilayered shell finite element with interlaminar continuous shear stresses: a refinement of the Reissner–Mindlin formulation. *International Journal for Numerical Methods in Engineering* 2000; **48**:843–874
75. Pandya BN, Kant T. Higher-order shear deformable for flexural of sandwich plates. Finite element evaluations. *International Journal of Solids and Structures* 1988; **24**:1267–1286.
76. Reddy JN. On computational models for composite laminate. *International Journal for Numerical Methods in Engineering* 1989; **27**:361–382.
77. Barboni R, Gaudenzi P. A class of C^0 finite elements for the static and dynamic analysis of laminated plates. *Computers and Structures* 1992; **44**:1169–1178.
78. Cho M, Parmerter RR. Efficient higher order composite plate theory for general lamination configurations. *American Institute of Aeronautics and Astronautics Journal* 1993; **31**:1299–1305.
79. Aitharaju VR, Averill RC. C^0 zig-zag kinematic displacement models for the analysis of laminated composites. *Mechanics of Composite Materials and Structures* 1996; **6**:31–56.
80. Idlbi A, Karama M, Touratier M. Comparison of various laminated plate theories. *Composite Structures* 1997; **37**:173–184.
81. Cho YB, Averill RC. First order zig-zag sublaminate plate theory and finite element model for laminated composite and sandwich panels. *Computers and Structures* 2000; **50**:1–15.
82. Polit O, Touratier M. Higher order triangular sandwich plate finite elements for linear and nonlinear analyses. *Computer Methods in Applied Mechanics and Engineering* 2000; **185**:305–324.
83. Pinsky PM, Kim KK. A multi-director formulation for elastic-viscoelastic layered shells. *International Journal for Numerical Methods in Engineering* 1986; **23**:2213–2224.
84. Reddy JN. An evaluation of equivalent single layer and layer-wise theories of composite laminates. *Composite Structures* 1993; **25**:21–35.
85. Robbins DH Jr, Reddy JN. Modeling of thick composites using a layer-wise theory. *International Journal for Numerical Methods in Engineering* 1993; **36**:655–677.
86. Gaudenzi P, Barboni R, Mannini A. A finite element evaluation of single-layer and multi-layer theories for the analysis of laminated plates. *Computers and Structures* 1995; **30**:427–440.
87. Botello S, Onate E, Canet JM. A layer-wise triangle for analysis of laminated composite plates and shells. *Computers and Structures* 1999; **70**:635–646.
88. Babuska I, Szabo, Actis. Hierarchy models for laminated composites. *International Journal for Numerical Methods in Engineering* 1992; **33**:503–535.
89. Fish J, Markolefas S. The *s*-version of the finite element method for multilayer laminates. *International Journal for Numerical Methods in Engineering* 1992; **33**:1081–1105.
90. Turn J-Q, Wang Y-B, Wang Y-M. Three-dimensional asymptotic finite element method for anisotropic inhomogeneous and laminated plates. *International Journal of Solids and Structures* 1996; **33**:1939–1960.
91. Pian THH, Mau ST. Some recent studies in assumed-stress hybrid models. In *Advances in Computational Methods in Structural Mechanics and Design*, Oden, Clought, Yamamoto (eds), 1972.
92. Spilker RL, Orringer O, Witmer O. Use of hybrid/stress finite element model for the static and dynamic analysis of multilayer composite plates and shells. *MIT ASRL TR* 181-2, 1976.
93. Spilker RL, Chou SC, Orringer O. Alternate hybrid-stress elements for analysis of multilayer composite plates. *Journal of Composite Materials* 1977; **11**:51–70.
94. Moriya K. Laminated plate and shell elements for finite element analysis of advanced fiber reinforced composite structure, laminated composite plates. *Transactions of the Society of Mechanical Engineers* 1986; **52**: 1600–1607 (in Japanese).
95. Liou WJ, Sun CT. A three-dimensional hybrid stress isoparametric element for the analysis of laminated composite plates. *Computers and Structures* 1987; **25**:241–249.
96. Jing H, Liao ML. Partial hybrid stress element for the analysis of thick laminate composite plates. *International Journal for Numerical Methods in Engineering* 1989; **28**:2813–2827.
97. Auricchio F, Sacco E. Partial mixed formulation and refined models for the analysis of composite laminates within and FSDT. *Composite Structures* 1999; **46**:103–113.
98. Rao KM, Meyer-Piening HR. Analysis of thick laminated anisotropic composites plates by the finite element method. *Composite Structures* 1990; **15**:185–213.
99. Carrera E. C^o Reissner–Mindlin multilayered plate elements including zig-zag and interlaminar stresses continuity. *International Journal for Numerical Methods in Engineering* 1996; **39**:1797–1820.
100. Carrera E, Kröplin B. Zig-zag and interlaminar equilibria effects in large deflection and postbuckling analysis of multilayered plates. *Mechanics of Composite Materials and Structures* 1997; **4**:69–94.

101. Carrera E, Krause H. An investigation on nonlinear dynamics of multilayered plates accounting for C_z^0 requirements. *Computers and Structures* 1998; **69**:463–486.
102. Carrera E. An improved Reissner–Mindlin-type model for the electromechanical analysis of multilayered plates including piezo-layers. *Journal of Intelligent Materials System and Structures* 1997; **8**:232–248.
103. Carrera E, Demasi L. Classical and advanced multilayered plate elements based upon PVD and RMVT. Part 2. Numerical implementations. 2000; **55**:(in press).
104. Reissner E. On a certain mixed variational theory and a proposed applications. *International Journal for Numerical Methods in Engineering* 1984; **20**:1366–1368.
105. Reissner E. On a mixed variational theorem and on a shear deformable plate theory. *International Journal for Numerical Methods in Engineering* 1986; **23**:193–198.
106. Washizu K. *Variational Method in Elasticity and Plasticity*. Pergamon Press: Oxford, 1968.
107. Antona E. *Mathematical Model and their Use in Engineering*. Miele A, Salvetti A (eds). Applied Mathematics in the Aerospace Science/Engineering, vol. 44, 1991; 395–433.
108. Zienkiewicz OC. *The Finite Element Method.* McGraw-Hill: London, 1986.

INTERNATIONAL JOURNAL FOR NUMERICAL METHODS IN ENGINEERING
Int. J. Numer. Meth. Engng 2002; **55**:253–291 (DOI: 10.1002/nme.493)

Classical and advanced multilayered plate elements based upon PVD and RMVT. Part 2: Numerical implementations

Erasmo Carrera*,† and Luciano Demasi

DIASP, Politecnico di Torino, Torino, Italy

SUMMARY

This paper presents numerical evaluations related to the multilayered plate elements which were proposed in the companion paper (Part 1). Two-dimensional modellings with linear and higher-order (up to fourth order) expansion in the z-plate/layer thickness direction have been implemented for both displacements and transverse stresses. Layer-wise as well as equivalent single-layer modellings are considered on both frameworks of the principle of virtual displacements and Reissner mixed variational theorem. Such a variety has led to the implementation of 22 plate theories. As far as finite element approximation is concerned, three quadrilaters have been considered (four-, eight- and nine-noded plate elements). As a result, 22×3 different finite plate elements have been compared in the present analysis. The automatic procedure described in Part 1, which made extensive use of indicial notations, has herein been referred to in the considered computer implementations. An assessment has been made as far as convergence rates, numerical integrations and comparison to correspondent closed-form solutions are concerned. Extensive comparison to early and recently available results has been made for sample problems related to laminated and sandwich structures. Classical formulations, full mixed, hybrid, as well as three-dimensional solutions have been considered in such a comparison. Numerical substantiation of the importance of the fulfilment of zig-zag effects and interlaminar equilibria is given. The superiority of RMVT formulated finite elements over those related to PVD has been concluded.

Two test cases are proposed as 'desk-beds' to establish the accuracy of the several theories. Results related to all the developed theories are presented for the first test case. The second test case, which is related to sandwich plates, restricts the comparison to the most significant implemented finite elements. It is proposed to refer to these test cases to establish the accuracy of existing or new higher-order, refined or improved finite elements for multilayered plate analyses. Copyright © 2002 John Wiley & Sons, Ltd.

KEY WORDS: finite element; plates; multilayers; classical and mixed formulation; composite materials

1. INTRODUCTION AND CONTENTS OF THE PAPER

This paper quotes numerical evaluations of the multilayered finite plate elements that have been proposed in the companion paper (Part 1) [1]. Reissner's mixed variational theorem

*Correspondence to: Erasmo Carrera, Department of Aeronautics and Aerospace Engineering, Politinecnico di Torino, Corso Duca degli Abruzzi, 24, 10129 Torino, Italy.
†E-mail: carrera@polito.it

Received 23 October 2000
Revised 4 April 2001

(RMVT) and the principle of virtual displacements (PVD) have been used to develop advanced and classical plate elements, respectively. Both layer-wise (LW) and equivalent single-layer (ESL) variable descriptions were employed (it is intended that the number of the unknown variables remains independent of the number of constitutive layers in the latter case).

The number of nodes N_n of the elements, as well as the order of the expansion N for both displacement and transverse stress variables in the plate thickness direction z, were taken as free parameters in the developments documented in Part 1. The numerical implementations, whose results are documented in this paper, have been restricted to the following cases:

1. Three quadrilater cases have been implemented, as far as the number of nodes is concerned: $N_n = 4,8$ and 9 (that is, four-, eight- and nine-noded plate elements have been considered)
2. $N \leqslant 4$, that is, theories which permit linear up to fourth-order expansion for displacement and/or transverse stress variables in the layer or whole plates have been addressed.

The latter choice, in conjunction with the possibilities of choosing between PVD or RMVT implementation, as well as layer-wise or equivalent single-layer description, lead to 22 possible two-dimensional theories. Referring to point (1), it follows that 22×3, multilayered finite elements have been implemented and compared in this paper. Some of these are classical finite elements (those based on PVD and linear field in layer/plate thickness). Nevertheless, about 20×3 of the multilayered plate elements discussed in this paper have neither been proposed nor evaluated by other scientists. These elements, herein called advanced, which are formulated on the basis of Reissner's mixed variational theorem are of particular interest.

The 22×3 finite elements have been implemented in a finite element code which is available at the DIASP. The possibilities of implementing all these elements in a single step is closely related to the following crucial facts, which were described in Part 1:

- the extensive use of indicial notations;
- the reduction of each type of finite element matrix to only five arrays (of dimension 3×3), which have already been called 'fundamental nuclei' (one for PVD formulations, see Equation (58) of Part 1, and four for RMVT ones, see Equations (69)–(72) of Part 1).

As a result, it was possible to implement the 22×3 multilayered plate elements, all together, by putting only 5×9 lines in appropriate loops of the written FORTRAN code. For the sake of clarity, these FORTRAN lines have been explicitly written in Appendix A.

The authors have found this technique very convenient and easy to check, and encourage other scientists to refer to it in the case where they are going to implement finite elements that are somewhat similar to the authors' one.

In spite of the large number of implemented elements, not all the possibilities described in Part 1 have herein been addressed. For instance, full mixed implementation has not been discussed. Mixed implementations have therefore been restricted to the case in which stress variables are eliminated at the element level; interlaminar loadings have not been addressed and so on. However, further implementations are in progress and the related results could be the subject of future studies.

The contents of this paper have been organized as follows. Section 2 quotes details on the implemented finite elements. The used shape functions, as well as displacement and transverse stress fields in the thickness directions, are given and explained with the help of figures.

Acronyms have been introduced in this section to denote the implemented finite elements. Section 3 describes the conducted numerical investigations. The data of the treated problems are firstly quoted. An assessment and comparison to other available results are then given in subsequent subsections. Section 4 discusses two test cases which are proposed as desk-beds to assess multilayered finite plate elements. Section 5 traces the final remarks. The FORTRAN list of the five used fundamental nuclei are explicitly given and briefly explained in Appendix A.

As far as notation and symbols are concerned, full reference should be made to Part 1.

2. IMPLEMENTED FINITE ELEMENTS

Apart from the number of nodes, the implemented multilayered finite elements are characterized by

- order N of the expansion in the z-thickness direction;
- used variational statement (PVD or RMVT);
- variables description (LWM or ESLM).

In order to denote in a concise manner the implemented finite elements, acronyms could be conveniently used. These acronyms have herein been built as illustrated in Figure 1:

- The first field of the acronym is related to the used variables description, L states for layer-wise and E states for equivalent single layer.
- The second field signifies the variational statements on which the correspondent finite element relay, D and M mean Principle of Virtual Displacements and Reissner's Mixed Variational theorem, respectively.
- The third and fourth fields (which are optional in the sense that they do compare only in particular cases related to ESL description) can assume the letter Z or/and C; that is zig-zag function is included in the displacement field and/or interlaminar continuity is guaranteed for transverse stresses.
- The last field is a number which denotes the used values for N.

Extensive reference to such acronyms will be made in the following.

2.1. *Used finite element approximations*

Following standard finite element method, the unknown variables in the generic layer points of the reference surface Ω are expressed in terms of their values with correspondence to the nodes. According to an isoparametric description displacements are written as follows:

$$\mathbf{u}_\tau^k = N_i \mathbf{q}_{\tau i}^k \quad (i = 1, 2, \ldots, N_n) \tag{1}$$

where N_i denote the shape functions and

$$\mathbf{q}_{\tau i}^k = [q_{u_x \tau i}^k \;\; q_{u_y \tau i}^k \;\; q_{u_z \tau i}^k]^{\mathrm{T}} \tag{2}$$

are the nodal values of displacements.

The same approximations have been introduced for stresses,

$$\boldsymbol{\sigma}_{n\tau}^k = N_i \mathbf{g}_{\tau i}^k \quad (i = 1, 2, \ldots, N_n) \tag{3}$$

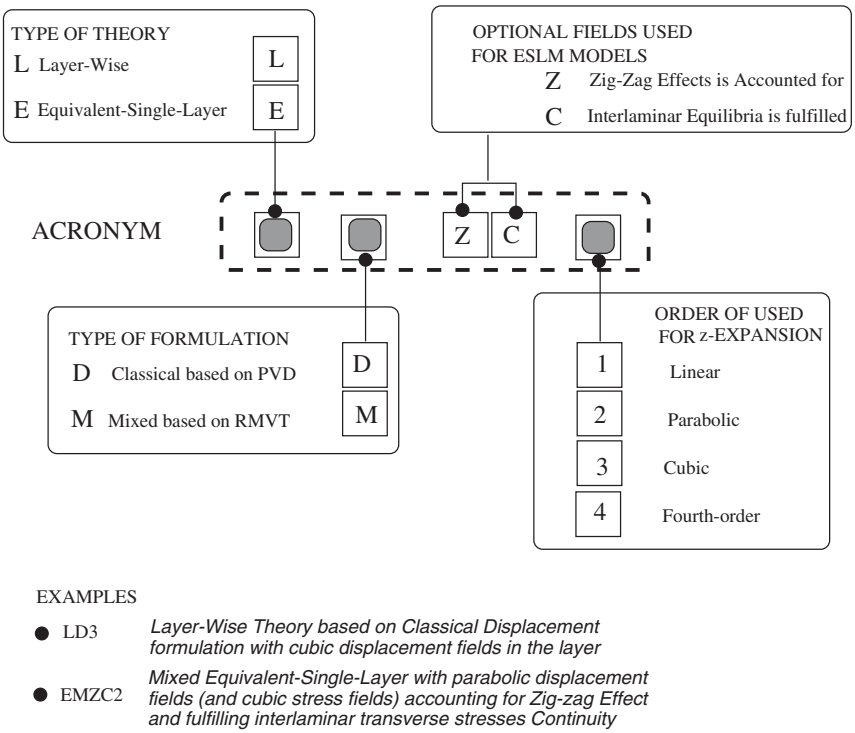

Figure 1. Acronyms used to denote implemented finite elements.

where

$$\mathbf{g}_{\tau i}^{k} = [g_{xz\tau i}^{k} \;\; g_{yz\tau i}^{k} \;\; g_{zz\tau i}^{k}]^{\mathrm{T}} \tag{4}$$

Three plate elements have been implemented with four (Q4), eight (Q8), nine (Q9) nodes, respectively. The explicit form of the shape function can be read in Reference [2]. According to isoparametric description, the problem co-ordinates are given in terms of their nodal values X_i and Y_i, according to

$$x = \sum_{1}^{N_n} N_i(\xi,\eta) X_i, \quad y = \sum_{1}^{N_n} N_i(\xi,\eta) Y_i$$

2.2. Multilayered plate elements based on PVD

Particular cases of displacement and stress fields which were introduced in Sections 5 and 6 of Part I are explicitly described here.

First, multilayered finite elements based on PVD are discussed. In such a framework, only displacements are assumed.

First- and higher-order ESLM cases: *ED1*, *ED2*, *ED3*, *ED4*: The order of the Taylor-type expansion varies from 1 up to 4. ESLM description requires a unique displacement fields for the whole multilayered plate,

$$\mathbf{u} = \mathbf{u}_0 + z^r \mathbf{u}_r, \quad r = 1,2,\ldots,N \tag{5}$$

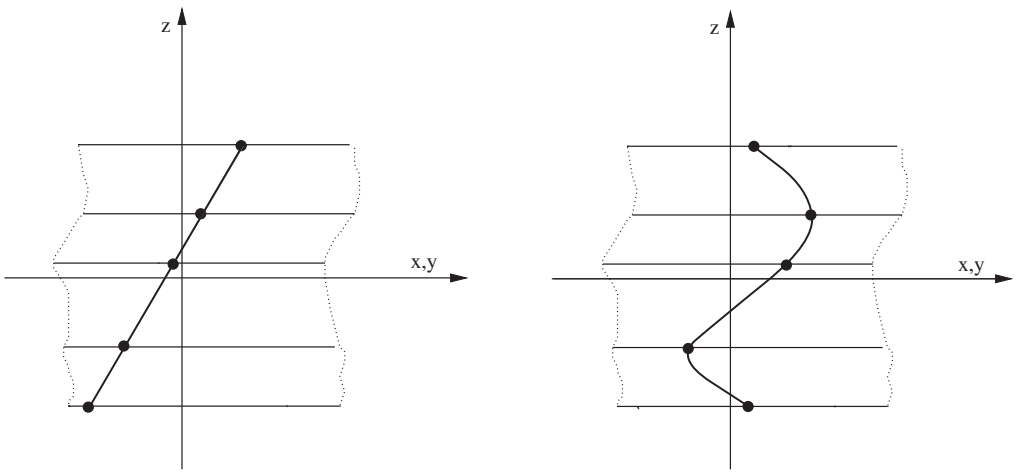

Figure 2. ESLM assumption. Linear and cubic cases.

Subscript $_0$ denotes displacement values with correspondence to the plate reference surface Ω. Linear and higher-order distributions in the z-direction are introduced by the r-polynomials. In a unified notation, the above expansion is rewritten in the following manners

$$\mathbf{u} = F_t\mathbf{u}_t + F_b\mathbf{u}_b + F_r\mathbf{u}_r = F_\tau\mathbf{u}_\tau, \quad \tau = t, b, r, \quad r = 1, 2, \ldots, N-1 \tag{6}$$

where

$$F_b = 1, \quad F_t = z^N, \quad F_r = z^r, \quad r = 1, 2, \ldots, N-1 \tag{7}$$

b and t subscripts in the LW cases will signify, see below, values of the displacement and/or stress variables with correspondence to layer bottom and top surfaces, respectively.

By varying N, from 2 to 4, four sub-cases are obtained. According to the acronyms of Figure 1, these four cases correspond to ED1, ED2, ED3, ED4 (E signifies equivalent single layer, D states that the related finite elements are formulated with only displacement variables and based on PVD, the final numbers denote the order of the used expansion). Linear and cubic cases are depicted in Figure 2.

First- and higher-order ESL cases with zig-zag function: *EDZ*1, *EDZ*2, *EDZ*3: zig-zag effect can be introduced in the finite element models with only displacement variables along with ESLM description, by referring to Murakami's zig-zag function. According to Murakami [3], a zig-zag function is added to the displacement field related to ED cases, as it follows

$$\mathbf{u} = \mathbf{u}_0 + (-1)^k\zeta_k\mathbf{u}_Z + z^r\mathbf{u}_r, \quad r = 1, 2, \ldots, N \tag{8}$$

Subscript Z refers to the introduced zig-zag term. Note that the unknown variables $\mathbf{u}_0, \mathbf{u}_Z, \mathbf{u}_r$ are k-independent. That is, ESLM description has been preserved. $\zeta_k = 2z_k/h_k$ is a non-dimensional layer co-ordinate (z_k is the physical co-ordinate of the k-layer whose thickness is h_k). The exponent k changes the sign of the zig-zag term in each layer.

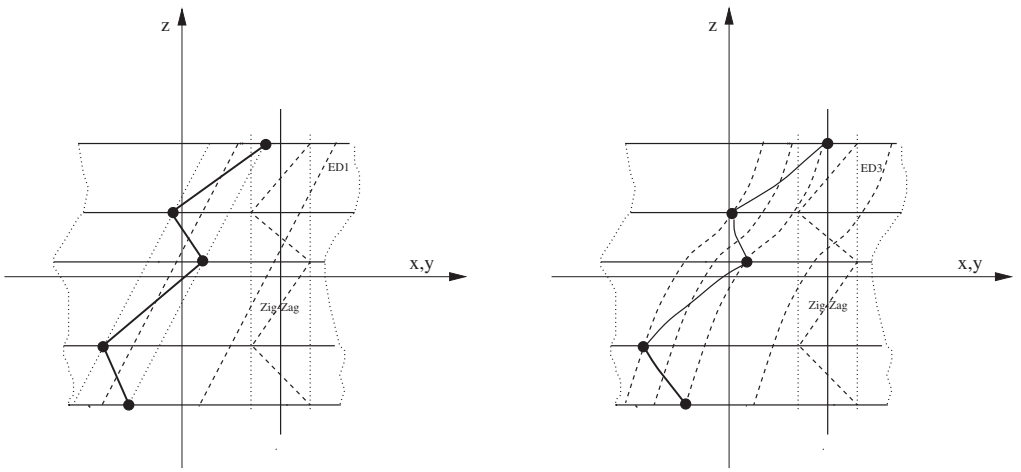

Figure 3. ESLM assumption with zig-zag function. Linear and cubic cases.

By employing a unified notations Equation (8) becomes

$$\mathbf{u} = F_t\mathbf{u}_t + F_b\mathbf{u}_b + F_r\mathbf{u}_r = F_\tau\mathbf{u}_\tau, \quad \tau = t,b,r, \quad r = 1,2,\ldots,N \tag{9}$$

Subscript t has been chosen to denote the zig-zag term ($\mathbf{u}_t = \mathbf{u}_Z$, $F_t = (-1)^k\zeta_k$).

The following three finite element implementations have been considered: EDZ1, EDZ2, EDZ3. The letter Z, before the order of the expansion, signifies that zig-zag effect is accounted for in these finite elements. The linear and cubic cases are depicted in Figure 3. The geometrical meanings of the zig-zag function become clear by the quoted picture: a zig-zag function of constant amplitude, which changes its sign with correspondence to each interface, is added to classical displacement field of ED-type. As a result, linear and higher-order displacement fields are obtained which reproduce derivative discontinuity at the interfaces.

First- and higher-order LW elements: *LD*1, *LD*2, *LD*3, *LD*4: Linear and higher-order displacement fields can be employed in the framework of layer-wise description. That is, the displacement field at Equation (6) is taken in each layer, in formulae

$$\mathbf{u}^k = F_t\mathbf{u}_t^k + F_b\mathbf{u}_b^k + F_r\mathbf{u}_r^k = F_\tau\mathbf{u}_\tau^k, \quad \tau = t,b,r, \quad r = 2,3,\ldots,N, \quad k = 1,2,\ldots,N_l \tag{10}$$

It is now intended that the subscripts t and b denote values related to the layer top and bottom surfaces, respectively. These two terms consist of the linear part of the expansion. The thickness functions $F_\tau(\zeta_k)$ have now been defined at the k-layer level,

$$F_t = \frac{P_0 + P_1}{2}, \quad F_b = \frac{P_0 - P_1}{2}, \quad F_r = P_r - P_{r-2}, \quad r = 2,3,\ldots,N \tag{11}$$

in which $P_j = P_j(\zeta_k)$ is the Legendre polynomial of j-order defined in the ζ_k-domain: $-1 \leqslant \zeta_k \leqslant 1$. The first five used Legendre polynomials are

$$P_0 = 1, \quad P_1 = \zeta_k, \quad P_2 = (3\zeta_k^2 - 1)/2, \quad P_3 = \frac{5\zeta_k^3}{2} - \frac{3\zeta_k}{2}, \quad P_4 = \frac{35\zeta_k^4}{8} - \frac{15\zeta_k^2}{4} + \frac{3}{8}$$

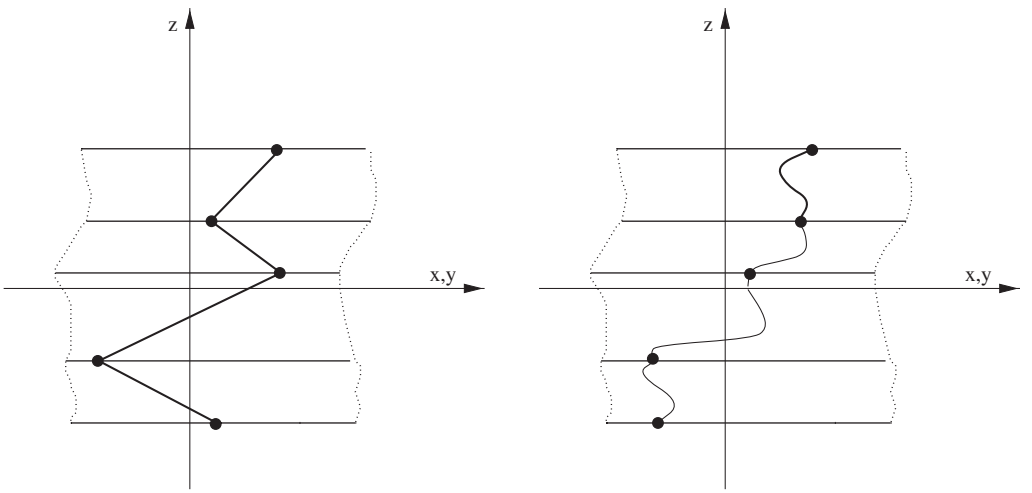

Figure 4. LWM assumption. Linear and cubic cases.

The chosen functions have the following properties:

$$\zeta_k = \begin{cases} 1, & F_t = 1,\ F_b = 0,\ F_r = 0 \\ -1, & F_t = 0,\ F_b = 1,\ F_r = 0 \end{cases} \tag{12}$$

The continuity of the displacement at each interface is easily linked:

$$\mathbf{u}_t^k = \mathbf{u}_b^{(k+1)}, \quad k = 1, N_l - 1 \tag{13}$$

The four finite elements LD1, LD2, LD3, LD4 have been implemented. L signifies layer-wise description, D states that the related finite elements are formulated with only displacement variables and based on PVD, the final numbers denote the order of the used expansion. Linear and cubic cases have been depicted in Figure 4.

2.3. Plate elements based upon RMVT

The finite elements described above are not able to fulfil *completely* and *a priori* the interlaminar equilibria for the transverse stresses. In order to meet such a requirement, stress assumptions should be made. According to Part 1, the description interlaminar continuous transverse shear and normal stresses require layer-wise modellings. Therefore, ESL description could be only given for displacement variables. Implemented finite elements which are based on different displacement and stress assumptions and on the application of RMVT are described in this subsection.

First- and higher-order ESLM cases: *EMC*1, *EMC*2, *EMC*3, *EMC*4: Equivalent single-layer finite elements based on RMVT (as discussed in Part 1) can be developed by using the displacement fields, already described in Equation (6). Such a field is herein, for convenience, rewritten as

$$\mathbf{u} = F_t \mathbf{u}_t + F_b \mathbf{u}_b + F_r \mathbf{u}_r = F_\tau \mathbf{u}_\tau, \quad \tau = t, b, r, \quad r = 1, 2, \ldots, N - 1 \tag{14}$$

Transverse shear and normal stresses are assumed according to the same assumption and notation that have been used for displacements. In formulae,

$$\boldsymbol{\sigma}^k_{n\mathrm{M}} = F_t\boldsymbol{\sigma}^k_{nt} + F_b\boldsymbol{\sigma}^k_{nb} + F_r\boldsymbol{\sigma}^k_{nr} = F_\tau\boldsymbol{\sigma}^k_{n\tau}, \quad \tau = t,b,r, \quad r = 2,3,\ldots,N, \quad k = 1,2,\ldots,N_l \tag{15}$$

The four cases EMC1, EMC2, EMC3, EMC4 have been implemented. E signifies equivalent single layer, M states that the related finite elements are formulated with mixed variables (stresses and displacements) and based on RMVT, C signifies that transverse stresses are *a priori* continuous at the interfaces; the final numbers denote the order of the used expansion. Linear and cubic cases have been depicted in Figure 2.

First- and higher-order ESLM cases with zig-zag function: *EMZC*1, *EMZC*2, *EMZC*3: The physics of multilayered structures demonstrated that interlaminar continuity and zig-zag effects are strongly connected to each other, as it is in solids for equilibrium and compatibility. Interlaminar continuous transverse stresses not accompanied by zig-zag effects description, as done for EMC-type finite elements, is physically inconsistent. To remove such inconsistency, a zig-zag function is used in the RMVT and ESLM framework. As a result, the displacement field at Equation (8) is employed in conjunction with the transverse stress assumption of Equation (15). Three multilayered finite elements herein denoted by EMZC1, EMZC2, EMZC3 have been implemented. With respect to that EMC case, a Z has been introduced in the acronyms to denote that zig-zag effects have been accounted for.

Linear and cubic cases have been depicted in Figure 2.

First- and higher-order LW cases: *LM*1, *LM*2, *LM*3, *LM*4: Full layer description based upon RMVT is simply obtained by using layer-wise description for both displacement and transverse stress variables. In formulae

$$\begin{aligned} \mathbf{u}^k &= F_t\mathbf{u}^k_t + F_b\mathbf{u}^k_b + F_r\mathbf{u}^k_r = F_\tau\mathbf{u}^k_\tau, \qquad \tau = t,b,r \\ & \qquad\qquad\qquad\qquad\qquad\qquad\quad r = 2,3,\ldots,N \\ \boldsymbol{\sigma}^k_{n\mathrm{M}} &= F_t\boldsymbol{\sigma}^k_{nt} + F_b\boldsymbol{\sigma}^k_{nb} + F_r\boldsymbol{\sigma}^k_{nr} = F_\tau\boldsymbol{\sigma}^k_{n\tau}, \quad k = 1,2,\ldots,N_l \end{aligned} \tag{16}$$

The four finite elements LM1, LM2, LM3, LM4 were implemented. Figure 4 depicts the related displacement and stress fields related to linear and cubic order cases.

3. RESULTS AND DISCUSSION

A large numerical investigation was conducted in order to assess the implemented finite elements. A number of convergence studies and comparison to analytical solutions, to three-dimensional exact analyses and to other available finite element results related to static response of bent orthotropic, multilayered very thick, thick, moderately thick and thin plates were made. Different loadings as well as boundary conditions were treated. Numerical performances have been established and transverse locking mechanisms were contrasted by extensive use of reduced and selective integration techniques. This was done according to the description given in Appendix C of Part 1.

3.1. Data of the treated problems

Data of the considered problems are described herein. For convenience, laminated data and boundary conditions are denoted by acronyms.

Mechanical properties of the lamina and lay-out of the laminates: The mechanical properties of the used lamina are:

$$\frac{E_1}{E_2}=25, \quad \frac{G_{12}}{E_2}=\frac{G_{13}}{E_2}=0.5, \quad \frac{G_{23}}{E_2}=0.2, \quad v_{12}=v_{13}=v_{23}=0.25$$

Cross-ply symmetrical and unsymmetrical laminated plates were investigated according to the following lay-outs and thicknesses:

- LAM1: $0°$;
- LAM2: $0°/90°/0°$, $h_i=\frac{1}{3}h$, $i=1,\ldots,3$;
- LAM3: $0°/90°/90°/0°$, $h_i=\frac{1}{4}h$, $i=1,\ldots,4$;
- LAM4: $0°/90°/0°/90°$, $h_i=\frac{1}{4}h$, $i=1,\ldots,4$.

Further to the above four cross-ply laminates, a sandwich plate will be analysed in Section 4. The mechanical properties of the laminae which are used as skins are those by Pagano [4]:

$$E_L=25, \quad E_T=1$$
$$G_{LT}=0.5G_{TT}=0.2v_{LT}=v_{TT}=0.25$$

The core material used for the sandwich plates is transversely isotropic with respect to the z-axis and is characterized by the following elastic properties:

$$E_{xx}=E_{yy}=0.04, \quad E_{zz}=0.5, \quad G_{xz}=G_{yz}=0.04$$
$$G_{xy}=0.016, \quad v_{xy}=v_{zy}=v_{zx}=0.25$$

Loading cases: Four types of loadings have been treated (Figure 5). These are all applied at the top surface of the investigated plates.

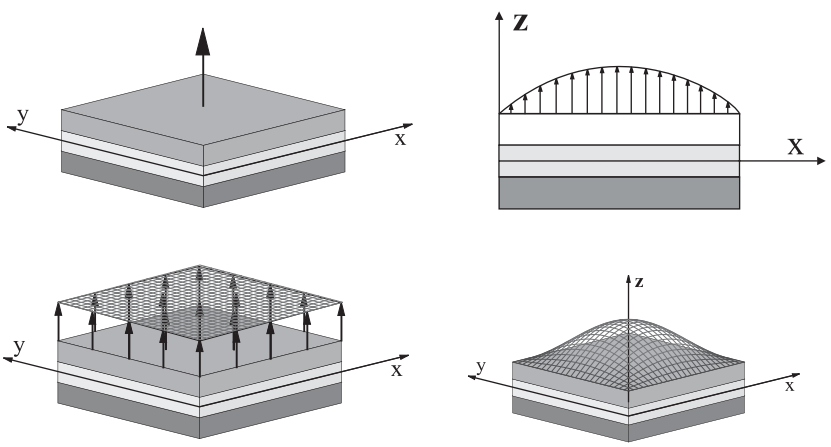

Figure 5. Considered loading cases. Concentrated load, constant and harmonic pressure distribution for cylindrical, bent and rectangular plates.

(1) Sinusoidal load:

$$P_z = p_z \sin\left(\frac{\pi x}{a}\right)$$

(2) Bi-sinusoidal load:

$$P_z = p_z \sin\left(\frac{\pi x}{a}\right) \sin\left(\frac{\pi y}{b}\right)$$

(3) Uniform pressure:

$$P_z = p_z$$

(4) Point load applied at the plate centre:

$$P_z = P$$

Boundary conditions: As far as boundary conditions are concerned, reference will be made to the two following cases:

- SS: simply supported;
- CL: clamped.

Adimensionalizations: Stresses and displacements are adimensionalized according to the following formulas:

$$(\bar{\sigma}_{xx}, \bar{\sigma}_{yy}, \bar{\sigma}_{xy}) = \frac{1}{p_z(a/h)^2}(\sigma_{xx}, \sigma_{yy}, \sigma_{xy})$$

$$(\bar{\sigma}_{zx}, \bar{\sigma}_{zy}) = \frac{1}{p_z(a/h)}(\sigma_{zx}, \sigma_{zy}), \quad \bar{\sigma}_{zz} = \frac{1}{p_z}\sigma_{zz}$$

$$(\sigma'_{xx}, \sigma'_{yy}, \sigma'_{xy}) = \frac{1}{p_z}(\sigma_{xx}, \sigma_{yy}, \sigma_{xy}), \quad (\sigma'_{zx}, \sigma'_{zy}) = \frac{1}{p_z}(\sigma_{zx}, \sigma_{zy})$$

$$\bar{U}_x = \frac{u_x E_2}{p_z h}, \quad \bar{U}_z = \frac{u_z 100 h^3 E_2}{p_z a^4}, \quad U'_z = \frac{u_z 100 h^3 E_2}{P a^2}$$

3.2. Finite element assessment and comparison to correspondent closed-form solutions

The acronyms that have been introduced in the previous paragraphs are used in the tables and figures to denote different theories as well as data description. Acronyms have also been used to denote results by other authors. A list of these has been provided in Table I. If not differently declared, it is intended that results are related to Q9 plate elements. Sinusoidal and bi-sinusoidal loadings are referred to cylindrical bending and square plate problems, respectively.

Convergence rates, locking mechanism and comparison to correspondent analytical, closed-form solution has been provided in Tables II–VI and Figures 6–22. The number of nodes N_n, the number of elements in the meshes N_e and the number of expansions used in the z-direction N have been used as parameters in the made assessment. Locking problems have,

Table I. List of acronyms frequently used in tables and figures to denote results for multilayered plates taken by open literature.

3D	Three-Dimensional solution (taken by different sources)
A&S	Auricchio and Sacco [18]
D&R	Di and Ramm [19]
D-1, D2	Linear and refined theory in Di Schiuva [20]
H&L	Jing and Liao [21]
IK&T	Idlbi, Karama and Touratier [22]
L&S	Liou and Sun [23]
LH&X	Liew, Han and Xiao [15]
Mindlin	Mindlin [24]
Morya	Morya [25]
P&K	Pandya and Kant [26]
P&T	Polit and Touratier [27]
R–E	Reddy [28]
R-H	Reddy [29]

Table II. $\bar{U}_z$ $(x = a/2, z = 0)$. Convergence rate with respect to number of elements. Data: IS integration, LAM2, sinusoidal load, SS.

	$a/h = 4$			$a/h = 6$		
N_e	$Q4$	$Q8$	$Q9$	$Q4$	$Q8$	$Q9$
			LD1			
2	2.4900	2.8204	2.7798	1.3619	1.6026	1.5802
4	2.7104	2.8004	2.7838	1.5263	1.5952	1.5837
6	2.7514	2.7925	2.7839	1.5582	1.5900	1.5838
8	2.7658	2.7891	2.7839	1.5695	1.5877	1.5839
10	2.7725	2.7874	2.7839	1.5747	1.5864	1.5839
LD1[a]		2.7830			1.5830	
			LM1			
2	2.4886	2.8372	2.7866	1.3702	1.6218	1.5960
4	2.7154	2.8126	2.7915	1.5406	1.6130	1.5998
6	2.7580	2.8028	2.7918	1.5735	1.6071	1.5999
8	2.7729	2.7985	2.7918	1.5851	1.6044	1.5999
10	2.7799	2.7963	2.7918	1.5905	1.6029	1.5999
LM1[a]		2.791			1.599	

at this stage, been contrasted by the use of reduced/selective integration techniques. These have been depicted in the correspondent analysis by adding the further letters IN, IS and IS2 in brackets to the correspondent finite elements. These integration schemes treat the different stiffness/compliance terms which were outlined in Appendix C of Part 1, in an alternate manner. The authors are not aware of the many other, more sophisticated, more elegant and more efficient integration techniques such as those described by Bathe and Dvorkin [5] and also used by the first author [6]. In fact, these advanced techniques permit one to avoid spurious modes that normally arise from reduced integration implementations. A discussion on these problems can be found in the articles by Briossilis [7–9], Zienkiewicz *et al*. [10]

Table III. $\bar{U}_z$ $(x = a/2, z = 0)$. Convergence rate with respect to N. Data: IS integration, LAM2, sinusoidal load, SS, mesh 8×1.

	$a/h = 4$				$a/h = 6$			
N	$Q4$	$Q8$	$Q9$	LD[a]	$Q4$	$Q8$	$Q9$	LD[a]
				LDN case				
1	2.7658	2.7891	2.7839	2.783	1.5695	1.5877	1.5839	1.583
2	2.8453	2.8700	2.8642	2.864	1.6156	1.6342	1.6302	1.630
3	2.8693	2.8407	2.8878	2.887	1.6205	1.5983	1.6351	1.635
4	2.8695	2.8410	2.8879	2.887	1.6206	1.5984	1.6351	1.635
3D		2.887				1.635		
				LMN case				
N	$Q4$	$Q8$	$Q9$	LM[a]	$Q4$	$Q8$	$Q9$	LM[a]
1	2.7729	2.7985	2.7918	2.791	1.5851	1.6044	1.5999	1.599
2	2.8581	2.8277	2.8767	2.891	1.6182	1.5953	1.6328	1.635
3	2.8693	2.8407	2.8878	2.887	1.6205	1.5983	1.6351	1.635
4	2.8695	2.8410	2.8879	2.887	1.6206	1.6206	1.6351	1.635
3D		2.887				1.635		

Table IV. $\bar{U}_x$ $(x = 0)$. Convergence to the elasticity solution by Pagano [30]. Data: $a/h = 4$, LAM1, sinusoidal load, SS, mesh 8×1.

z/h	3D	LM4[a]	LM4 (IN)	LM4 (IS)	LM4 (IS2)	LD4[a] LD4	(IN)	LD4 (IS)	LD4 (IS2)
−0.5	0.6894	0.6855	0.6780	0.6880	0.6882	0.6855	0.6780	0.6880	0.6882
−0.3	0.2260	0.2225	0.2197	0.2230	0.2228	0.2225	0.2197	0.2230	0.2228
−0.1	0.0632	0.0520	0.0497	0.0503	0.0502	0.0520	0.0497	0.0503	0.0502
0.1	−0.0333	−0.0222	−0.0253	−0.0259	−0.0258	−0.0222	−0.0253	−0.0259	−0.0258
0.3	−0.2090	−0.2053	−0.2082	−0.2114	−0.2112	−0.2053	−0.2082	−0.2114	−0.2112
0.5	−0.7161	−0.7122	−0.7116	−0.7216	−0.7221	−0.7122	−0.7116	−0.7216	−0.7221

and Carrera [11]. On the other hand, this present paper is more oriented towards two-dimensional modellings of multilayered plates. In this respect, the previously mentioned advanced techniques could be implemented in future works.

The convergence rates of Q4, Q8 and Q9 elements have been documented in Table II and Figures 6 and 7 with respect to the number of elements in a cylindrical bent plate. Two thick plates are considered. Both mixed (LM1) and classical (LD1) approaches are compared. The analytical closed-form solutions are taken from (Carrera's) previous works [12–14]. The latter have been denoted by adding superscript a to the correspondent finite element acronyms. An excellent convergence rate has to be registered for both classical and mixed cases. It should be noted that the comparison that has been made with the closed-form solutions consists of the best test that could be made in order to assess the reliability of FE approximations. Finite element results could not in fact be better, in any case, than those of corresponding closed-form solutions.

Table V. Convergence to the analytical solution. Data: $a=b$, LAM4, bi-sinusoidal load, SS, mesh 4×4.

a/h		$\bar{\sigma}_{xx}$ $a/2, a/2, \pm\frac{1}{2}$	$\bar{\sigma}_{yy}$ $a/2, a/2, \pm\frac{1}{4}$	$\bar{\sigma}_{xy}$ $0, 0, \pm\frac{1}{2}$	$\bar{\sigma}_{zx}$ $0, a/2, 0$	$\bar{\sigma}_{zy}$ $a/2, 0, 0$	$\bar{\sigma}_{zz}$ $a/2, a/2, 0$	$\bar{U}_z$ $a/2, a/2, 0$
2	LM4[a]	0.1918 −0.9447	0.0265 −0.7808	−0.0877 0.0694	0.1625	0.1947	0.4512	5.2632
	LM4(IN)	0.2053 −0.9885	0.0260 −0.8147	−0.0928 0.0733	0.1727	0.2058	0.4512	5.2642
10	LM4[a]	0.0453 0.5360	0.0114 0.4966	−0.0291 0.2921	0.2713	0.2719	0.4996	0.7623
	LM4(IS)	0.0474 −0.5611	0.0121 −0.5239	−0.0302 0.0304	0.2638	0.2645	0.5015	0.7629
100	LM4[a]	0.0358 −0.4873	0.0112 −0.4627	−0.2539 0.2541	0.2803	0.2803	0.5000	0.5092
	LM4(IS2)	0.0377 −0.5111	0.0119 −0.4851	−0.0262 0.0262	0.3032	0.3033	0.5302	0.5094

The following further comments can be made:

- Q9 elements show the best convergence rate.
- As known, stiffness reduces for Q4 and Q9 elements with N_e increasing, vice versa for the Q8 case.
- Mixed (LM1) and classical elements (LD1) show the same numerical behaviour, that is, RMVT does not introduce any complicating numerical effects to the corresponding PVD ones. This happens even with the quite different mathematical structures of the differential operators of RMVT matrices with respect to PVD ones.

Convergence to elasticity solutions and comparison to correspondent analytical ones have been analysed in Table III and Figure 8. The effect of an increase in N has been monitored. A mesh of eight elements has been used. Twenty four ($2\times4\times3$) multilayered finite elements are compared: four LD (LD4, LD3, LD2, LD1) and four LMN (LM4, LM3, LM2, LM1) cases for each of Q4, Q8 and Q9 implementations. The following conclusions can be drawn:

- Finite element results closely match the correspondent analytical ones for each N value and for both classical and mixed finite elements.
- An increase of N the elasticity solutions is obtained.

The made analysis has demonstrated the suitability of the implemented elements. Furthermore, to obtain the desired accuracy and, at the same time, to cut down computational costs, a compromise has to be made between the number of used elements N_e as well as element type N_n, and the order of the used expansion for the variables in the plate thickness directions N.

Further assessments which also take the implemented numerical integration schemes and their effects into account on different theories are documented in Tables IV–VII and Figures 9–22. Comparison to three-dimensional solutions and/or to analytical ones have been provided in these analyses. Local values of transverse displacements, related to layer-wise descriptions, are reported in Table IV, for a thick plate. Finite elements and closed-form (analytical) solutions for transverse displacements are compared to three-dimensional ones in six positions of

Table VI. Convergence to the elasticity solution. Data: $a=b$, LAM3, bi-sinusoidal load, SS, mesh 4×4.

a/h		$\bar{\sigma}_{xx}$ $a/2, a/2, \pm\frac{1}{2}$	$\bar{\sigma}_{yy}$ $a/2, a/2, \pm\frac{1}{4}$	$\bar{\sigma}_{xy}$ $0, 0, \pm\frac{1}{2}$	$\bar{\sigma}_{zx}$ $0, a/2, 0$	$\bar{\sigma}_{zy}$ $a/2, 0, 0$	$\bar{\sigma}_{zz}$ $a/2, a/2, 0$	$\bar{U}_z$ $a/2, a/2, 0$
2	3D	1.388 −0.912	0.835 −0.795	−0.0863 0.0673	0.153	0.295	—	5.075
	LM4(IN)	1.4405 −0.9477	0.8478 −0.8116	−0.0911 0.0710	0.1601	0.3105	0.4576	5.0800
4	3D	0.720 −0.6840	0.663 −0.6660	−0.0467 0.0458	0.219	0.292	—	1.937
	LM4(IN)	0.7456 −0.7093	0.6897 −0.6937	−0.0493 0.0484	0.2294	0.3148	0.4964	1.9374
10	3D	0.559 −0.559	0.401 −0.403	−0.0275 0.0276	0.301	0.196	—	0.737
	LM4(IS)	0.5909 −0.5915	0.4225 −0.4244	−0.0286 0.0287	0.3073	0.1607	0.5018	0.7376
20	3D	0.543 −0.5430	0.308 −0.3090	−0.0230 0.0230	0.328	0.156	—	0.513
	LM4(IS2)	0.5732 −0.5741	0.3239 −0.3247	−0.0239 0.0240	0.3592	0.1697	0.5342	0.5133
50	3D	0.539 −0.539	0.276 −0.276	−0.0216 0.0216	0.337	0.141	—	0.446
	LM4(IS2)	0.5673 −0.5674	0.2894 −0.2895	−0.0225 0.0225	0.3665	0.1533	0.5305	0.4449
100	3D	0.539 −0.539	0.271 −0.271	−0.0214 0.0214	0.339	0.139	—	0.435
	LM4(IS2)	0.5655 −0.5655	0.2841 −0.2841	−0.0224 0.0224	0.3665	0.1505	0.5302	0.4348
1000	LM4(IS2)	0.5646 −0.5646	0.2823 −0.2823	−0.0223 0.0223	0.3663	0.1496	0.5301	0.4315

the plate thickness. It should be noticed that a plate consisting of one single layer has been investigated. Good performance of the implemented elements should be confirmed for local value evaluations. The three integration schemes are also compared in Table V: very thick ($a/h=2$), moderately thick ($a/h=4$) and thin plates are considered. The plate being made of one layer, the quoted comparisons are of particular interest, as far as numerical behaviour is concerned:

- The plate being made of one layer, RMVT and PVD statements must lead to the same numerical result. This is demonstrated by the fact that the two closed-form solutions LM4[a] and LD4[a] give the same numbers.
- Such a coincidence is preserved in the finite element solutions.
- Furthermore, PVD and RMVT finite element results are the same for the three different integration schemes (IN, IS, IS2) that have been implemented.

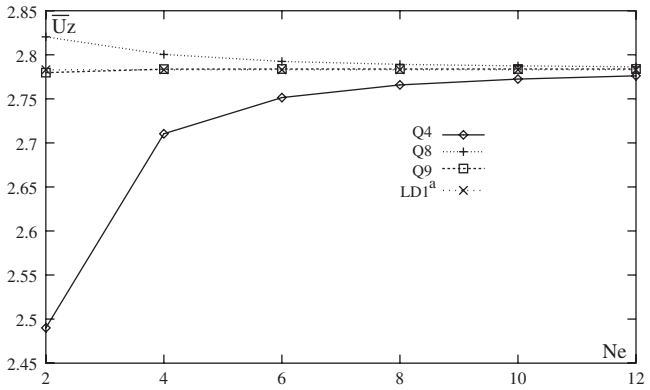

Figure 6. $\bar{U}_z(a/2, a/2, 0)$ vs N_e. Convergence to the analytical solution. Data: $a/h = 4$, LD1, IS integration, LAM2, sinusoidal load, SS.

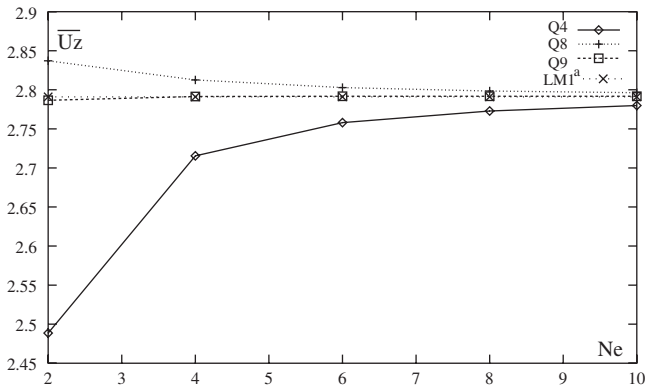

Figure 7. $\bar{U}_z(a/2, a/2, 0)$ vs N_e. Convergence to the analytical solution. Data: $a/h = 4$, LM1, IS integration, LAM2, sinusoidal load, SS.

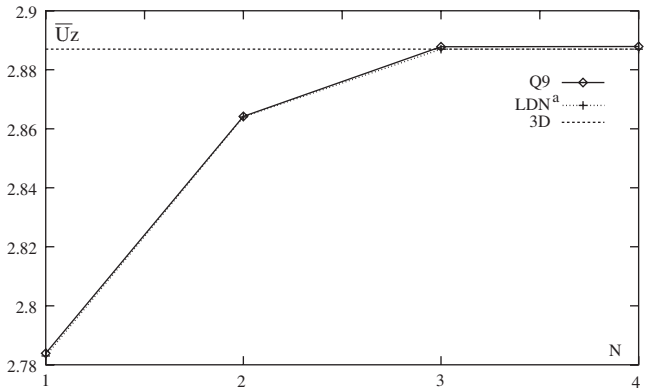

Figure 8. $\bar{U}_z(a/2, a/2, 0)$ vs N. Convergence at the analytical solution. Data: $a/h = 4$, LDN case, IS, LAM2, sinusoidal load, SS.

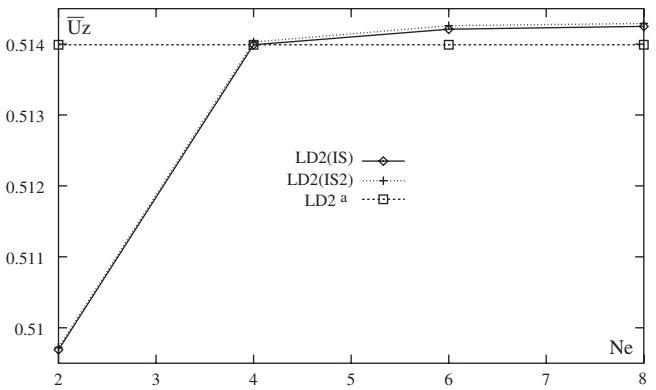

Figure 9. $\bar{U}_z(a/2, a/2, 0)$ vs N_e. Convergence to the analytical solution. Data: $a/h = 100$, LD2 case, LAM2, sinusoidal load, SS.

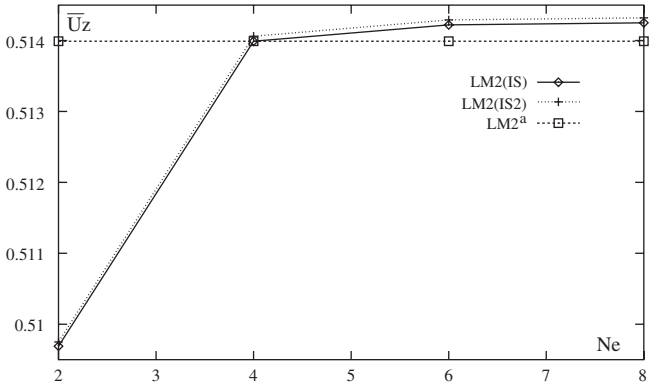

Figure 10. $\bar{U}_z(a/2, a/2, 0)$ vs N_e. Convergence to the analytical solution. Data: $a/h = 100$, LM2 case, LAM2, sinusoidal load, SS.

- These three points permit one to conclude that the connections (which were established in Appendix C of Part 1) between stiffness/compliance terms and different integration schemes should be considered to be consistent for both PVD and RMVT cases.

Further to what has just been written, the authors have made additional analyses, which are not documented herein, to compare eigenvalues of finite element matrices related to the problem discussed in Table IV. A perfect agreement between the classical and mixed layer-wise finite elements was confirmed by this eigenvalue analysis. It should once again be noted that the mathematical structure of the matrices related to the PVD and RMVT applications is completely different. Nevertheless, it leads to the same numbers: in these magic results probably lies the truth of variational statements.

The convergence rates of transverse displacements by an increase of N_e of LD2 and LD2 cases for IS and IS2 integration schemes are detailed in Figures 9 and 10. Thin plates are

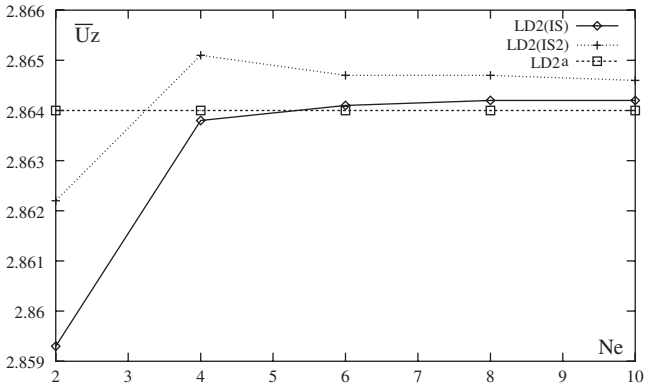

Figure 11. $\bar{U}_z(a/2, a/2, 0)$ vs N_e. Convergence to the analytical solution. Data: $a/h = 4$, LD2 case, LAM2, sinusoidal load, SS.

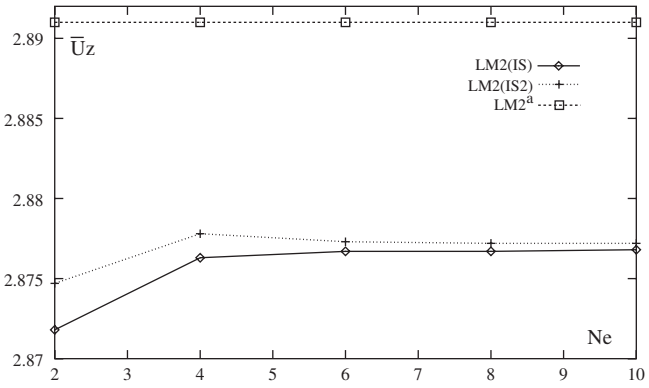

Figure 12. $\bar{U}_z(a/2, a/2, 0)$ vs N_e. Convergence to the analytical solution. Data: $a/h = 4$, LM2 case, LAM2, sinusoidal load, SS.

treated in the two latter figures while corresponding thick plates are addressed in Figures 11 and 12. The thickness behaviour of in-plane displacements of thick and thin plates are given in Figures 13–16 for different integration schemes and LD and LM finite elements.

The classical patch test on transverse displacements vs thickness ratio is presented in Figure 17. Such a test proves that the three different integration schemes all work well to evaluate transverse displacements of very thick and very thin multilayered plates. On the contrary, quite a different response has been obtained as far as transverse stress evaluations are concerned, see Figures 18 and 19. In such a case, the use of the IS2 integration scheme becomes mandatory for thin-plate geometries.

The effects of the number of elements on transverse displacements and transverse stresses in thin-plate analyses have been addressed in Figures 20–22. The superiority of the IS2 integration scheme is confirmed. It is further demonstrated that the accuracy of the three

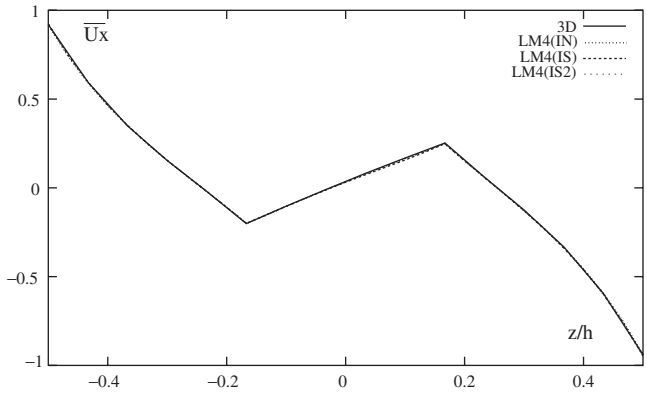

Figure 13. $\bar{U}_x$ $(x=0)$ vs z/h. Convergence to the elasticity solution. Data: $a/h=4$, LM4 case, LAM2, sinusoidal load, SS.

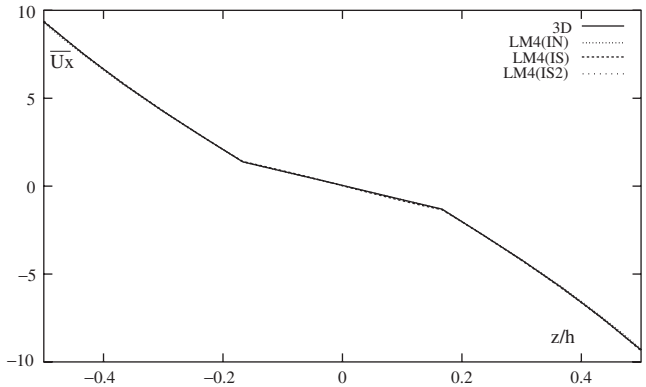

Figure 14. $\bar{U}_x$ $(x=0)$ vs z/h. Convergence to the elasticity solution. Data: $a/h=10$, LM4 case, LAM2, sinusoidal load, SS.

integration schemes increases by the number of elements that increase, that is, the differences between the three different schemes is a numerical problem.

A more comprehensive evaluation of displacements and stresses for the different layer-wise theories is given in Tables V and VI. To complete the picture, transverse displacements of layer-wise and equivalent single-layer finite elements, which are based on both PVD and RMVT for thin plates, are compared in Table VII. The following final comments can be made on these latter analyses:

- The introduced integration schemes work in the same manner for both classical and mixed finite elements, that is, the choice made in Appendix C of Part 1 when the different terms were selected, should be considered reasonable.
- Thick and thin plates can be modelled by appropriate selection of integration schemes.
- As far as displacement evaluations are concerned, the three integration schemes lead to the same results. This conclusion cannot be confirmed as far as stresses are concerned. In such a case, IN and IS evaluations could be completely wrong.

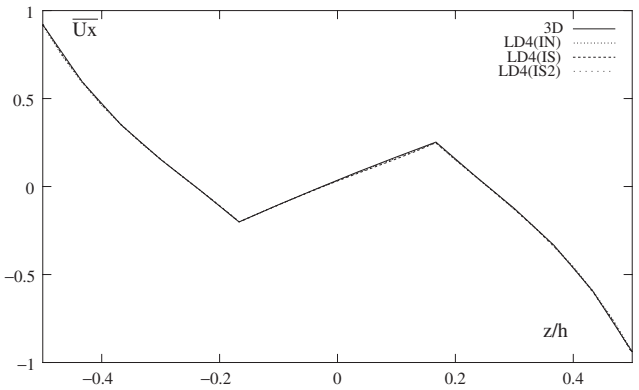

Figure 15. $\bar{U}_x$ $(x=0)$ vs z/h. Convergence to the elasticity solution. Data: $a/h=4$, LD4 case, LAM2, sinusoidal load, SS.

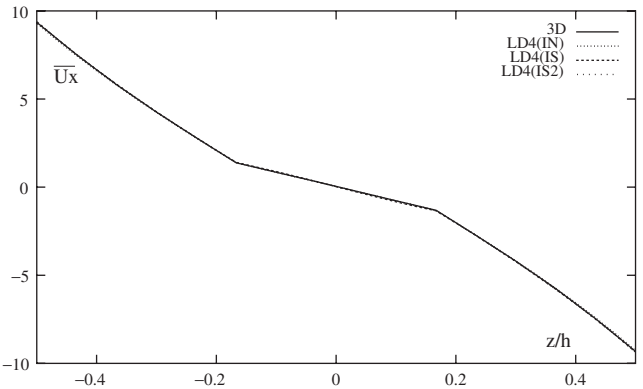

Figure 16. $\bar{U}_x$ $(x=0)$ vs z/h. Convergence to the elasticity solution. Data: $a/h=10$, LD4 case, LAM2, sinusoidal load, SS.

The conclusions reached on the analyses presented here have been used in the results that are discussed in the next paragraphs. Q9 finite elements in particular are employed in the implemented FE model.

3.3. Comparison with other results in the literature

A comprehensive comparison with available computational results has been documented in Tables VIII–XIII. Some of the most relevant multilayered plate elements that have been proposed in open literature have been considered in these tables. Different geometries, loadings and boundary conditions are considered. Problems treated by other authors have been compared with the implemented finite elements. In a few cases, closed-form solutions have also been given and, wherever available, three-dimensional solution has been quoted too. For

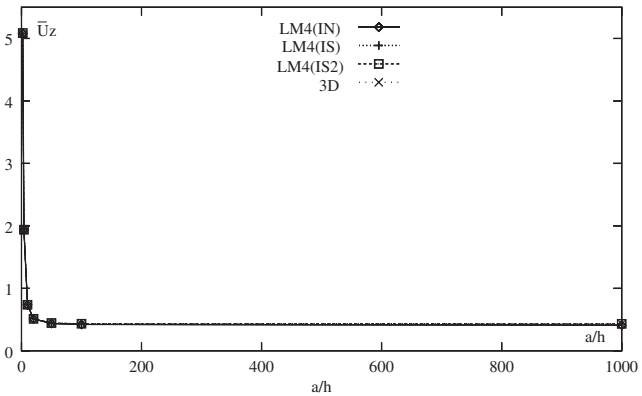

Figure 17. $\bar{U}_z(a/2, a/2, 0)$ vs N_e. Convergence to the elasticity solution. Data: LM4 case, LAM3, bi-sinusoidal load, SS.

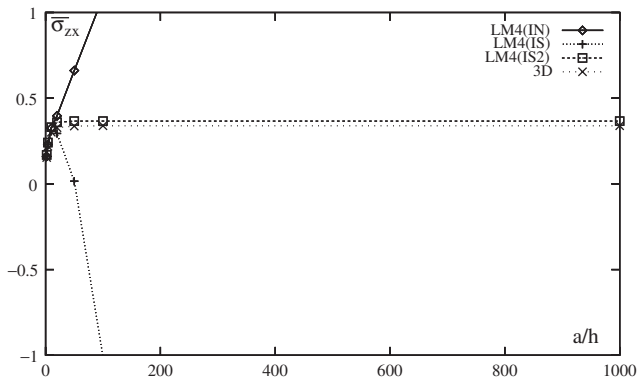

Figure 18. $\bar{\sigma}_{zx}(0, a/2, 0)$ vs a/h. Convergence to the elasticity solution. Data: LM4 case, LAM3, bi-sinusoidal load, SS.

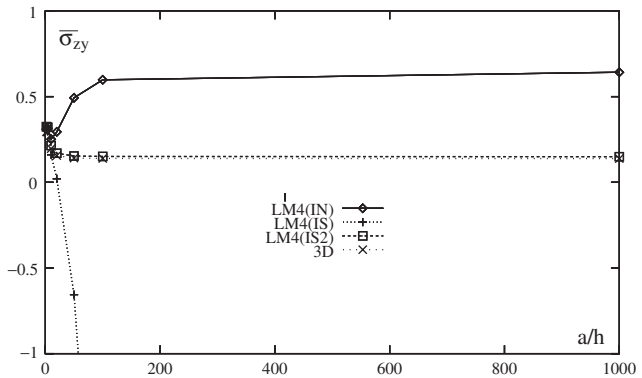

Figure 19. $\bar{\sigma}_{zy}(a/2, 0, 0)$ vs a/h. Convergence at the elasticity solution. Data: LM4, LAM3, bi-sinusoidal load, SS.

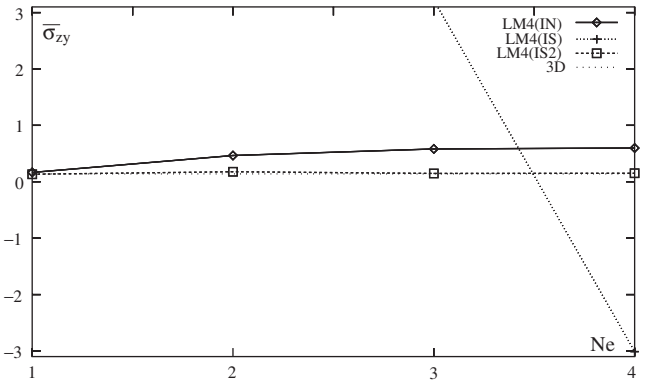

Figure 20. $\bar{\sigma}_{zy}(a/2, 0, 0)$ vs N_e. Convergence to the elasticity solution. Data: $a/h = 100$, LM4, LAM3, bi-sinusoidal load.

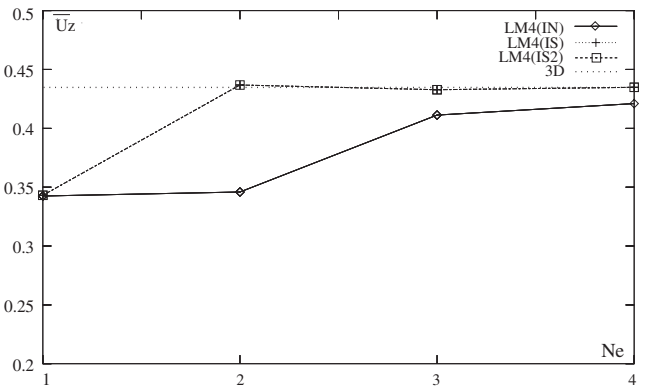

Figure 21. $\bar{U}_z(a/2, a/2, 0)$ vs N_e. Convergence to the elasticity solution. Data: $a/h = 100$, LM4, LAM3, bi-sinusoidal load, SS.

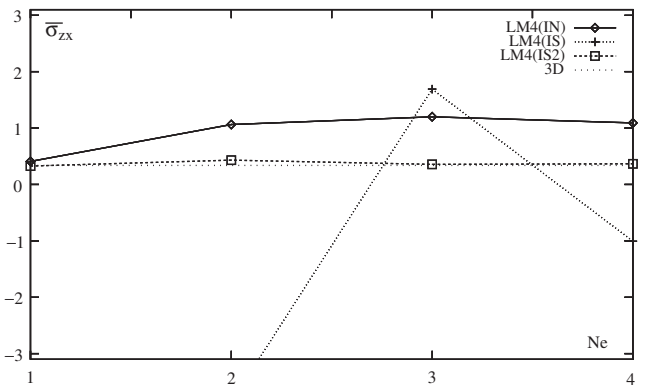

Figure 22. $\bar{\sigma}_{zx}(0, a/2, 0)$ vs N_e. Convergence to the elasticity solution. Data: $a/h = 100$, LM4 case, LAM3, bi-sinusoidal load, SS.

Table VII. $\bar{U}_z(a/2, a/2, 0)$. Comparison of various theories. Data: IS integration, $a/h = 100$, case of Table VI.

			Exact 3D value: 0.435				
LM4	0.43482	LM3	0.43482	LM2	0.43482	LM1	0.43477
LD4	0.43482	LD3	0.43482	LD2	0.43481	LD1	0.43390
—	—	EMZC3	0.43708	EMZC2	0.43700	EMZC1	0.43183
EMC4	0.43688	EMC3	0.43690	EMC2	0.43577	EMC1	0.43067
—	—	EDZ34	0.43708	EDZ2	0.43698	EDZ1	0.43180
ED4	0.43684	ED3	0.43684	ED2	0.43572	ED1	0.43054

Table VIII. $\bar{U}_z(a/2, a/2, 0)$. Comparison to available results. Data: $a = b$, bi-sinusoidal load, LAM3, SS, mesh 3×3. 3D solution by Pagano [31].

a/h	4	10	20	100
3D	1.937	0.737	0.513	0.435
		Results from literature		
R-H	1.8937	0.7147	0.5060	0.4343
R-F	1.7100	0.6628	0.4912	0.4337
P&K	1.8744	0.7185	—	0.4346
D&R	1.9530	0.7377	0.5122	0.4333
A&S	–	0.6693	—	—
LH&X	1.7095	0.6627	0.4912	0.4337
		Present LW analysis		
LM3[a]	1.9385	0.7370	0.5130	0.4346
LD3[a]	1.9371	0.7370	0.5130	0.4346
LM3(IS)	1.9381	0.7358	0.5114	0.4328
LD3(IS)	1.9381	0.7358	0.5114	0.4328
		Present ESL analysis		
EMZC3(IS)	1.9633	0.7443	0.5167	0.4368
EMC4(IS)	1.9506	0.7303	0.5121	0.4366
EDZ3(IS)	1.9633	0.7441	0.5166	0.4368
ED4(IS)	1.9506	0.7272	0.5112	0.4366

those cases in which a three-dimensional solution is not available, reference could be made to the present LM4 finite elements.

Thick and thin square plates are considered in Table VIII. Early and recent computational results are compared to the proposed classical and advanced finite elements. Classical (R–E) Reissner–Mindlin-type and refined (R–E and P&K) finite elements with only displacement variables are considered. D-R consists of a hybrid finite plate/shell element while A-S consists of a very recent mixed re-elaboration of FSDT statements. The alternative computational techniques, called differential quadrature approach by Liew *et al.* [15] are also taken into account in the comparison. These five referenced analyses are compared to the present

Table IX. $\bar{U}_z(a/2, b/2, 0)$. Comparison to available results. Data: $b = 3a$, bi-sinusoidal load, LAM2, SS, mesh 3×9. 3D solution by Pagano [4].

a/h	4	10	20	100
3D	2.820	0.919	0.610	0.508
		Results from literature		
D&R	2.8370	0.920	0.6086	0.5061
D-1	2.7172	0.8810	0.5987	0.50721
D-2	2.7756	0.9197	0.6098	0.5077
R-H	2.6411	0.862	0.5937	0.5070
L&S	2.828	0.921	0.611	—
IK&T	2.729	0.918	0.609	—
P&T	2.73	0.918	0.610	0.508
		Present LW analysis		
LM3[a]	2.8216	0.9189	0.6095	0.5077
LD3[a]	2.8210	0.9189	0.6095	0.5077
LM3(IS)	2.8167	0.9163	0.6072	0.5054
LD3(IS)	2.8167	0.9163	0.6072	0.5054
		Present ESL analysis		
EMZC3(IS)	2.8554	0.9182	0.6077	0.5057
EMC4(IS)	2.7648	0.8744	0.5953	0.5052
EDZ3(IS)	2.8527	0.9182	0.6077	0.5057
ED4(IS)	2.7328	0.8686	0.5938	0.5051

Table X. $\bar{U}_z(a/2, a/2, 0)$. Comparison to available results. Data: $a = b$, LAM2, uniform load, SS, mesh 3×3.

a/h	4	10	100
		Results from literature	
P&K	2.8765	1.0968	0.6713
R-H	2.9091	1.0900	0.6705
Mindlin	2.6559	1.0211	0.6701
		Present LW analysis	
LM3(IS)	3.0547	1.1593	0.6743
LD3(IS)	3.0548	1.1593	0.6743
		Present ESL analysis	
EMZC3(IS)	3.1702	1.1787	0.6806
EMC4(IS)	3.1099	1.1272	0.6799
EDZ3(IS)	3.1667	1.1788	0.6806
ED4(IS)	3.0797	1.1204	0.6798

Table XI. $U_z'(a/2, a/2, 0)$. Comparison to available results. Data: $b = a$, LAM2, central point load, SS, mesh 4×4.

a/h	4	10	100
	Results from literature		
P&K	21.709	5.3434	2.1593
Mindlin	15.6905	4.3989	2.1177
	Present ESL analysis		
EMZC3(IS)	22.811	5.6052	2.1740
EMC4(IS)	24.831	5.5074	2.1703
EDZ3(IS)	22.680	5.5906	2.1739
ED4(IS)	24.595	5.4671	2.1697

Table XII. $\bar{U}_z(a/2, a/2, 0)$. Comparison to available results. Data: $b = a$, LAM2, bi-sinusoidal load, CL, mesh 3×3.

a/h	4	10	100
	Results from literature		
P&K	1.3146	0.3752	0.1081
Mindlin	1.3376	0.3452	0.1054
	Present LW analysis		
LM3(IS)	1.3612	0.3961	0.1072
LD3(IS)	1.3594	0.3958	0.1072
	Present ESL analysis		
EMZC3(IS)	1.3387	0.3948	0.1072
EMC4(IS)	1.3250	0.3766	0.1068
EDZ3(IS)	1.3318	0.3943	0.1072
ED4(IS)	1.3121	0.3732	0.1067

layer-wise and equivalent single-layer finite elements. Both classical and mixed implementations have been given with correspondence to the highest N-values. The following comments can be made:

- The differences in the several theories vanish in thin-plate cases.
- Present LW finite elements are in excellent agreement with three-dimensional solutions.
- Among the considered analyses, the present LW finite elements lead to the best two-dimensional description.
- The present ESL analyses, based on RMVT, are more effective than those related to the referenced refined finite elements.

Correspondent rectangular-plate cases are addressed in Table IX. Apart from the already considered refined models (R-H and D-R), the hybrid multilayered elements by Liou and Sun (L&S),

Table XIII. $\bar{U}_z(a/2, a/2, 0)$. Comparison to available results. Data: $b = a$, LAM2, uniform load, CL, mesh 3×3.

a/h	4	10	100
		Results from literature	
P&K	1.8891	0.5247	0.1421
Mindlin	1.9203	0.4829	0.1388
		Present LW analysis	
LM3(IS)	1.9612	0.5589	0.1442
LD3(IS)	1.9577	0.5583	0.1442
		Present ESL analysis	
EMZC3(IS)	1.9278	0.5570	0.1442
EMC4(IS)	1.9100	0.5311	0.1436
EDZ3(IS)	1.9176	0.5563	0.1442
ED4(IS)	1.8914	0.5262	0.1435

Table XIV. $U_z'(a/2, a/2, 0)$. Comparison to available results. Data: $b = a$, LAM2, central point load, CL, mesh 4×4.

a/h	4	10	100
		Results from literature	
P&K	19.5659	4.0740	0.8478
Mindlin	14.1203	3.1840	0.8186
		Present ESL analysis	
EMZC3(IS)	19.862	4.2257	0.8522
EMC4(IS)	21.805	4.1679	0.8484
EDZ3(IS)	19.719	4.2093	0.8521
ED4(IS)	21.600	4.1305	0.8478

as well as the refined models D-1, D-2, P&T, and IK&T (which are based on Ambartsumian–Whitney–Rath–Das theory given in Part 1), are compared. The quoted results confirm the conclusions outlined for Table VIII. The superiority of the present ESL finite elements EMZC3 and EDZ3 (based on RMVT and PVD, respectively) over the other available ESL refined models, such as D-1, D-2, P&T and IK&T is in particular confirmed. The four latter referenced analyses, by discarding normal stresses effects, in fact violate Koiter's recommendations discussed in Section 2 of Part 1. Such a stress is indeed fully retained by the present EMZC3 and EDZ3 analyses. In particular, EMZC3 describes an interlaminar continuous transverse stress field.

Further similar analyses, related to different loadings and boundary conditions, are dealt with in Tables X–XIV. The previously reached conclusions can be confirmed. These tables could also be used to assess future, refined models for multilayered plates.

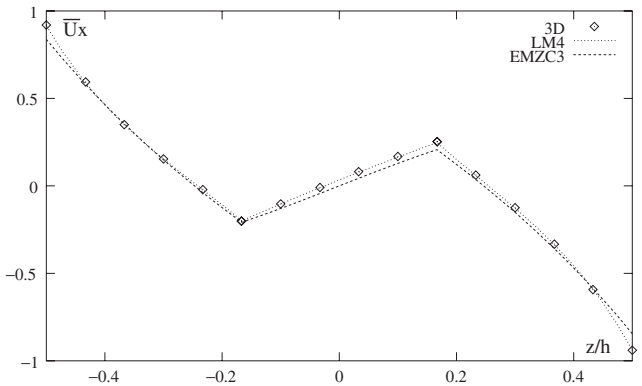

Figure 23. $\bar{U}_x$ $(x=0)$ vs z/h. Comparison to the elasticity solution. Data: $a/h=4$, IN integration, LAM2, sinusoidal load, SS.

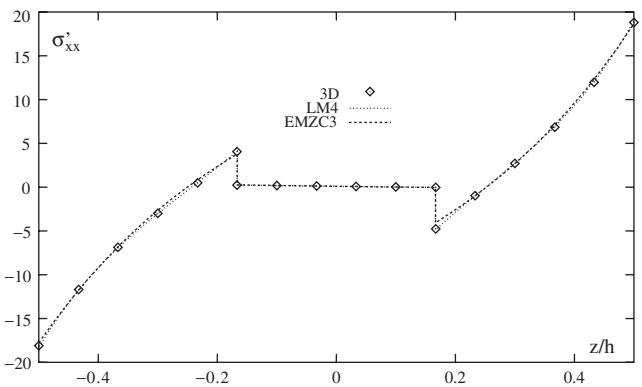

Figure 24. σ'_{xx} $(x=a/2,)$ vs z/h. Convergence to the elasticity solution. Data: $a/h=4$, IN integration, LAM2, sinusoidal load, SS.

3.4. Further results obtained by comparing the implemented classical and advanced elements

Quite a comprehensive evaluation of the implemented finite elements as a tool to trace the response of multilayered plates is given in Figures 23–33. In-plane displacements, in-plane stresses, transverse stresses (both shear and normal components) vs multilayered plate thickness plots are given. Thick $(a/h=4)$ and moderately thick plates are considered. Plotted transverse stresses are those assumed *a priori* for mixed cases. In-plane stresses are those obtained from the corresponding Hooke's law. Transverse stresses related to PVD formulated finite elements are those obtained by integration of three-dimensional indefinite equilibrium equations.

The implemented comparisons permit one to make the following comments:

- It is confirmed that LM4 analyses lead to three-dimensional descriptions of static response of multilayered plates.

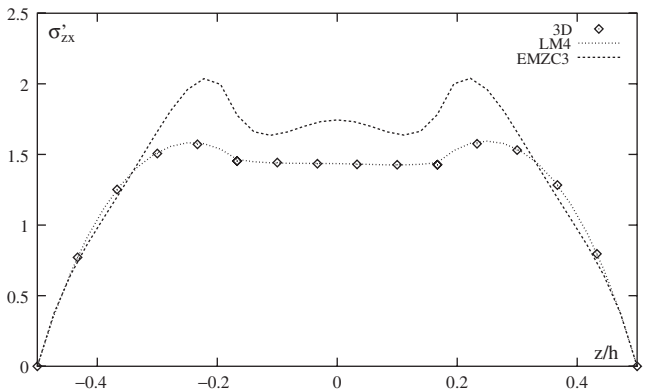

Figure 25. σ'_{zx} $(x = 0,)$ vs z/h. Convergence to the elasticity solution. Data: $a/h = 4$, IN integration, LAM2, sinusoidal load, SS.

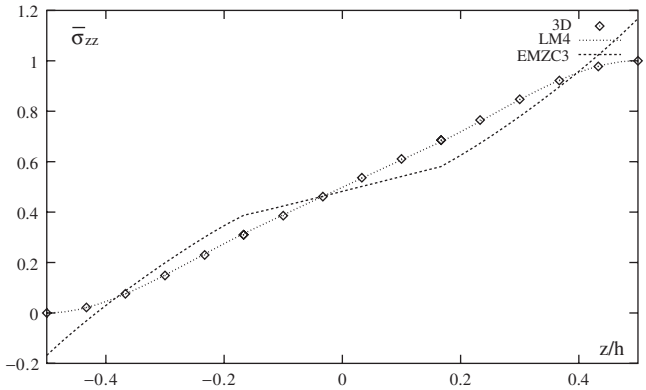

Figure 26. $\bar{\sigma}_{zz}$ $(x = a/2,)$ vs z/h. Convergence to the elasticity solution. Data: $a/h = 4$, IN integration, LAM2, sinusoidal load, SS.

- Among the implemented analysis, layer-wise finite elements (e.g. LM4) are the only ones that give *a priori* transverse stresses (Figure 25) and such a description meets the corresponding three-dimensional, exact analysis with excellent agreement.
- Among the implemented ESL finite elements, those formulated on RMVT offer the best descriptions. In any case, very thick plates demand the use of layer-wise finite elements.
- The largest differences among the different finite elements are mostly located at the layer interfaces.
- σ_{zz} can play a predominant role, as it is extremely influenced by a/h. It should be noticed that the considered laminated plates barely being transversely anisotropic (i.e. $E_z = E_T$ does not vary in the thickness direction) the zig-zag terms u_{Zz} could introduce an unmotivated constraint (see Figure 33). The zigzag form has, in fact, barely been exhibited by the LM4 analysis.

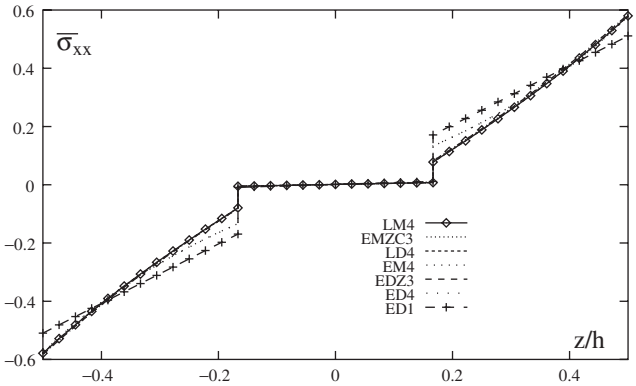

Figure 27. $\bar{\sigma}_{xx}$ $(x = a/2, y = a/2)$ vs z/h. Evaluation of different finite elements. Data: $a/h = 10$, IS, LAM2, bi-sinusoidal load, SS, mesh 5×5.

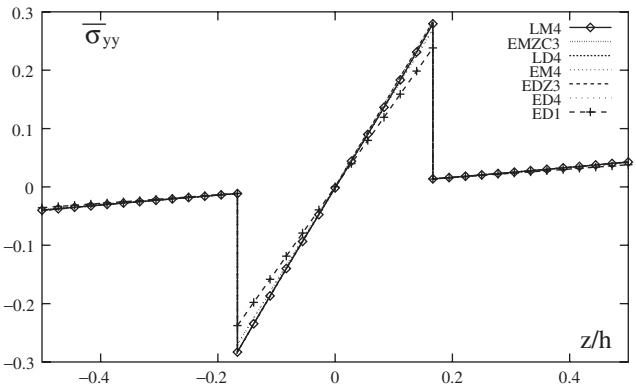

Figure 28. $\bar{\sigma}_{yy}$ $(x = a/2, y = a/2)$ vs z/h. Evaluation of different finite elements. Data: $a/h = 10$, IS integration,LAM2, bi-sinusoidal load, SS, mesh 5×5.

3.5. Final comments on the analyses

Further to the discussion made in the previous subsections, the following comments and conclusions can be drawn on the conducted numerical investigations.

- Advanced layer-wise LM and equivalent single-layer finite elements, which are based on RMVT (LM- and EM-types), completely fulfil interlaminar equilibria and account for the zig-zag effects. These elements *a priori* furnish transverse shear normal stresses without requiring any post-processing procedures. Worst description has been found in the ESL cases, due to the assumed, non-physical independence of the zig-zag function from the k-layer.

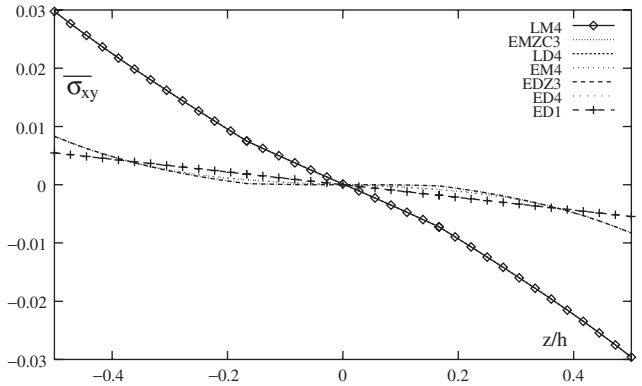

Figure 29. $\bar{\sigma}_{xy}$ $(x=0, y=0)$ vs z/h. Evaluation of different finite elements. Data: $a/h=10$, IS integration, LAM2, bi-sinusoidal load, SS, mesh 5×5.

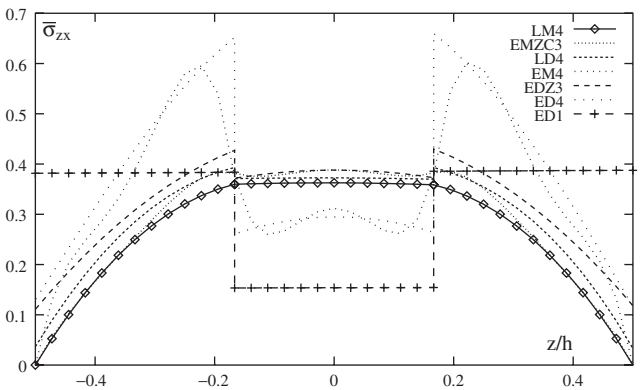

Figure 30. $\bar{\sigma}_{zx}$ $(x=0, y=a/2)$ vs z/h. Evaluation of different finite elements. Data: $a/h=10$, IS integration, LAM2, bi-sinusoidal load, SS, mesh 5×5.

- LD- and ED-type finite elements do not *a priori* fulfil interlaminar continuous transverse stresses while zig-zag effects can be included in ED cases by considering the related EDZ-type theories.
- LM- and LD-type elements are more computationally expensive than the corresponding EM and ED ones; the number of independent variables in fact depends on the number of constitutive layers N_l. On the other hand, the use of layer-wise description is essential for those cases in which an accurate description of σ_{zz} and related effects is required.
- LWM descriptions are more accurate than the corresponding ESLM ones.
- Advanced, M mixed descriptions based on RMVT are more accurate than the corresponding classical D formulation, based on PVD.

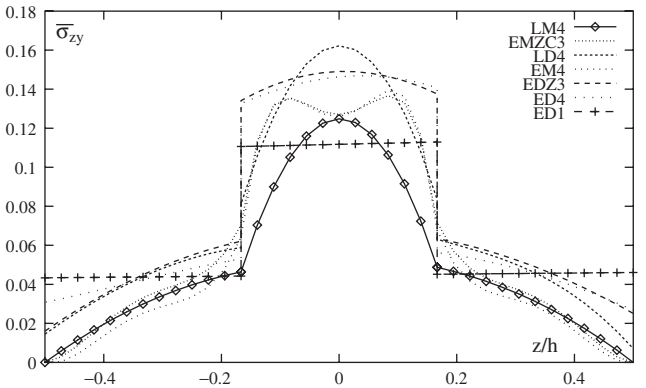

Figure 31. $\bar{\sigma}_{zy}$ $(x = a/2, y = 0)$ vs z/h. Evaluation of different finite elements. Data: $a/h = 10$, IS integration, LAM2, bi-sinusoidal load, SS, mesh 5×5.

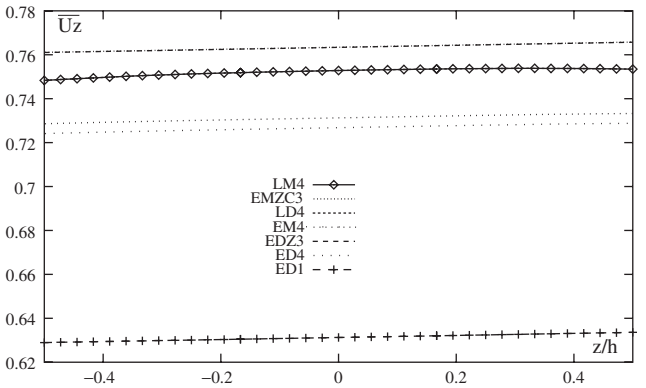

Figure 32. $\bar{U}_z$ $(x = a/2, y = a/2)$ vs z/h. Evaluation of different finite elements. Data: $a/h = 10$, IS integration, LAM2, bi-sinusoidal load, SS, mesh 5×5.

- EM finite elements are more accurate than ED ones, in other words RMVT is much more effective for ESLM formulations.
- M mixed analyses do not require any post-processing procedure to obtain transverse stresses.
- The order of the used expansion N plays a very important role, especially as far as unsymmetrical laminates are concerned. One should note that the quadratic expansions are much more effective for unsymmetrical laminates. With an increase of N the differences between LM and LD tends to disappear.

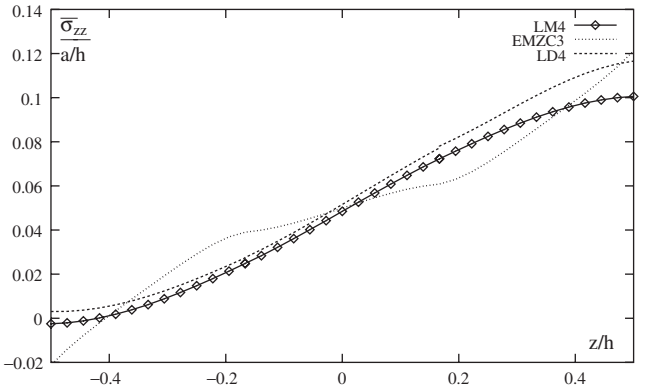

Figure 33. $\frac{1}{a/h}\bar{\sigma}_{zz}$ $(x = a/2, y = a/2)$ vs z/h. Evaluation of different finite elements. Data: $a/h = 10$, IS integration, LAM2, bi-sinusoidal load, SS, mesh 5×5.

- The zig-zag function already improves the related results: the EDZ analyses are more accurate than the ED ones. Advantages also arise from imposing interlaminar continuity, i.e. the EMC results are more accurate than the ED ones.

4. PROPOSED TEST CASES

The companion paper (Part 1) has proposed advanced and classical finite elements as tools to describe the static response of multilayered plates with different levels of accuracy and from a two-dimensional point of view. Furthermore, the present paper has shown results that have been obtained by implementing some of the finite elements proposed in the companion paper. Nevertheless, the numerical analysis conducted in the previous sections has documented that quite a different level of accuracy could be reached by the several implemented finite elements. Such a level of accuracy can, in fact, vary considerably from element to element. For instance, a three-dimensional description can be obtained by implementing layer-wise finite elements (e.g. LM4) while thin-plate results of a Kirchhoff-type can be obtained by implementing classical equivalent single layer elements (e.g. ED1).

Many other finite elements exist between these two extreme finite elements, related to the highest and lowest level of accuracy. Two 'test cases' are then proposed by the authors in Tables XV(a)–XVI(d) and Figures 34 and 35. A layered, moderately thick plate is considered in Tables XV(a) and XV(b) where 20 additional finite element results have been quoted between the LM4 and ED1 analyses. Very thick ($a/h = 2$), thick ($a/h = 4$), moderately thick ($a/h = 10$) and thin sandwich plates are considered in Tables XVI(a) and XVI(b) where results of six finite elements have been compared. These six elements correspond to most representative implemented finite elements. In-plane displacements vs thickness of the sandwich plate are given in Figures 34 and 35; these two figures are related to the two thickest plates.

Tables XV(a)–XVI(d) also represent a summary of the analysis present in this paper. Three-dimensional results, as well as a few other finite element results by other authors, have been

Table XV. Test case I. Results for the 22 implemented $Q9$ finite elements. Data: $a = b$, LAM2, bi-sinusoidal load, SS, mesh 5×5, $a/h = 10$.

	$\bar{\sigma}_{xx}$ $a/2, a/2, \pm h/2$	$\bar{\sigma}_{yy}$ $a/2, a/2, \pm h/6$	$\bar{\sigma}_{xy}$ $0, 0, \pm h/2$	$\bar{\sigma}_{zx}$ $0, a/2, 0$	$\bar{\sigma}_{zy}$ $a/2, 0, 0$	$\bar{U}_z$ $a/2, a/2, 0$
3D	0.590 − 0.590	0.285 −0.288	−0.0289 0.0289	0.357	0.1228	0.7530
			Results from literature			
L&S	0.580 − 580	0.285 −0.289	−0.0283 0.0284	0.367	0.127	0.7546
Moriya	0.5759 − 0.5785	0.2820 −0.2890	−0.02861 0.02878	0.3993	0.1296	0.7512
R-H	0.5684 —	—	—	0.1033	—	0.7125
H&L	0.5884 − 0.5879	0.2834 −0.2873	−0.02880 0.02896	0.3627	0.1284	0.7531
			Present LW analysis			
LM4(IS2)	0.5801 − 0.5784	0.2796 −0.2831	−0.0296 0.0297	0.3626	0.1249	0.7528
LM3(IS2)	0.5801 − 0.5784	0.2797 −0.2831	−0.0296 0.0298	0.3626	0.1249	0.7528
LM2(IS2)	0.5796 − 0.5781	0.2772 −0.2807	−0.0296 0.0297	0.3518	0.1191	0.7524
LM1(IS2)	0.5760 − 0.5748	0.2525 −0.2562	−0.0294 0.0296	0.3615	0.0937	0.7500
LD4(IS2)	0.5801 − 0.5784	0.2796 −0.2831	−0.0296 0.0297	0.3724	0.1623	0.7528
LD3(IS2)	0.5801 − 0.5784	0.2797 −0.2831	−0.0296 0.0297	0.3724	0.1623	0.7528
LD2(IS2)	0.5792 − 0.5777	0.2791 −0.2826	−0.0296 0.0297	0.3711	0.1362	0.7519
LD1(IS2)	0.5608 − 0.5598	0.2740 −0.2776	−0.0288 0.0289	0.3726	0.1338	0.7371
			Present ESL analysis			
EMZC3(IS)	0.5856 − 0.5826	0.2829 −0.2823	−0.0083 0.0083	0.3884	0.1270	0.7634
EMZC2(IS)	0.5685 − 0.5654	0.2766 −0.2761	−0.0076 0.0076	0.3955	0.1486	0.7503
EMZC1(IS)	0.5674 − 0.5658	0.2747 −0.2741	−0.0077 0.0077	0.3986	0.1546	0.7442
EMC4(IS)	0.5787 − 0.5764	0.2708 −0.2706	−0.0084 0.0083	0.3118	0.1259	0.7313
EMC3(IS)	0.5803 − 0.5773	0.2710 −0.2705	−0.0085 0.0086	0.2687	0.1450	0.7323
EMC2(IS)	0.5128 − 0.5097	0.2417 −0.2411	−0.0055 0.0055	0.1442	0.1124	0.6441
EMC1(IS)	0.5106 − 0.5090	0.2411 −0.2406	−0.0051 0.0051	0.1979	0.0723	0.6449
EDZ3(IS)	0.5856 − 0.5825	0.2834 −0.2828	−0.0083 0.0083	0.3879	0.1491	0.7634

Table XV *Continued.*

EDZ2(IS)	0.5664 −0.5633	0.2780 −0.2775	−0.0075 0.0075	0.3838	0.1411	0.7487
EDZ1(IS)	0.5642 −0.5625	0.2762 −0.2757	−0.0076 0.0076	0.3777	0.1408	0.7417
ED4(IS)	0.5776 −0.5753	0.2694 −0.2692	−0.0083 0.0083	0.2948	0.1464	0.7268
ED3(IS)	0.5783 −0.5753	0.2687 −0.2681	−0.0085 0.0085	0.2849	0.1445	0.7246
ED2(IS)	0.5131 −0.5101	0.2405 −0.2399	−0.0056 0.0056	0.1671	0.1137	0.6395
ED1(IS)	0.5113 −0.5096	0.2382 −0.2376	−0.0055 0.0055	0.1538	0.1117	0.6313

Table XVI. Test case II. Results for the most representative $Q9$ finite elements. Data: sandwich plate, SS, mesh 5×5.

	$\bar{\sigma}_{xx}$ $(a/2, b/2, \pm1)$	$\bar{\sigma}_{yy}$ $(a/2, b/2, \pm1)$	$\bar{\sigma}_{zx}$ $(0, b/2, 0)$	$\bar{\sigma}_{zy}$ $(a/2, 0, 0)$	$\bar{U}_z$ $(a/2, b/2, 0)$
(a) $a/h=2$ case					
3D	3.278 −2.653	0.452 −0.392	0.185	0.139	26.0
		Present layer-wise analysis			
LM4	3.2430 −2.6233	0.4537 −0.3829	0.1897	0.1444	22.103
LM2	3.2352 −2.6172	0.4541 −0.3832	0.1853	0.1404	22.103
LD3	3.2426 −2.6233	0.4544 −0.3834	—	—	22.103
		Present ESL analysis			
EMZC3	3.1594 −2.5612	0.5041 −0.4338	0.2403	0.1600	23.313
EMZC2	3.1255 −2.5286	0.5021 −0.4319	0.2489	0.1648	23.298
ED3	3.0752 −2.5015	0.4825 −0.4241	—	—	21.960
(b) $a/h=4$ case					
3D	1.556 −1.512	0.260 −0.253	0.239	0.107	8.0
		Present layer-wise analysis			
LM4	1.5425 −1.4956	0.2582 −0.2486	0.2459	0.1143	7.5947
LM2	1.5412 −1.4944	0.2584 −0.2487	0.2435	0.1118	7.5943
LD3	1.5426 −1.4957	0.2583 −0.2487	—	—	7.5948

Table XVI *Continued.*

	$\bar{\sigma}_{xx}$ $(a/2, b/2, \pm 1)$	$\bar{\sigma}_{yy}$ $(a/2, b/2, \pm 1)$	$\bar{\sigma}_{zx}$ $(0, b/2, 0)$	$\bar{\sigma}_{zy}$ $(a/2, 0, 0)$	$\bar{U}_z$ $(a/2, b/2, 0)$
			Present ESL analysis		
EMZC3	1.5932 −1.5467	0.2804 −0.2713	0.2759	0.1192	7.8723
EMZC2	1.5852 −1.5388	0.2801 −0.2709	0.2767	0.1186	7.8689
ED3	1.5645 −1.5228	0.2656 −0.2592	—	—	7.3560
(c) $a/h = 10$ case					
3D	1.153 −1.152	0.110 —	0.3	0.053	2.5
			Present layer-wise analysis		
LM4	1.1323 −1.1293	0.1093 −0.1076	0.3042	0.05354	2.2001
LM2	1.1323 −1.1293	0.1093 −0.1077	0.3032	0.05237	2.2001
LD3	1.1324 −1.1293	0.1093 −0.1076	—	—	2.2001
			Present ESL analysis		
EMZC3	1.1488 −1.1467	0.1137 −1.127	0.3313	0.06388	2.2342
EMZC2	1.1588 −1.1568	0.1146 −0.1135	0.3264	0.06765	2.2313
ED3	1.5645 −1.5228	0.2656 −0.2592	—	—	2.1132
(d) $a/h = 50$ case					
3D	±1.099	±0.057	0.323	0.031	1.10
			Present layer-wise analysis		
LM4	±1.0786	±0.0559	0.3287	0.0312	0.9343
LM2	±1.0785	±0.0558	0.3280	0.0305	0.9343
LM1	±1.0791	±0.0563	0.3281	0.0305	0.9343
LD3	±1.0785	±0.0558	—	—	0.9343
			Present ESL analysis		
EMZC3	±1.0714	±0.0572	0.4094	0.1055	0.9354
EMZC2	±1.0843	±0.0589	0.4672	0.0795	0.9303
ED3	±1.0706	±0.0569	—	—	0.9297

quoted for comparison purposes. Transverse displacement as well as in-plane and out-of-plane stress values are compared.

The authors propose to refer to the two introduced test cases as desk-beds in order to establish the level of accuracy of multilayered finite elements to evaluate stresses and displacements of multilayered plates. In other words, the authors propose that any new FE

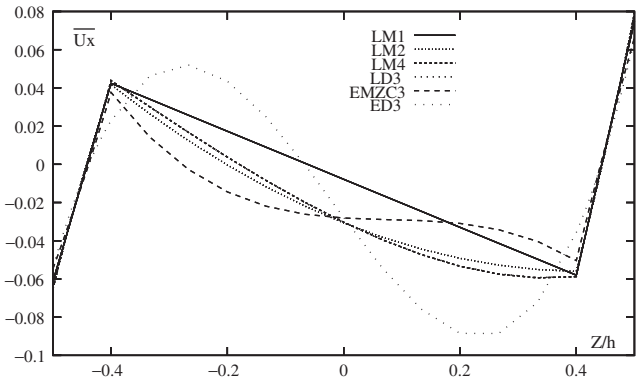

Figure 34. Test case II. In-plane displacement $\bar{U}_x$ vs thickness. Very thick sandwich plate $a/h = 2$.

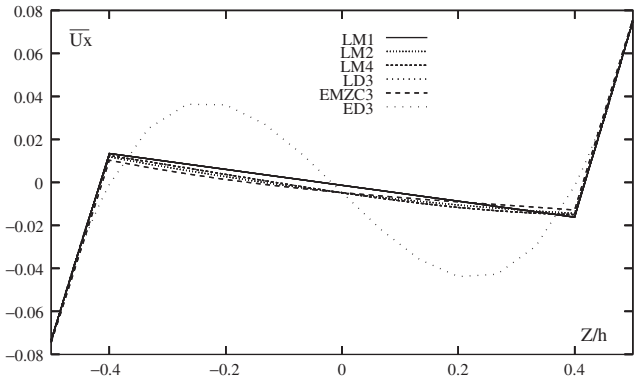

Figure 35. Test case II. In-plane displacement $\bar{U}_x$ vs thickness. Thick sandwich plate $a/h = 4$.

contribution directed to a better understanding of multilayered structures and which proposes a 'refined', 'advanced' or 'improved' multilayered finite element should clearly state the level of accuracy that such a finite element assumes in the hierarchy that has been established in Tables XV(a)–XV(d) and Figures 34 and 35.

5. CONCLUDING REMARKS

This paper has reported results of a numerical investigation directed to implement advanced (based on Reissner's mixed variational theorem) and classical (based on the principle of virtual displacements) multilayered finite elements that have been proposed in the companion paper. Linear up to fourth-order displacement and transverse stress fields have been considered in the layer/plate thickness. Both layer-wise and equivalent single-layer descriptions have been addressed, leading to 22 possible two-dimensional models. Three finite elements (four,

eight and nine nodes) have been considered. As a result, 22×3 finite elements have been implemented and compared. A condensed indicial notation has been used for implementation purpose.

Cross-ply symmetrical and unsymmetrical multilayered plates, as well as sandwich plates subject to various loadings and boundary conditions, have been analysed. A numerical assessment has been made. Comparisons to available three-dimensional solutions, to corresponding analytical solutions and other available computational implementations have been made.

From a numerical point of view, the following conclusion can be made:

- The implemented Q4, Q8 and Q9 elements have shown convergence rates typical of that class of finite elements.
- Advanced multilayered plate elements based on RMVT have shown the same numerical behaviour as corresponding classical elements based on PVD, that is, RMVT does not introduce any further numerical complications than those usually obtained from standard PVD applications.
- In order to contrast shear locking, a choice has been made, with respect to reduced and selective integration schemes, on the stiffness/compliance contributions of the finite element matrices related to RMVT applications. Numerical tests have shown that such a choice was consistent to that made for PVD cases.

As far as the two-dimensional point of view is concerned, the following conclusions can be drawn:

- The *a priori* fulfilment of interlaminar continuity for σ_{zz} makes mixed models more attractive than other available models that violate such a continuity.
- Thick-plate analysis has shown that any refinements of existing theories can be meaningless unless both interlaminar continuous transverse shear and normal stresses are taken into account in a refined theory.
- The number of independent variables should conveniently be taken as being dependent on N_l in very thick-plate analysis.
- It has been confirmed that the Reissner mixed variational theorem remains a valuable tool to analyse multilayered plates.
- Layer-wise analyses furnish a quasi-three-dimensional description of displacement and stress fields even though very thick plates are considered ($a/h\geqslant2$). Transverse stress evaluations do not require any post-processing (*a posteriori*) procedure such as the integration of three-dimensional indefinite equilibrium equations. These stresses are in fact computed *a priori* and with excellent accuracy directly by the assumed models.
- The accuracy given by equivalent single layer models is extremely subordinate to the order of the used expansion in the displacement and stress fields, to laminate layouts and to geometrical parameters. The case of cubic displacement field (EMZC3) has led to the best results.

Two 'Test cases' have been described; these have been proposed as desk-beds to assess future, 'refined' multilayered plate elements. The presented finite element evaluations have a strong practical interest in many problems. In general, accurate stress–strain evaluations are required to detect a certain damage in the structure. As a further example, the recent 'Meyer–Piennig [16] test case' related sandwich structures have to be mentioned. In this case, LW description is required even though a thin structure is considered [17].

Future works should be directed to a comparison of whole implemented finite elements to solve practical problems related to multilayered structures. More complex geometries as well as multilayered layouts, boundary and loading conditions (including dynamic loadings) should be considered in these analyses. Further attempts should consider alternative techniques, such as assumed strain field concept, in order to contrast numerical, locking mechanisms. The different techniques described in Part 1 as far as treatment of stress variables is concerned should be compared too. Extension to non-linear problems could be a further development of the present work.

APPENDIX A: FORTRAN FORM OF FUNDAMENTAL NUCLEUS

A.1. $K^{k\tau s}$ matrix for PVD applications

```
c
c
Nine FORTRAN statements follow.
      UD(1,1) = ETSUU(k,τ,s) * QPP(k,1,1) * FXX (i,j) + ETSUU(k,τ,s) * QPP(k,1,3) * FYX (i,j)
                +ETSUU(k,τ,s) * QPP(k,1,3) * FXY (i,j) + ETSUU(k,τ,s) * QPP(k,3,3) * FYY (i,j)
                +ETZSZUU(k,τ,s) * QNN(k,1,1) * F00(i,j)
      UD(1,2) = ETSUU(k,τ,s) * QPP(k,1,2) * FXY (i,j) + ETSUU(k,τ,s) * QPP(k,2,3) * FYY (i,j)
                +ETSUU(k,τ,s) * QPP(k,1,3) * FXX (i,j) + ETSUU(k,τ,s) * QPP(k,3,3) * FYX (i,j)
                +ETZSZUU(k,τ,s) * QNN(k,1,2) * F00(i,j)
      UD(1,3) = ETSZUU(k,τ,s) * QPN(k,1,3) * FX0(i,j) + ETSZUU(k,τ,s) * QPN(k,3,3) * FY0(i,j)
                +ETZSUU(k,τ,s) * QNN(k,1,1) * F0X(i,j) + ETZSUU(k,τ,s) * QNN(k,1,2) * F0Y(i,j)
      UD(2,1) = ETSUU (k,τ,s) * QPP(k,1,2) * FYX(i,j) + ETSUU (k,τ,s) * QPP(k,1,3) * FXX(i,j)
                +ETSUU (k,τ,s) * QPP(k,2,3) * FYY(i,j) + ETSUU (k,τ,s) * QPP(k,3,3) * FXY(i,j)
                +ETZSZUU (k,τ,s) * QNN(k,1,2) * F00(i,j)
      UD(2,2) = ETSUU (k,τ,s) * QPP(k,2,2) * FYY(i,j) + ETSUU (k,τ,s) * QPP(k,2,3) * FXY(i,j)
                +ETSUU (k,τ,s) * QPP(k,2,3) * FYX(i,j) + ETSUU (k,τ,s) * QPP(k,3,3) * FXX(i,j)
                +ETZSZUU (k,τ,s) * QNN(k,2,2) * F00(i,j)
      UD(2,3) = ETSZUU(k,τ,s) * QPN(k,2,3) * FY0(i,j) + ETSZUU(k,τ,s) * QPN(k,3,3) * FX0(i,j)
                +ETZSUU(k,τ,s) * QNN(k,1,2) * F0X(i,j) + ETZSUU(k,τ,s) * QNN(k,2,2) * F0Y(i,j)
      UD(3,1) = ETSZUU(k,τ,s) * QNN(k,1,1) * FX0(i,j) + ETSZUU(k,τ,s) * QNN(k,1,2) * FY0(i,j)
                +ETZSUU(k,τ,s) * QNP(k,3,1) * F0X(i,j) + ETZSUU(k,τ,s) * QNP(k,3,3) * F0Y(i,j)
      UD(3,2) = ETSZUU(k,τ,s) * QNN(k,1,2) * FX0(i,j) + ETSZUU(k,τ,s) * QNN(k,2,2) * FY0(i,j)
                +ETZSUU(k,τ,s) * QNP(k,3,2) * F0Y(i,j) + ETZSUU(k,τ,s) * QNP(k,3,3) * F0X(i,j)
      UD(3,3) = ETSUU (k,τ,s) * QNN(k,1,1) * FXX(i,j) + ETSUU (k,τ,s) * QNN(k,1,2) * FYX(i,j)
                +ETSUU (k,τ,s) * QNN(k,1,2) * FXY(i,j) + ETSUU (k,τ,s) * QNN(k,2,2) * FYY(i,j)
                +ETZSZUU(k,τ,s) * QNN(k,3,3) * F00(i,j)
c
c
```

The 3×3 elements of the $K^{\tau sk}$ matrix are denoted by the array UD. ET...-type arrays denote the thickness integrals. These are affected by τ and s indexes which come from the product of used expansion in $zF_\tau F_j$. QPP, QPN, QNP, QNN are the Hooke's law lamina arrays. ET...-type as well as QPP, QPN, QNP, QNN arrays are all affected by layer index k. F...-type arrays are the integral on Ω. These are affected by i and j indexes which come from the product of used shape function (e.g. N_iN_j, $N_{ix}N_j$). By putting the above 3×3 elements in appropriate loops with indexes k, τ, s, i, j, layer and multilayered stiffness matrices are obtained. The

four fundamental nuclei related to RMVT applications are treated likewise. $K_{u\sigma}^{k\tau s}$ is written in what follows.

A.2. $K_{u\sigma}^{k\tau s}$ matrix

```
c
c
US(1,1) = ETZSUS(k,τ,s) * F00(i,j)
US(1,2) = 0.0
US(1,3) = ETSUS (k,τ,s) * CPN(k,1,3) * FX0(i,j) +ETSUS (k,τ,s) * CPN(k,3,3) * FY0(i,j)
US(2,1) = 0.0
US(2,2) = ETZSUS(k,τ,s) * F00(i,j)
US(2,3) = ETSUS (k,τ,s) * CPN(k,2,3) * FY0 (i,j) + ETSUS (k,τ,s) * CPN(k,3,3) * FX0 (i,j)
US(3,1) = ETSUS (k,τ,s) * FX0(i,j)
US(3,2) = ETSUS (k,τ,s) * FY0(i,j)
US(3,3) = ETZSUS(k,τ,s) * f00(i,j)
c
c
```

REFERENCES

1. Carrera E, Demasi L. Classical and advanced multilayered plate elements based upon PVD and RMVT. Part 1. Derivation of finite element matrices. *International Journal for Numerical Methods in Engineering* 2002; **55**:191–231.
2. Reddy JN. *An Introduction to the Finite Element Method*. McGraw-Hill: New York, 1993.
3. Murakami H. Laminated composite plate theory with improved in-plane response. *Journal of Applied Mechanics* 1986; **53**:661–666.
4. Pagano NJ. Exact solutions for rectangular bidirection composites and sandwich plates. *Journal of Composite Materials* 1970; **4**:20–34.
5. Bathe KJ, Dvorkin EN. A four node plate bending element based on Mindlin/Reissner plate theory and mixed interpolation. *International Journal for Numerical Methods in Engineering* 1985; **21**:367–383.
6. Brank B, Carrera E. Multilayered shell finite element with interlaminar continuous shear stresses: a refinement of the Reissner–Mindlin formulation. *International Journal for Numerical Methods in Engineering* 2000; **48**: 843–874.
7. Briossilis D. The C^0 structural finite elements reformulated. *International Journal for Numerical Methods in Engineering* 1992; **35**:541–561.
8. Briossilis D. The four node C^0 Mindlin plate bending elements reformulated. Part I: formulation. *Computer Methods in Applied Mechanics and Engineering* 1993; **107**:23–43.
9. Briossilis D. The four node C^0 Mindlin plate bending elements reformulated. Part II: verification. *Computer Methods in Applied Mechanics and Engineering* 1993; **107**:45–100.
10. Zienkiewicz O, Xu Z, Zeng LF, Samuelsson N, Wiberg NE. Linked interpolation for Reissner–Mindlin plate element: Part I—A simple quadrilater. *International Journal for Numerical Methods in Engineering* 1993; **36**:3043–3056.
11. Carrera E. C^0 Reissner–Mindlin multilayered plate elements including zig-zag and interlaminar stresses continuity. *International Journal for Numerical Methods in Engineering* 1996; **39**:1797–1820.
12. Carrera E. Evaluation of layer-wise mixed theories for laminated plates analysis. *American Institute of Aeronautics and Astronautics Journal* 1998; **36**:830–839.
13. Carrera E. A study of transverse normal stress effects on vibration of multilayered plates and shells. *Journal of Sound and Vibration* 1999; **225**(5):803–829.
14. Carrera E. Single-layer vs multi-layers plate modellings on the basis of Reissner's mixed theorem. *American Institute of Aeronautics and Astronautics Journal* 2000; **38**:342–353.
15. Liew KM, Han B, Xiao M. Differential quadrature method for thick symmetric cross-ply laminates with first-order shear flexibility. *International Journal of Solids and Structures* 1996; **33**:2647–2658.
16. Meyer-Piening H-R. Experiences with 'exact' linear sandwich beam and plate analyses regarding bending, instability and frequency investigations. vol. I. ETH Zürich, Switzerland, 37–48.

17. Carrera E, Demasi L. Sandwich plate analysis by finite element method and Reissner's mixed theorem, vol. I. ETH Zürich, Switzerland, 301–312, 2000.
18. Auricchio F, Sacco E. A mixed-enhanced finite element for the analysis of laminated composite plates. *International Journal for Numerical Methods in Engineering* 1999; **44**:1481–1504.
19. Di S, Ramm E. Hybrid stress formulation for higher-order theory of laminated shell analysis. *Computer Methods in Applied Mechanics and Engineering* 1993; **109**:359–376.
20. D'schiuva. Multilayered anisotropic plate models with continuous interlaminar stresses. *Composite Structures* 1992; **22**:149–167.
21. Jing HJ, Liao ML. Partial hybrid stress element for the analysis of thick laminated composite plates. *International Journal for Numerical Methods in Engineering* 1989; **28**:2813–2827.
22. Idlbi A, Karama M, Touratier M. Comparison of various laminated plate theories. *Composite Structures* 1997; **37**:173–184.
23. Liou WJ, Sun CT. A three-dimensional hybrid stress isoparametric element for the analysis of laminated composite plates. *Computers and Structures* 1985; **25**:241–249.
24. Mindlin RD. Influence of rotatory inertia and shear deformation on flexural motions of isotropic elastic plates. *Journal of Applied Mechanics* 1951; **18**:31–38.
25. Moriya K. Laminated plate and shell elements for finite element analysis of advanced fiber reinforced composite structures. *Transactions of the Japan Society of Mechanical Engineering* (*Series A*) 1986; **52**(478):1600–1607. (in Japanese).
26. Pandya BN, Kant T. Flexural analysis of laminated composites using refined higher-order C^0 plate bending elements. *Computer Methods in Applied Mechanics and Engineering* 1985; **66**:173–198.
27. Polit O, Touratier. High-order triangular sandwich plate finite element for linear and non-linear analyses. *Computer Methods in Applied Mechanics and Engineering* 2000; **185**:305–324.
28. Reddy JN, Chao WC. A comparison of closed-form and finite-element solutions of thick laminated anisotropic rectangular plates. *Nuclear Engineering Design* 1981; **64**:153–167.
29. Reddy JN. A simple higher-order theory for laminated composite plates. *Journal of Applied Mechanics* 1984; **51**:745–752.
30. Pagano NJ. Exact solutions for composite laminates in cylindrical bending. *Journal of Composite Materials* 1969; **3**:398–411.
31. Pagano NJ, Hatfield SJ. Elastic behaviour of multilayered bidirectional composites. *American Institute of Aeronautics and Astronautics Journal* 1972; **10**:931–933.

